ELECTROCHEMISTRY FOR ENVIRONMENTAL APPLICATIONS: WATER DISINFECTION, PHARMACEUTICAL ANALYSIS, AND CO_2 REDUCTION

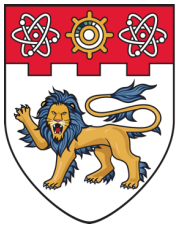

NANYANG TECHNOLOGICAL UNIVERSITY SINGAPORE

TONANON PANYAWUT

School of Chemistry, Chemical Engineering, and Biotechnology

A thesis submitted to the Nanyang Technological University
in partial fulfillment of the requirements for the degree of
Doctor of Philosophy

2025

Statement of Originality

I hereby certify that the work embodied in this thesis is the result of original research done by me except where otherwise stated in this thesis. The thesis work has not been submitted for a degree or professional qualification to any other university or institution. I declare that this thesis is written by myself and is free of plagiarism and of sufficient grammatical clarity to be examined. I confirm that the investigations were conducted in accord with the ethics policies and integrity standards of Nanyang Technological University and that the research data are presented honestly and without prejudice.

January 2025

Date

Tononan Panyawut

Supervisor Declaration Statement

I have reviewed the content and presentation style of this thesis and declare it of sufficient grammatical clarity to be examined. To the best of my knowledge, the thesis is free of plagiarism and the research and writing are those of the candidate's except as acknowledged in the Author Attribution Statement. I confirm that the investigations were conducted in accord with the ethics policies and integrity standards of Nanyang Technological University and that the research data are presented honestly and without prejudice.

January 2025

.....

Date

.....

Assoc Prof Richard D. Webster

Authorship Attribution Statement

This thesis contains material from 3 papers published in the following peer-reviewed journals in which I am listed as an author.

Part of chapter 1 is published as Tonanon, P.; Webster, R. D. Recent Electrode and Electrolyte Choices for Use in Small Scale Water Treatment Applications—A Short Review. *Current Opinion in Electrochemistry* **2023**, 38, 101211.

https://doi.org/10.1016/j.coelec.2023.101211.

The contributions of the co-authors are as follows:

- A/Prof Webster provided initial paper direction and edited the manuscript drafts.
- I prepared the manuscript drafts.

Part of chapter 3 is published as Tonanon, P.; Jalando-On Agpoon, K.; Webster, R. D. A Comparison of the Detection and Quantification of Praziquantel via Electrochemical and Gas Chromatography Methods in Freshwater and Saltwater Samples. *Analytical Methods* **2024**, 16 (9), 1323–1329.

https://doi.org/10.1039/D3AY01905E.

The contributions of the co-authors are as follows:

- A/Prof Webster provided the initial project direction and edited the manuscript drafts.
- I prepared the manuscript drafts. The manuscript was revised by Ms Agpoon
- I codesigned the study with A/Prof Webster and Ms Agpoon and performed electrochemical and GC-MS analysis at the School of Chemistry, Chemical Engineering, and Biotechnology.
- Ms Agpoon assisted in the experiment design and provided guidance in the interpretation of GC-MS data.

Part of chapter 5 is published as Tonanon P.; Webster, R. D. Probing the Molecular Interactions of Electrochemically Reduced Vitamin B_2 with CO_2. *The Journal of Physical Chemistry B* **2024** 128 (44), 10853-10860.

https://doi.org/10.1021/acs.jpcb.4c05952

The contributions of the co-authors are as follows:

- A/Prof Webster provided the initial project direction and edited the manuscript drafts.

- I prepared the manuscript drafts.
- I codesigned the study with A/Prof Webster, performed electrochemical and spectroscopic analysis at the School of Chemistry, Chemical Engineering, and Biotechnology.

January 2025

Date

Tonanon Panyawut

Acknowledgements

First and foremost, I am deeply grateful to my supervisor, Professor Richard D. Webster, for his invaluable guidance, unwavering support, and tireless encouragement throughout my doctoral journey. His expertise in electrochemistry has been instrumental in shaping my research. I am especially grateful for his patience and encouragement during challenging times and for fostering a stimulating intellectual environment that allowed me to grow as a researcher.

I also express my sincere appreciation to the members of my thesis advisory committee, Professor Yeow Kok Lee Edwin, and Professor Mihaiela Stuparu, for their insightful feedback and constructive criticism, which significantly strengthened this thesis.

This research was made possible by generous funding from the Singapore Agency for Science, Technology and Research and Nanyang Technological University. Their financial support allowed me to access essential resources and fully dedicate myself to my research endeavors.

I am indebted to my fellow lab mates Jing Song, Aisha, and Kendric for their camaraderie, intellectual stimulation, and countless hours of fruitful discussion. Their willingness to share their knowledge and experience has been a tremendous asset in my research.

I express my deepest gratitude to all participants who generously shared their time, experiences, and perspectives with me. I am also grateful to all my colleagues at Nanyang Technological University for their support and encouragement, especially Katherine Jalando-On Agpoon, Arvin Liangdy, and Haruethai Kongcharoen. Their contributions have been invaluable in shaping this research and enriching our understanding of electrochemistry.

Finally, I extend my heartfelt gratitude to my family, especially my parents, my sister, and my partner, Suchayada Mahavana, for their unconditional love, unwavering

belief in me, and constant encouragement, without which this journey would not have been possible.

Tonanon Panyawut, January 2025

Contents

List of Figures

List of Tables

List of Schemes

Abstract

This thesis explores novel applications of analytical electrochemistry in addressing environmental challenges and advancing pharmaceutical analysis, focusing on three main areas: water disinfection, pharmaceutical compound detection, and carbon dioxide capture and utilization.

In the first study, platinized titanium electrodes were investigated for their efficacy in inactivating *Escherichia coli* in water through electrochemical processes. The research elucidated the mechanisms underlying the disinfection process, particularly the generation and role of reactive oxygen species, demonstrating feasible rapid disinfection even at low electrolyte concentrations.

The second study developed and optimized methods for detecting and quantifying praziquantel, an important antiparasitic drug, in water samples. Two techniques were compared: gas chromatography-mass spectrometry (GC-MS) and voltammetry, both utilizing solid phase extraction for sample preparation. While GC-MS showed lower detection limits, the voltametric method demonstrated comparable accuracy and precision, offering a potentially more cost-effective and portable alternative for on-site testing.

The final study explored the electrochemistry of organic molecules, specifically quinones and flavins (vitamin B_2), for potential applications in carbon dioxide capture and energy storage. The research investigated the molecular interactions between reduced organic species and CO_2, as well as their electrochemical behavior under various conditions, providing insights into the development of novel carbon capture technologies and organic-based energy storage systems.

Throughout these investigations, the thesis demonstrates the versatility and power of analytical electrochemistry in addressing diverse challenges in environmental remediation, pharmaceutical analysis, and sustainable energy technologies. The research contributes to the advancement of electrochemical methods and their practical applications in these critical areas.

Chapter 1

Introduction

1.1 Background and Motivation

In an era marked by escalating environmental concerns, the field of analytical and physical chemistry has emerged as a critical discipline in identifying, quantifying, and understanding the complex pollutants that threaten our ecosystems. Electrochemistry, with its inherent versatility and potential for green remediation strategies, plays an increasingly pivotal role in addressing these challenges. By harnessing the power of electron transfer reactions, electrochemical techniques offer promising avenues to address diverse topics, ranging from environmental remediation, detection and quantification of pollutants/pharmaceutical compounds, and potentially limiting the environmental effects of CO_2 emissions leading to climate change. Three problems are specifically studied in this thesis:

- Potable water has always been an essential component in sustaining human life, yet globally today, millions of people still lack access to a reliable supply.
- The accurate detection and quantification of active pharmaceutical ingredients (APIs) represents critical aspects of analytical chemistry research, development, and quality control. Accurate API detection and quantification methods are essential in surveillance and regulatory compliance. In recent years, advancements in analytical techniques and instrumentation have led to more sophisticated and sensitive methods for API detection and quantification, contributing significantly to analytical chemistry research.
- The increase in atmospheric CO_2 levels due to continuing industrialization is contributing to climate change. Carbon capture and storage (CCS) is a way of reducing carbon dioxide emissions, which could be key to helping to tackle global climate change. Through the lens of electrochemistry, fundamental studies and applications could be applied as a unique approach toward CCS.

Electrochemical methods have emerged as a powerful toolkit for addressing environmental challenges due to their inherent sensitivity, selectivity, and versatility. This thesis explores the diverse applications of electrochemical methods in environmental analysis, ranging from the development of novel sensors for trace-level detection to the implementation of electrochemical remediation strategies for CO_2 in atmosphere.

While water treatment, pharmaceutical analysis, and CO_2 reduction may appear unrelated, these three topics share fundamental electrochemical principles that make them naturally complementary areas of study. All three applications rely on controlled electron transfer processes at electrode surfaces - in water treatment, these process generate reactive oxygen species for disinfection; in pharmaceutical analysis, they enable selective detection through characteristic oxidation or reduction potentials; and in CO_2 reduction, they facilitate the conversion of CO_2 through specific redox mediators. The development of understanding of electron transfer kinetics can benefit all three areas simultaneously. Moreover, these applications face similar practical challenges: the need for stable electrode materials, the influence of solution conditions and interfering species, and the requirement for scalable, cost-effective implementations. Advances in fundamental electrochemistry, such as improved understanding of surface process or proton-coupled electron transfer can therefore drive progress across all three domains. This thesis demonstrates how electrochemical expertise can be leveraged to address these seemingly distinct environmental challenges through a unified analytical and mechanistic approach.

1.2 Fundamentals of Electrochemical Systems

Electrochemistry is a branch of physical and analytical chemistry in which the electrochemical parameters are correlated to the chemical changes of the system under study. In potentiometry, the potential difference is measured between two electrodes when there is minimal current flow, which can be used to measure concentration changes of the analyte-of-interest. For coulometry, to determine the analyte concentration, a constant potential must be applied to the surface of the working electrode to either fully oxidize/reduce the target analyte or to ensure that the analyte has completely reacted with an intermediate reagent that has been electrochemically produced at the working electrode. Electrochemical reactions are heterogeneous in nature and occur in the region in the vicinity of an electrode (diffusion layer). Three steps are involved: mass transfer from the bulk to the electrode surface, heterogeneous electron transfer at the electrode surface, and mass transfer back to the bulk solution. Electrochemical techniques can be separated into two classes with respect to the bulk solution and diffusion layer: (a) techniques that attempt to change the composition of the bulk solution, and, (b)

techniques that are limited to the diffusion layer.[1] The first class is bulk electrolysis or coulometry, which requires a large ratio of electrode area to surface volume, and effective mass transfer is required. The second class is electroanalytical techniques that usually use small electrodes that do not result in alteration bulk concentration of the analyte. Examples of techniques in this class are cyclic voltammetry and square wave voltammetry. Descriptions of the three main electrochemical procedures used in this thesis (cyclic voltammetry, square-wave voltammetry and electrolysis methods) are discussed subsequently.

1.2.1 Cyclic Voltammetry

Cyclic voltammetry (CV) is a fundamental electrochemical technique that is used to study redox behavior of chemical species. It involves linearly sweeping the potential applied to a working electrode in a cycle (hence the name cyclic) and recording the resulting current. This generates characteristic current-potential curves, known as cyclic voltammograms, which reveal a wealth of information about thermodynamics and kinetics of electron transfer processes.

In a typical CV experiment, the potential is linearly swept from an initial value (E_0) to a switching potential (E_1) and then back to E_0 in a sawtooth waveform (right-hand pane in Figure 1.1). This cycle can be repeated as needed, with the scan rate ($\mathrm{V\,s^{-1}}$) determining how quickly the potential changes.

The left-hand pane in Figure 1.1 shows the CV for the oxidation of ferrocene (Fc), while the right-hand pane shows applied potential and resulting current. During the forward scan, as the potential approaches the formal potential of the analyte (E_0^f), the anodic current increases due to the oxidation of the ferrocene that exits in its natural uncharged reduced (Red) state. This current eventually peaks and then decreases as Red is depleted near the electrode surface. Upon reversing the scan, a cathodic current emerges as the oxidized ferrocene (Ox) is reduced, peaking and then decaying as Ox is consumed. The resulting current-potential plot, the cyclic voltammogram, provides valuable insights into the electrochemical behavior of the analyte.[2]

For chemically and electrochemically reversible redox couples with fast electron transfer kinetics, the voltammogram displays symmetrical anodic and cathodic peaks,

with the peak current i_p directly proportional to the analyte concentration and the square root of the scan rate, as described by the Randles-Sevcik equation ((1.1)). However, chemically irreversible reactions, where the oxidized or reduced species undergoes further chemical transformations on the timescale of the voltametric scan, result in asymmetric voltammograms with altered peak shapes and positions. Analysis of the peak shapes with the aid of digital modelling such as with the commercial software, DigiElch, can be used to determine thermodynamic and kinetic parameters associated with the homogeneous reactions following electron transfer.

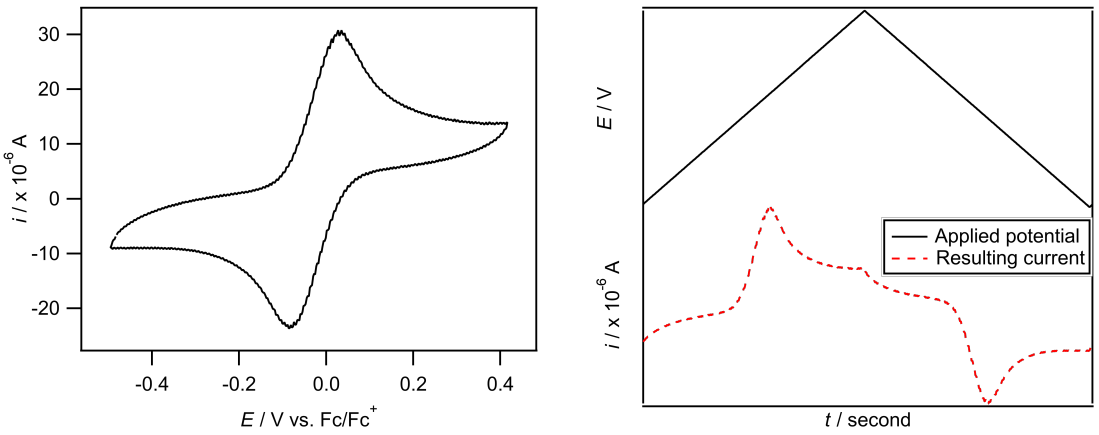

FIGURE 1.1: (Left) Cyclic voltammogram of 1 mM Ferrocene in 0.5 M nBu_4NPF_6 in MeCN. (Right) (Solid black line) applied potential, and (Dashed red line) resulting current from the same cyclic voltammogram.

EQUATION 1.1: Randles-Sevcik equation

$$i_p = 0.4463nFAC\left(\frac{nFvD}{RT}\right)^{\frac{1}{2}} \tag{1.1}$$

where i_p = current maximum in A; n = number of electrons transferred in the redox event; A = electrode surface area in cm^2; F = Faraday constant in $C\,mol^{-1}$; D = diffusion coefficient in $cm^2\,s^{-1}$; v = scan rate in $V\,s^{-1}$; R = Gas constant in $J\,K^{-1}\,mol^{-1}$; and T = temperature in K.

1.2.2 Square Wave Voltammetry

Square wave voltammetry (SWV), invented by G. C. Barker and A. W. Gardner, is an advanced pulse voltammetry technique designed to enhance detection capabilities by minimizing capacitive background current and maximizing the signal-to-noise

ratio.[3] It achieves this by superimposing a square wave onto a staircase potential waveform applied to the working electrode. Figure 1.2 (right-hand pane) illustrates the combined applied potential (solid black line) as a result of a combination between square potential (dashed red line) and staircase potential (dashed blue line). This unique waveform subjects the electrode to alternating forward and reverse potential pulses at each step of the staircase.

SWV measures current twice during each pulse: once at the end of the forward pulse and again at the end of the reverse pulse. The current difference between these two measurements is then plotted against the staircase potential, effectively eliminating capacitive current and isolating the faradaic current, which is directly related to the analyte's redox reactions. This approach significantly improves sensitivity and allows for faster scan rates compared to traditional differential pulse voltammetry.[4] The recording at the forward pulse (dashed red line) and backward pulse (dashed blue line) can be seen in Figure 1.2 (left-hand pane), while the resulting current (δ current, solid black line), can be seen in the same figure.

The resulting square wave voltammogram provides valuable information about the analyte. The peak potential corresponds to the formal potential of the analyte, the peak height is directly proportional to its concentration, and the peak width offers insights into the reversibility of the electron transfer process. By analyzing these parameters, SWV enables both qualitative identification and quantitative determination of electroactive species in a solution. Square wave voltammetry has various applications, ranging from biological systems (human blood serum,[5] flavonoids in human urine[6]), to industrial uses (SB-14 in fuel samples).[7]

1.2.3 Electrolysis

Contrary to techniques focused on analyzing reactions that occur only at the electrode surface within the diffusion layer (resulting in minimal loss of the analyte from solution), coulometry, specifically controlled potential electrolysis (CPE), measures the charge passing between two electrodes that are used to completely oxidize or reduce a target compound. This enables solutions prepared by bulk electrolysis to be used for subsequent isolation of electrolyzed products for characterization or further experimentation. CPE can be performed in two-electrode (working and counter) or three-electrode (working, auxiliary and reference) mode. Three electrode mode

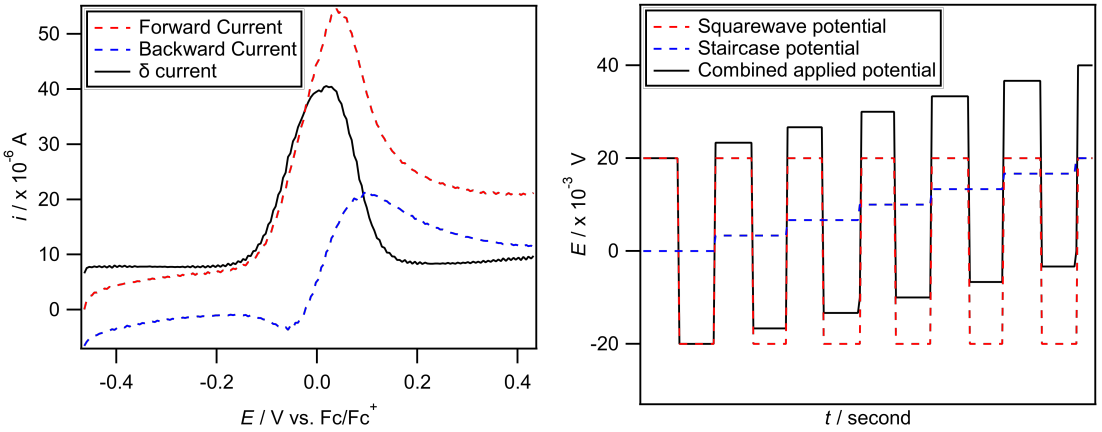

FIGURE 1.2: (Left) Separated forward (dashed red line), backward (dashed blue line) and delta current (solid black line) of 1 mM ferrocene in 0.5 M nBu_4NPF_6 in MeCN. (Right) Separated square potential (dashed red line), staircase potential (dashed blue line) and combined applied potential (solid black line) of the same experiment.

helps considerably with reducing the effects of solution resistance but requires an expensive potentiostat, while two-electrode mode is usually preferred if performing experiments on a large scale where very high currents are needed, and a simpler DC power supply can be used. In this study, experiments were conducted in both two-electrode and three-electrode mode depending on the required data.

CPE can be used to determine the number of electrons transferred during a redox reaction and scaled up for the production of oxidized or reduced products. Large surface area working electrodes, such as meshes or cylinders, are often used to expedite the electrolysis process. Inert gas bubbling, such as nitrogen or argon, deoxygenates the solution and facilitates mass transfer of products away from the electrode, ensuring faster electrolysis.

Cyclic voltammetry (CV) usually precedes CPE to identify the peak potential of the analyte to so that the required applied potential can be identified. During CPE, a potential 100-200 mV more positive (for oxidation) or negative (for reduction) than this peak is applied. The recorded current-time plot decays until negligible, indicating exhaustive electrolysis. Integrating this plot with respect to time yields the total charge transferred, revealing the number of electrons involved in the redox reaction.

Figure 1.3 shows an example of the CPE process by plotting the graph of current over time (solid black line), and the resultant integrated charge (dashed red line).

This figure was obtained from an experiment in chapter 4.

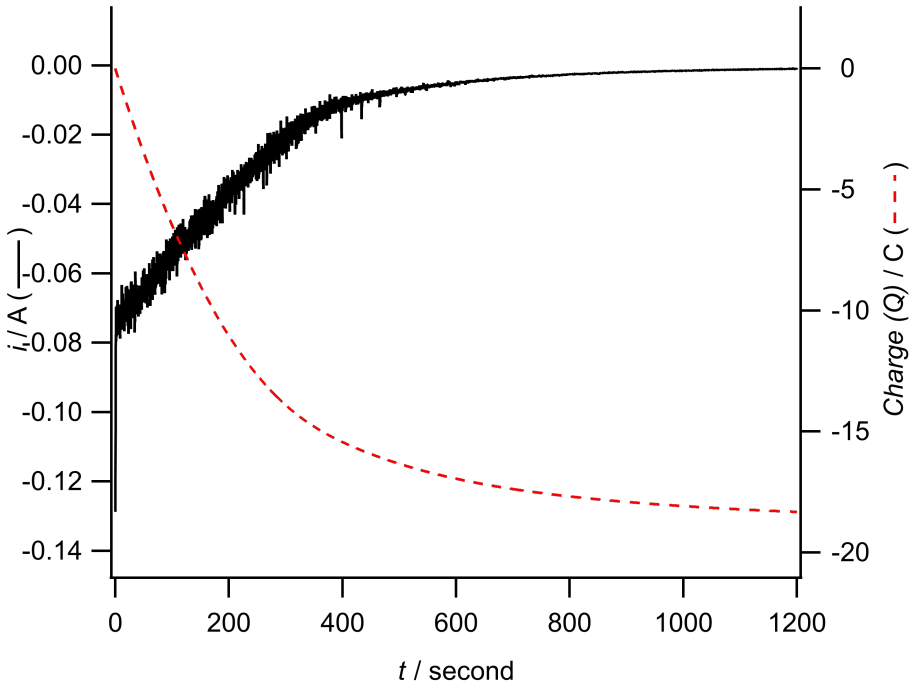

FIGURE 1.3: (solid black line) example plots of resulting current from CPE experiments, and (dashed red line) integrated charge resulting from the same experiment.

1.3 Electrochemical Water Treatment

Potable water has always been an essential component in sustaining human life, yet globally today, millions of people still lack access to a reliable supply.[8] The United Nations, seeing the importance of water to universal prosperity, established the mission to ensure availability and sustainable management of water and sanitation for all as the Sustainable Development Goal (SDG) number 6, under the broader overarching 17 SDGs that are intended to be achieved by the year 2030. The purpose is to alleviate the rapid degradation of accessible water due to extensive use and reducing supplies due to global climate change. Should there be no extensive collaborative effort to address the issue, a considerable fraction of the global population will experience water scarcity problems. Though the target year is approaching, there are still many countries and regions exhibiting difficulties in reaching these goals.[9]

Even worse, the rapid rate of global climate change has magnified droughts in both frequency and severity, putting pressure on securing water supplies. Take as an example Sub-Saharan Africa; during 2000-2015, only 57.6% of the total population had access to basic drinking water services (compared to 90.6% for North Africa and Western Asia), and 28.1% for basic sanitation (compared to 86.1% in North Africa and Western Asia).[8,9] Though progress has been made since 2015 to secure water access in the Sub-Saharan Africa region, global climate change has reduced the percentage of the population with water access.[10] Efforts to secure water access in this region, as with other regions, is partly to treat used and naturally accessible water – grey water – to become drinkable water

Electrochemistry, particularly electrolysis, has the ability to function as a water purifying process, either through directly killing microorganisms via the applied electric fields or by generating chemical species that kills pathogens. There have been a number of recent developments in novel electrode materials and reagents that can potentially be used in electrochemically based water treatment devices. It is envisioned that the devices would be for small scale applications using natural source waters in remote locations that have limited chemical contamination but with likely biological contamination from animal sources such as livestock or wild animals, rather than full-scale industrial applications where existing membrane-based solutions have cost and energy advantages.

Some major contaminants in surface water involves biological and chemical contamination, including but not limited to, *Escherichia coli* (*E. coli*), *Giardia*, *Cryptosporidium*, viruses, pesticides, synthetic and pharmaceutical compounds, heavy metals, and metalloids. Many systems and technologies have been developed to remove these contaminants that differ in scale and complexity. A significant problem in providing the entire global population with clean drinking water (in addition to water shortages) lies in the difficulty in establishing large scale water treatment systems in remote regions. Distances and lack of the required infrastructure make creating high volume efficient water treatment plants not viable, thus smaller scale systems employing the necessary technologies for onsite treatment are suggested as a replacement in remote communities. These facilities are usually stand-alone with no connection or back up to a water grid and are small in scale, which comes with their own set of challenges. Contrary to the traditional primary treatment processes, electrochemical technologies are more compact and convenient, and are

an interesting alternative to be explored. In this section, advances in electrode materials and co-chemical reagents that may be used in possible future decentralized water treatment systems are discussed.

1.3.1 Challenges associated with decentralized small-scale water treatment

Considering the scale of water treatment, the size and the complexity of such systems can be used as a general guideline to separate between a small scale (aiming for the point-of-use) versus a large scale (industrial, centralized) system. The difference, and the limitation preventing the transition between small scale and large scale, lies in the scalability (or the lack thereof) of various technologies employed in each construction. For small scale low volume systems, conventional technologies rely on passive treatment processes without external energy or chemicals added into the system. These conventional technologies are precipitation, and filtration. Since without energy or chemicals, these systems are useful in treating relatively clean natural water to non-potable applications such as washing. However, for large scale treatment with more stringent matrix requirements, the filtration processes become more complicated, partly because the time requirement necessitates that the purification occurs much more quickly compared with the small-scale system. A typical public water treatment system starts from coagulation and flocculation, sedimentation, filtration, disinfection, adsorption on biologically activated carbon, to chemical treatment. Though lengthy, these steps are necessary to meet the standard of potable water. The challenges that are faced for small-scale remote purification processes include the availability of resources, energy requirements[11] and degradation in water quality if some of the steps are missed.[12] There is a current research gap on producing potable water with stringent quality requirements while maintaining a small footprint with limited energy and resources required.[11,13]

Aiming to address the challenges of potable water production with a small footprint, electrochemical methods for water treatment have been receiving interest in recent years. By passing current to water, electrochemical methods can trigger a cascade destruction of pathogens and chemical contaminants, providing water treatment without requiring reactive supplementary chemicals or elevated pressures. Considering that electrochemical treatment systems can overcome the mentioned limitations,

the continuing investigation of electrochemical water treatment techniques, and ultimately the development of small-scale treatment devices are worthwhile endeavors. Nevertheless, electrochemical methods for water treatment still cope with serious engineering challenges[14–17] such as fouling, power control requirements, robustness to operate in all water characteristics, and geometry and spatial placement considerations for the electrodes. The following sections present two approaches toward pathogen/pollutant mitigation, either through direct water oxidation, or with the help of added chemicals.

1.3.1.1 Organic contaminant decomposition through electrochemical advanced water oxidation

Using electrochemical techniques, organic contaminant decomposition is typically achieved through cascade radicalization, a process whereby contaminants are decomposed through destructive oxidation with $OH^{\bullet}$.[18] Several reviews in recent years have focused on this field, ranging from choice of anode material,[19] mechanisms,[20] or substrate scope (e.g., antibiotics,[17,21] dyes,[22] or pesticides).[23] The greatest degree of decontamination is achieved by generating as many $OH^{\bullet}$ as possible, either catalytically or directly.

This procedure, named electrochemical advanced oxidation process (EAOP) can be divided into two broad categories depending on the mechanism of radical generation: anodic oxidation (AO) and electro-Fenton (EF). For AO, $OH^{\bullet}$ radicals are generated directly through water oxidation, whilst the electro-Fenton process generates $OH^{\bullet}$ radicals using the Fe^{2+}/Fe^{3+} redox pair as a catalyst.[16] The EF process shows better decontamination properties than direct water oxidation. However, the EF process suffers from a low pH requirement, the presence of the catalyst and the high cost of oxidant, and sludge generation, preventing it from being adopted at a scale necessary for decentralized water treatment.[16,24–27] AO, on the other hand, is a cleaner process, though limited by lower decontamination efficiency. The water oxidation process can be divided into two approaches based on the definition by Comninellis, depending on whether the electrode material actively participates on the oxidation processes or not: active anodes which suffer from a constant replacement requirement, and non-active anodes, which are more robust.[14,28,29]

1.3.1.2 Pathogens disinfection through in-situ electrochemical generation of disinfectants

The drawback of direct oxidation is that the decontamination is limited to the electrode diffusion layer, since $OH^{\bullet}$ have a very limited lifetimes;[20] hence electrochemical generation of other disinfectants can increase the degree of oxidation degradation reactions. Therefore, the aim of adding chemicals is to help with decontamination and disinfection, where $OH^{\bullet}$ fall short. There is a long history of how electrochemical disinfection works and it can be achieved in many ways, including by direct oxidation, the addition of oxidizable chemicals, and integrating photoelectrocatalytic systems.[30–32] In addition, electrochemical generation of disinfectants aids in mitigating backcontamination of treated water by allowing the generation of trace amounts of disinfectants, especially useful in growing concern over current and future pandemics. This allows a similar approach to swimming pool water disinfection where only trace amounts of chlorine and chlorine dioxide need to be present in the pool water to prevent new pathogen contamination.

1.3.2 Critical evaluation of electrochemical water treatment approaches

Despite the significant advantages offered by electrochemical water treatment over conventional methods, several fundamental challenges warrant critical examination. These limitations not only affect current applications but also guide future research directions in the field.

1.3.2.1 Material and Design Constraints

Choosing electrode materials involves a critical balance between performance and cost. Although noble metal electrodes, such as platinum, offer excellent activity and stability, their high expense significantly hampers large-scale application.[33,34] On the other hand, alternative materials like metal oxides and carbon-based electrodes frequently experience decreased stability over extended use, slower electron transfer rates, and varied performance in diverse water conditions.[35] These challenges underscore an important research opportunity to develop economical materials that uphold high performance levels.[36]

1.3.2.2 Operational Challenges

There are numerous challenges when it comes to practical implementation, including the suboptimal energy efficiency caused by high overpotentials needed for water oxidation, mass transport limitations that greatly reduce treatment efficiency at larger scales, and the impact of variable water composition on the stability and efficacy of the process.[15–17] Moreover, current research lacks comprehensive solutions for integrating these systems with renewable energy sources, especially in remote applications where grid electricity might be unreliable or inaccessible.

1.3.2.3 Performance Assessment

Evaluating treatment effectiveness presents distinct obstacles, including the lack of standardized testing protocols, which hinders direct comparisons between different techniques. Furthermore, there is a limited understanding of how different oxidative species interact during treatment, and insufficient long-term performance data under real-world conditions complicates evaluations. For instance, the conductivity of water, influenced by the supporting electrolyte, impacts both the generation of reactive species and consequently the efficacy of water treatment. Variations in experimental setup and the amount of supporting electrolyte used make it challenging to compare results in existing literature reports.[14] These gaps highlight the need for more comprehensive validation studies across a variety of operating conditions.

1.4 Electrochemical detection and quantification of praziquantel

1.4.1 Introduction to praziquantel

Praziquantel (PZQ), a synthetic anthelmintic drug discovered by Bayer in the 1970s, is a cornerstone in treating schistosomiasis and various cestode and trematode infections.[37] Its broad-spectrum efficacy and tolerability in diverse patient populations underscore its significance in both human and veterinary medicine.[38,39]

While the exact mechanism of action remains elusive, the prevailing hypothesis suggests multiple pharmacological targets synergizing to exert detrimental effects on parasites.[39] PZQ is a stable crystalline powder, practically insoluble in water but soluble in organic solvents.[40] Notably, PZQ exhibits low toxicity in animal studies, further solidifying its safety profile.[41,42] The drug's widespread use, particularly in aquaculture, necessitates robust analytical methods for its detection and quantification in complex environmental matrices. Monitoring PZQ levels in water sources is crucial due to its potential impact on aquatic life, making the development of sensitive and reliable analytical techniques a pivotal endeavor for environmental research and protection.

1.4.2 Various detection methods of praziquantel

The precise detection and measurement of active pharmaceutical ingredients (APIs), including PZQ, are crucial components of analytical chemistry research, development, and quality control. Reliable API detection and quantification methods play a vital role in monitoring and ensuring compliance with regulations. Recent progress in analytical techniques and instrumentation has resulted in the development of more advanced and sensitive methods for API detection and quantification, making significant contributions to analytical chemistry research. Various review articles have addressed the different approaches to API detection.[43–50]

High Performance Liquid Chromatography (HPLC) is one of the most widely used techniques for PZQ detection.[51,52] This method offers high sensitivity, selectivity, and reproducibility, making it suitable for both qualitative and quantitative analysis. Another chromatographic technique, Liquid Chromatography with Tandem Mass Spectrometry (LC-MS/MS), has gained popularity due to its enhanced specificity and ability to detect trace amounts of PZQ in complex matrices.[53,54]

Spectroscopic methods, such as Near Infrared Spectroscopy (NIS), have also been employed for PZQ detection.[55] NIS is a non-destructive technique that allows for rapid and cost-effective analysis, making it suitable for high-throughput screening and on-site testing.

Capillary Electrophoresis (CE) is another technique that has been used for PZQ detection.[56] CE offers high resolution, fast analysis times, and requires small sample volumes, making it an attractive option for certain applications.

Electrochemical methods have emerged as promising alternatives to chromatographic and spectroscopic techniques. These methods offer good sensitivity, simpler instrumentation, and the potential for portable and on-site analysis. However, electrochemical methods may be more susceptible to interference from complex sample matrices compared to chromatographic methods.

1.4.3 Previous electrochemical and chemical studies on praziquantel

Electrochemical methods have emerged as promising techniques for the detection and quantification of praziquantel (PZQ) in various matrices. The electrochemistry of PZQ in aqueous solution was first investigated by Rizk et al. using a dropping mercury electrode under basic conditions.[57] They proposed that PZQ underwent reduction at the carbonyl group and successfully applied this method to analyze spiked human urine and blood plasma without pretreatment, obtaining nearly identical recoveries. In another study, Ghoneim, Mabrouk, and Tawfik observed a single 2-electron irreversible reduction wave of PZQ in acidic aqueous conditions.[58] Based on this finding, they developed a voltametric procedure using cathodic adsorptive stripping differential-pulse voltammetry on a hanging mercury drop electrode.

An alternative approach was proposed by Radia and Hassanein, who suggested the indirect determination of praziquantel through nitration to produce more electroactive nitro-praziquantel derivatives.[59] This method also relied on the adsorptive properties of a hanging mercury drop electrode and employed differential-pulse techniques. However, despite the development of various voltametric detection methods for PZQ determination, the use of hanging mercury drop electrodes has largely been phased out due to safety and environmental concerns associated with mercury use.

As the field of analytical chemistry continues to evolve, there is a growing need for safer, more environmentally friendly, and sensitive electrochemical methods for

PZQ detection. The development of mercury-free electrodes and novel voltametric techniques could provide new opportunities for the accurate and reliable quantification of PZQ in complex matrices, contributing to advancements in pharmaceutical analysis, environmental monitoring, and public health.

1.4.4 Comparative analysis of detection methods

The detection and quantification of pharmaceutical compounds in environmental matrices present unique analytical challenges that have led to the development of various complementary approaches. Each method offers distinct advantages while facing specific limitations.

1.4.4.1 Chromatographic Techniques

Traditional chromatographic techniques are still considered the benchmark for pharmaceutical analysis, yet they encounter several challenges: substantial upfront investment and ongoing expenses, intricate sample preparation needs, limited portability and use in the field, and the necessity for considerable expertise for both operation and upkeep.[60,61] Despite their remarkable sensitivity and selectivity, their use in routine monitoring situations proves to be difficult.

1.4.4.2 Electrochemical Methods

Electrochemical detection techniques offer promising alternatives but require diligent consideration of factors such as matrix effects and interfering substances, electrode fouling and degradation, variable performance across different sample types, and decreased selectivity compared to chromatographic methods. Advantages of electrochemical techniques involve compact apparatus and reduced costs. Applications in this domain include the detection of heavy metals,[62] pesticides,[23] and active pharmaceutical ingredients.[63] These advantages make them pertinent for on-site and routine monitoring. Current research challenges involve developing more selectively tailored electrodes and improving stability in complex sample matrices. Key topics that warrant additional inquiry include: Establishment of solid sample preparation strategies, Combination of various detection techniques to enhance dependability,

Verification across a range of environmental matrices, and Improvement of detection thresholds while preserving the simplicity of the method.

1.5 Electrochemical CO_2 reduction

1.5.1 Electrochemical approaches to CO_2 reduction

The relentless rise in atmospheric carbon dioxide (CO_2) levels over the past century has emerged as one of the most pressing environmental challenges of our time, driving global climate change and posing unprecedented threats to ecosystems, human health, and socioeconomic stability worldwide. This increase in CO_2 concentration is primarily attributed to human activities, particularly the burning of fossil fuels, solid waste, and biomass, as well as certain industrial chemical reactions. As economic activity grows, it introduces significant changes to the global carbon cycle, adding more CO_2 to the atmosphere while simultaneously affecting the capacity of natural carbon sinks, such as forests. Although CO_2 can be naturally removed from the atmosphere through plant absorption as part of the carbon life cycle, increased economic activity coupled with deforestation and changing land use patterns have compromised the Earth's natural ability to sequester carbon.

As of June 2024, atmospheric CO_2 concentrations have surpassed 420 ppm, a level unprecedented in recent geological history.[64] The strong correlation between human greenhouse gas emissions and rising global average temperatures underscores the urgent need for action (Figure 1.4). This alarming trend not only disrupts ecosystems and weather patterns but also threatens food security, water resources, and human health on a global scale, making the mitigation of CO_2 emissions and the development of effective carbon capture and utilization technologies critical priorities for scientific research and policy interventions.

In response to this critical challenge, the international community has established a series of treaties and agreements aimed at reducing CO_2 emissions and combating climate change. These range from the 1979 Geneva Convention on long-distance cross-border air pollution to more recent and comprehensive accords such as the 1997 Kyoto Protocol, the 2012 Doha Amendment, and the 2015 Paris Agreement.

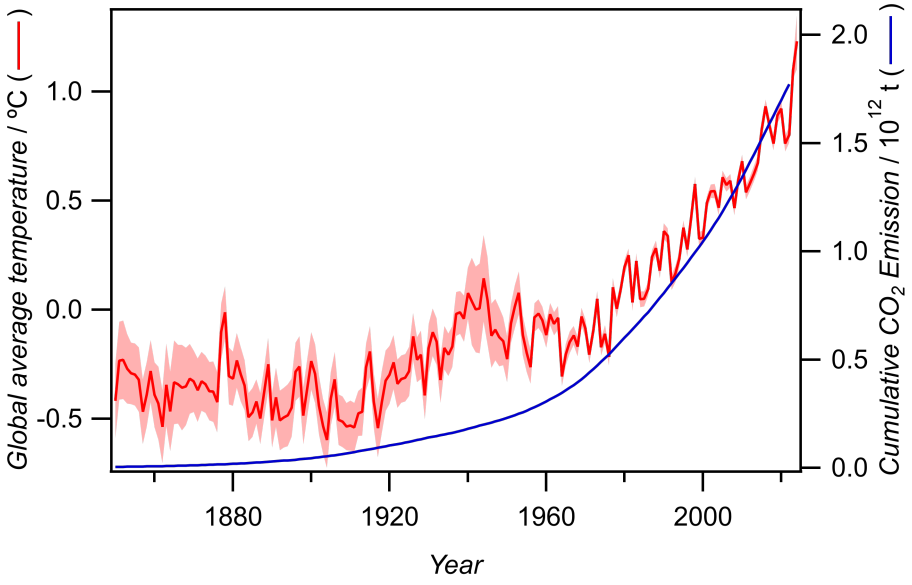

FIGURE 1.4: Global average land-sea temperature anomaly relative to the 1961-1990 average temperature,[65] and cumulative CO2 emissions[66,67] versus time.

The Kyoto Protocol, adopted in 1997 and implemented in 2005, was a landmark agreement that obliged participating countries to reduce their greenhouse gas emissions based on scientific consensus. It recognized the principle of common but differentiated responsibilities, acknowledging that developed countries bear a greater historical responsibility for current greenhouse gas concentrations.[68]

Building on the Kyoto Protocol, the Paris Agreement of 2015 represents the most recent and ambitious global effort to address climate change. As of April 2018, 175 countries had ratified this agreement, which aims to limit global temperature rise to well below 2 °C above pre-industrial levels, with efforts to limit the increase to 1.5 °C. The Paris Agreement requires all parties to put forward their best efforts through "nationally determined contributions" (NDCs) and to strengthen these efforts in the years ahead.[69]

These international agreements underscore the urgent need for coordinated global action to mitigate CO_2 emissions and reduce atmospheric CO_2 levels. They provide a framework for countries to work together in addressing this critical challenge, emphasizing the importance of both developed and developing nations in contributing to climate change mitigation efforts.

To limit global temperature rising below 2 °C, immediate curtailment of industrial emissions along with direct air capture strategies are required.

Current state-of-the-art CO_2 capture technology is the thermal swing adsorption process, which uses an aqueous base to selectively absorb CO_2 from the industrial waste stream followed by thermal stripping to release CO_2 for further sequestration.[70] This process is limited by Carnot efficiency and requires a substantial amount of thermal energy for stripping, making it inefficient and costly.[70]

Electrochemical CO_2 direct-air-capture (DAC) has emerged as a promising approach to address the urgent challenge of reducing atmospheric CO_2 levels. This technology offers a potential solution by directly extracting CO_2 from ambient air or diluted sources, providing a versatile and scalable method to combat climate change.

The primary goal of electrochemical DAC is to selectively capture CO_2 from the complex mixture of gases in the atmosphere and produce a concentrated stream of high-purity CO_2. This captured CO_2 can then be safely stored underground or utilized in various industrial processes, effectively closing the carbon cycle.

Electrochemical methods for CO_2 capture are particularly attractive due to their ability to efficiently utilize renewable electricity and their adaptable designs for easy integration into existing systems. These techniques can potentially be combined with electrochemical valorization processes to create compounds for liquid fuels, offering exciting possibilities for sectors like aviation and automotive industries.

The development of electrochemical DAC technologies could lead to the creation of CO_2 capture devices for use in vehicles and commercial aircraft, significantly reducing emissions from these hard-to-decarbonize sectors. However, the effectiveness of these systems in mitigating climate change will depend heavily on the availability of clean energy sources to power them.

An example of industrial scale DAC is by the Swiss company Climeworks, which commenced the largest DAC facility in Iceland,[71] based on the CO_2 capture via solid amine-containing compounds, then injecting them underground toward basaltic rock for mineralization with calcium, magnesium, and iron compounds to create solid carbonate materials.[72]

As DAC technologies continue to advance, they have the potential to play a crucial role in achieving climate goals, complementing other carbon reduction strategies and negative emissions technologies. By directly addressing the issue of atmospheric

CO_2 concentrations, electrochemical DAC offers a powerful tool in the global effort to combat climate change and transition towards a more sustainable future.

Addressing these challenges requires removing CO_2 from the atmosphere or mitigating point source emissions through the separation and concentration of CO_2 from diluted sources. This requires a reduction in energetic and monetary costs of DAC technologies relative to traditional thermal and pressure swing methods.

1.5.2 Electrochemical CO_2 binding mechanisms and reduction pathways

Electrochemical CO_2 direct air capture is an emerging technology that aims to extract CO_2 from dilute gas mixtures, including ambient air. This process utilizes redox-active systems to produce a pure CO_2 stream, offering potential advantages over traditional capture methods. Electrochemical processes have been described that can operate with the full range of source concentrations (0.04% from air to flue gas concentrations near 15%). Electrochemical methods fall under two general classes of separations: direct processes where a sorbent is reduced or oxidized to modulate CO_2 binding affinity, and indirect processes, where electrochemistry acts on a secondary aspect of the system to modulate sorbent affinity for CO_2.[73] Figure 1.5 illustrates this direct process in four steps: Sorbent activation through oxidation or reduction, CO_2(g) capture on the activated sorbent, sorbent deactivation through the reverse electrochemical process, CO_2(g) release.

Several classes of compounds have been investigated as catalysts for electrochemical CO_2 DAC. Quinones, derived from aromatic compounds, have garnered significant attention due to their strong CO_2 binding affinity in their reduced form. Examples include 9,10-phenanthrenequinone, 2,6-di-tert-butyl-1,4-benzoquinone (DTBQ), and 1,4-naphthoquinone (1,4-NQ). Other promising catalysts include bipyridines,[74] which can form stable radical anion CO_2 adducts, and sulphur-containing compounds like benzyl disulfide (BDS),[75] which form thiolate anions capable of reacting with CO_2. The organic systems listed above are shown in Scheme 1.1 and a detailed discussion pertaining those system containing quinones will be discussed in detail in Section 1.5.3. Transition metal complexes, particularly binuclear complexes of nickel and copper with amino and pyridyl ligands, have also shown potential for CO_2 capture and release through M^{2+}/M^{+} redox reactions,[76] although in this thesis

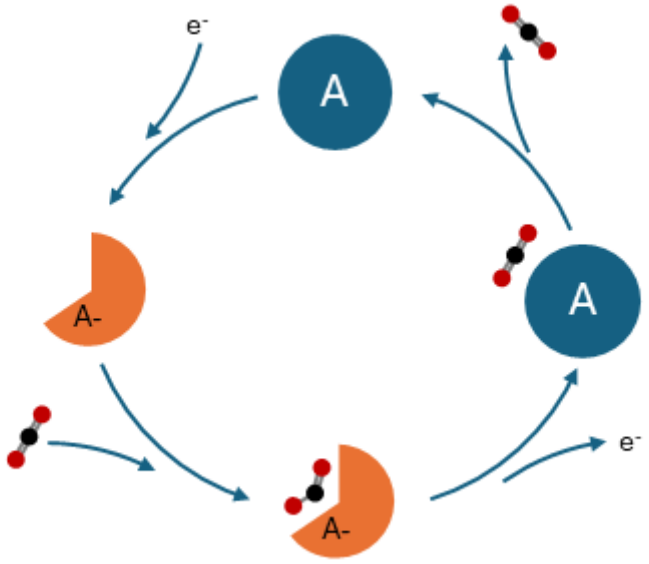

FIGURE 1.5: Illustration of the direct process where a sorbent is reduced or oxidized to modulate CO2 binding affinity.

work is concentrated on organic systems. Despite its promise, electrochemical CO_2 DAC faces several challenges that require further research and development, which are discussed in the following sections below.

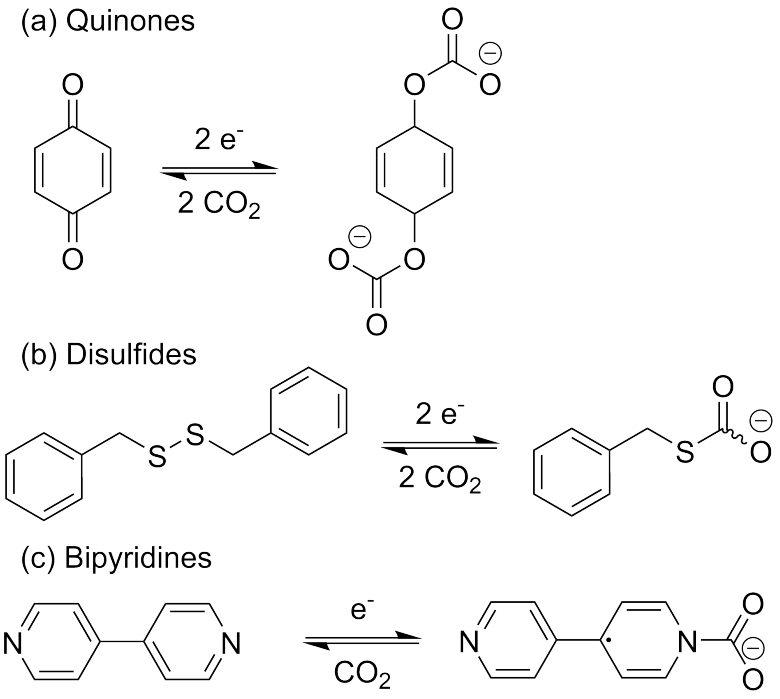

SCHEME 1.1: Examples of organic system capable of capturing CO_2 through electrochemical CO_2 capture process.

1.5.2.1 Redox potential landscape

The selection of appropriate redox-active molecules is crucial and challenging. These molecules must have reversible redox-active sites, significant changes in CO_2 binding affinity between oxidized and reduced states, and high selectivity for CO_2. The redox potentials of current molecules span from approximately -0.4 to -1.4 V versus the standard hydrogen electrode (SHE). This presents several issues: a) Many of these potentials necessitate non-aqueous media to avoid the water reduction window, limiting the choice of electrolytes. b) More negative reduction potentials, while offering higher CO_2 affinities, also increase the risk of parasitic reactions with trace water and especially oxygen. c) There is a need to decouple CO_2 binding affinities from O_2 reactivity for practical separation systems.

1.5.2.2 Energy efficiency

The energy requirements for the redox reactions and overall process efficiency are significantly challenging: a) The correlation between more negative reduction potentials and higher CO_2 affinities means that more energy-intensive processes often yield better capture performance. b) Parasitic reactions, especially with oxygen, can significantly reduce the Faradaic efficiency of the process. c) The energy input for the electrochemically induced reversible binding must be optimized to make the process competitive with other CO_2 capture technologies.

1.5.2.3 Scalability

Scaling up electrochemical CO_2 DAC systems from laboratory to industrial scale faces several hurdles: a) The need for specialized non-aqueous electrolytes or ionic liquids may pose challenges for large-scale operations. b) Electrode design and cell architecture must be optimized for efficient mass transfer in large-scale systems. c) The stability and longevity of redox-active molecules over many cycles need to be ensured for continuous operation.

1.5.2.4 Economic viability

The economic feasibility of electrochemical CO_2 DAC is a significant challenge: a) The cost of specialized redox-active molecules and electrolytes may be prohibitive for large-scale deployment. b) The energy costs associated with the electrochemical process must be balanced against the value of captured CO_2 or environmental benefits. c) Competition with other CO_2 capture technologies and the need for supportive policies or carbon pricing mechanisms to make the process economically attractive.

1.5.2.5 Selectivity and contaminant handling

The presence of other gases and contaminants in air poses challenges: a) The redox-active molecules must maintain high selectivity for CO_2 in the presence of other atmospheric gases. b) Strategies are needed to handle or mitigate the effects of trace contaminants that may interfere with the capture process or degrade the capture materials over time.

1.5.2.6 System integrations and process design

Developing a complete, integrated system involves several challenges: a) Balancing the electrochemical capture process with subsequent steps for CO_2 concentration, purification, and utilization or storage. b) Designing systems that can handle the intermittent nature of renewable energy sources if the process is to be powered by clean electricity. c) Optimizing the overall process flow, including electrolyte management and CO_2 release mechanisms.

Addressing these challenges requires interdisciplinary research efforts, combining advances in materials science, electrochemistry, process engineering, and system design. Future developments in molecular design, electrolyte formulation, and cell architecture will be crucial in overcoming these obstacles and making electrochemical CO_2 DAC a viable technology for large-scale carbon dioxide removal from the atmosphere.

1.5.3 Quinones as redox-active molecule for CO_2 capture

Literature reports have shown that quinones in their reduced forms can undergo supramolecular bonding with carbon dioxide (CO_2) leading to substantial changes in their formal reduction potentials (E_f^0) compared to those observed under inert Ar of N_2 atmospheres.[77] This binding relationship between quinone and CO_2 has been proposed for utilization for CO_2 capture and concentration.[78–84] Electrochemical methods for carbon dioxide capture and concentration have gained significant interest as alternatives to traditional thermal swing processes. Among these, systems utilizing redox-active quinone molecules as CO_2 binding agents have shown promise. Several studies have investigated the electrochemistry and CO_2 binding properties of various quinone structures to optimize their performance as capture agents.

Mizen and Wrighton (1989) conducted a seminal study on the electrochemical reduction of 9,10-phenanthrenequinone (PAQ) in the presence of CO_2.[85] Using cyclic voltammetry, they observed that PAQ undergoes two reversible one-electron reductions in acetonitrile without CO_2. However, in the presence of CO_2, a larger cathodic current was observed, suggesting a change from a one-electron to a two-electron process. Through UV-vis and IR spectroelectrochemistry, they determined that two moles of CO_2 were consumed per mole of PAQ reacted, forming a bis(carbonate) adduct $[\mathrm{PAQ} \cdot 2\,\mathrm{CO_2}]^{2-}$. The authors proposed an ECEC (electrochemical-chemical-electrochemical-chemical) mechanism for this process, with initial one-electron reduction of PAQ followed by CO_2 addition, a second one-electron reduction, and addition of a second CO_2 molecule. Importantly, they demonstrated that oxidation of the CO_2 adducts resulted in quantitative regeneration of PAQ and CO_2, establishing the chemical reversibility of the system.

Building on this work, Simpson and Durand (1990) expanded the investigation to various quinones including benzoquinone (BQ), anthraquinone (AQ), naphthoquinone (NQ), duroquinone (DQ), and 2,6-dimethylbenzoquinone (DMQ) in dimethyl sulfoxide (DMSO).[77] They observed similar electrochemical behavior across all studied quinones in the presence of CO_2, characterized by a shift in the second reduction wave to more positive potentials, resulting in a single irreversible two-electron wave. This behavior further supported the ECE mechanism proposed by Mizen and Wrighton.[85] Using rotating disk voltammetry, they determined second-order rate constants for the reaction of quinones with CO_2, finding them to be in the order of

10^2 to 10^3 M^{-1} s^{-1}. Notably, they observed a correlation between the reduction potential of the quinones (as an indicator of nucleophilicity) and their reaction rate with CO_2, suggesting that the nucleophilicity of the reduced quinones plays a role in their reactivity towards CO_2.

Scovazzo et al. (2003) took these fundamental studies a step further by demonstrating the practical application of quinones for electrochemical CO_2 separation and concentration.[86] Using 2,6-di-tert-butyl-1,4-benzoquinone (DtBBQ) as a redox-active CO_2 carrier in propylene carbonate (PC) or the ionic liquid [bmim][PF_6], they showed that CO_2 could be selectively separated from sub-1% levels and concentrated to nearly 100% at atmospheric pressure. In PC, they achieved a 200-fold increase in CO_2 partial pressure, from 0.5% to 97%. The system demonstrated high efficiency, with a molar ratio of CO_2 pumped per electron transferred of 0.43, close to the theoretical maximum of 0.50.

These studies collectively highlight the potential of quinone-based systems for electrochemical CO_2 capture and concentration. The work of Mizen and Wrighton[85] established the fundamental mechanism of CO_2 binding to reduced quinones, while Simpson and Durand[77] expanded this understanding to a range of quinone structures and identified key structure-reactivity relationships. Scovazzo et al.[86] then demonstrated the practical application of these principles in a working separation and concentration system.

However, challenges remain. The oxygen sensitivity of many quinones, including DtBBQ used by Scovazzo et al.,[86] limits their practical application for atmospheric CO_2 capture. Future work should focus on developing oxygen-stable quinone derivatives or protective strategies to enable their use in ambient conditions. Additionally, further optimization of solvent systems, cell designs, and process parameters will be crucial for improving the efficiency and scalability of these systems.

Quinones undergo reversible reduction to form semiquinone radical anions and dianions, which can bind CO_2 via nucleophilic addition reactions. The electrochemistry and CO_2 binding properties of various quinone structures have been systematically investigated to optimize their performance as capture agents. Simeon et al. examined a wide range of para- and ortho-quinones using cyclic voltammetry, categorizing them as either "weakly complexing" or "strongly complexing" based on their interactions with CO_2.[83] Weakly complexing quinones showed two distinct

reduction waves under CO_2, with only the second wave shifted positively compared to under an N_2 atmosphere. In contrast, strongly complexing quinones exhibited merging of the two reduction waves under a CO_2 atmosphere, indicating rapid reaction of the semiquinone with CO_2 followed by further reduction. The CO_2 binding constants were found to correlate with quinone basicity, with electron-donating substituents generally enhancing CO_2 affinity.

While quinones show promise for CO_2 capture, a key challenge is their sensitivity to oxygen, which can lead to degradation of the reduced species. Barlow and Yang addressed this issue by utilizing alcohol additives to shift the reduction potentials of quinones to more positive values.[80] They found that hydrogen bonding interactions with ethanol could shift the reduction potential of tetrachloro-p-benzoquinone by up to 350 mV, making it stable in the presence of O_2. The alcohol additives also enhanced CO_2 binding in some cases. By optimizing the pKa of the alcohol additive, they achieved both O_2 stability and improved CO_2 capture performance. However, the alcohol itself underwent weak molecular binding with the reduced quinone through a hydrogen-bonding mechanism, which would likely affect the ability of the reduced quinone to bind with CO_2.

Building on these fundamental studies, Diederichsen et al. advanced the concept of a continuous-flow electrochemical CO_2 capture process utilizing liquid quinones.[81] They synthesized a naphthoquinone derivative that remained liquid at room temperature and combined it with low-volatility glymes to create a redox-active liquid sorbent. This approach achieved high quinone concentrations (1 M) and eliminated the need for water as a solvent. In a dual-cell flow system, they demonstrated continuous CO_2 capture and release with promising initial energetics between 50-200 kJ mol^{-1} CO_2. The liquid quinone system offers the potential for large-area distributed capture with centralized CO_2 release.

1.5.4 Vitamin B_2 as a potential redox mediator for CO_2 reduction

Riboflavin is the crucial component responsible for redox activity in the cofactors flavin adenine dinucleotide (FAD) and flavin mononucleotide (FMN). These cofactors power numerous biological redox reactions by facilitating electron movement

across diverse chemical groups.[87,88] Examples of these reactions include the dehydrogenation of NADPH and D-amino acids. Within membranes, flavoenzymes exhibit greater electron-transfer adaptability than nicotinamide coenzymes (NAD/NADP), handling both single-electron and two-electron transfers.[89–92] This flexibility lets flavins bridge the gap between two-electron donors (like NADH) and single-electron acceptors (like heme Fe). Importantly, flavins engage in key aerobic processes due to their distinct oxygen interactions.[90]

Like quinones, flavins can exist in three oxidation states: flavoquinone (Fl_{ox}), flavosemiquinone radical ($Fl_{rad}{}^{\bullet-}$), and flavohydroquinone dianion ($Fl_{red}{}^{2-}$). The electrochemical reduction mechanism for vitamin B_2 in aprotic solution is an ECE (where E represents an electron transfer and C represents a chemical step) process for cyclic voltammograms recorded between –0.5 and –1.6 V vs. Fc/Fc^+ (where Fc = ferrocene).[93] For larger potential windows, additional electron transfer and chemical steps are observed. In buffered aqueous solutions a chemically reversible electron transfer involving the transfer of two electrons and two protons occurs.[94]

Considering the similar electrochemical behavior of quinones and flavins, experiments were performed in this thesis to test whether reduced flavins were also able to undergo molecular interactions with dissolved CO_2, and to determine how the overall reduction mechanism changed in a CO_2-rich environment. The ability of flavins to undergo reversible redox transformations and potential for CO_2 interactions make it an interesting candidate for CO_2 utilization applications. Therefore, the exploration of riboflavin's electrochemical behavior in the presence of CO_2 could provide valuable insights into bio-inspired approaches for CO_2 reduction and utilization.

1.5.5 Investigation of quinones in energy storage systems

In parallel with CO_2 utilization, the development of efficient energy storage systems is crucial for the widespread adoption of renewable energy sources. The intermittent nature of solar and wind power necessitates robust storage solutions to ensure a stable and reliable energy supply. Redox flow batteries (RFBs) have emerged as promising candidates for large-scale energy storage due to their ability to decouple power and energy capacity, as well as their potential for long cycle life and scalability.

Organic redox-active compounds, including quinones and flavins, offer several advantages for RFB applications, such as structural diversity, tailorable redox properties, and potential for low-cost, sustainable production. The electrochemical properties that make these compounds interesting for CO_2 utilization also render them attractive for energy storage applications. The ability to fine-tune their redox potentials and solubility through molecular engineering provides opportunities for optimizing their performance in RFBs.

This thesis investigates the dual potential of quinones for CO_2 utilization and energy storage applications. By exploring their electrochemical behavior, CO_2 binding properties, and potential for reversible redox cycling, we aim to contribute to the development of innovative solutions at the nexus of carbon management and sustainable energy technologies. The research presented here spans fundamental electrochemical studies to proof-of-concept demonstrations, providing insights into the challenges and opportunities in harnessing organic redox-active compounds for addressing critical environmental and energy challenges.

Through this exploration, we seek to advance the understanding of structure-function relationships in organic electroactive materials, elucidate mechanisms of CO_2 interactions and electron transfer processes, and assess the feasibility of integrating CO_2 utilization with energy storage functionalities. The findings from this research could pave the way for the development of novel, multifunctional systems that simultaneously address CO_2 mitigation and energy storage needs, contributing to a more sustainable and low-carbon future.

1.5.6 Critical assessment of CO_2 reduction strategies

Electrochemical CO_2 reduction represents a promising approach for carbon capture and utilization, yet significant challenges remain before widespread implementation becomes feasible.

1.5.6.1 Fundamental Challenges

Several critical constraints influence current CO_2 reduction strategies: Thermodynamic barriers hindering CO_2 activation, Rivalry with the oxygen reduction reaction, Complex multi-electron transfer mechanisms, and a limited understanding

of reaction pathways. Electrochemical capture of carbon dioxide using redox-active molecules such as quinone necessitates a careful equilibrium between the binding affinity of reduced species and their redox potential, which contends with the oxygen reduction reaction.[95] Addressing these challenges demands precise catalyst development and optimization of operational conditions. Recent advancements in this domain have shifted focus from basic quinone to other redox mediators, including modified quinones,[81] guanidinos,[96] and isoindigos.[97]

1.5.6.2 Practical Implementation

Translating laboratory results into real-world applications encounters multiple obstacles: Limitations in mass transport at current densities pertinent to industry, Challenges in integrating systems with renewable energy sources, Requirements for product separation and purification, and Economic competitiveness against current technologies.[98]

1.5.6.3 Research Priorities

Significant topics that require further investigation encompass: the development of catalysts with improved selectivity and stability, an enhanced understanding of reaction mechanisms and the intermediate species involved, the refinement of system designs to boost efficiency, and research on long-term stability in realistic environments. Additionally, exploring the effects of molecular interactions and stabilization brought about by CO_2 binding for applications like energy storage and redox flow batteries is also of interest.

1.6 Objective and scope of the thesis

This thesis aims to explore and advance the applications of analytical electrochemistry in addressing critical environmental and pharmaceutical challenges. The primary objective is to demonstrate the versatility and effectiveness of electrochemical techniques in three key areas: water disinfection, pharmaceutical compound detection, and carbon dioxide capture and utilization. By focusing on these diverse

yet interconnected fields, the thesis seeks to contribute to the development of sustainable solutions for pressing global issues.

The study focuses on the feasibility of employing platinized titanium electrodes for electrochemically deactivating *Escherichia coli* in water. The goal is to create a water treatment process that minimizes the need for additional supporting electrolytes and conductivity, which is crucial when treating potable water to limit electrolyte content. This research investigates the disinfection mechanisms, the key factors impacting inactivation efficiency, and evaluates varying electrode designs. A significant emphasis is placed on analyzing how reactive oxygen species, notably hydroxyl radicals, contribute to bacterial inactivation. The research aspires to offer insights for creating effective, sustainable, and eco-friendly water disinfection methods, especially beneficial in regions lacking access to conventional water treatment systems.

The objectives of this thesis in pharmaceutical analysis are to establish and refine methods for detecting and measuring praziquantel, a crucial antiparasitic medication, in water samples. This investigation encompasses a comparison between two analytical techniques: gas chromatography-mass spectrometry (GC-MS) and voltammetry. The methods are assessed based on detection limits, accuracy, precision, and their viability for field applications. This research seeks to advance the environmental monitoring of pharmaceutical compounds and explore the potential of electrochemical methods as either alternatives or complements to conventional chromatographic approaches, enabling cost-effective routine on-site detection.

In the area of carbon dioxide capture and energy storage, the research objective is to explore the electrochemistry of organic molecules, specifically quinones and riboflavin (vitamin B_2), for potential applications in CO_2 capture and utilization. The scope of this study includes investigating the supramolecular interactions between reduced organic species and CO_2, examining their electrochemical behavior under various conditions, and assessing their potential for energy storage applications. This research aims to provide fundamental insights that could guide the development of novel carbon capture technologies and organic-based energy storage systems.

Overall, the thesis seeks to bridge the gap between fundamental electrochemistry and practical applications in environmental remediation, pharmaceutical analysis, and sustainable energy technologies. By addressing these diverse yet interconnected

areas, the research aims to demonstrate the broad applicability and potential impact of electrochemistry in solving complex global challenges. The scope of the thesis extends from laboratory-based investigations to considerations of real-world applicability, with the goal of contributing to the development of sustainable solutions for water treatment, environmental monitoring, and carbon management.

1.7 Thesis organization and chapter overview

This thesis is organized into six chapters, each focusing on different aspects of electrochemistry and its applications in addressing environmental and pharmaceutical challenges. The structure of the thesis reflects a progression from fundamental electrochemical studies to practical applications in water treatment, pharmaceutical analysis, and carbon dioxide utilization. Below is an overview of each chapter:

Chapter 1: Introduction

The introductory chapter provides a comprehensive background on the importance of electrochemistry in environmental and pharmaceutical sciences. It outlines the global challenges related to water quality, pharmaceutical pollution, and carbon dioxide emissions. The chapter also introduces the key concepts and techniques in electrochemistry that form the foundation for the subsequent research chapters.

Chapter 2: Electrochemical Water Treatment

This chapter focuses on the development and optimization of an electrochemical system for water disinfection using platinized titanium electrodes. It begins with a literature review on current water treatment technologies and the potential advantages of electrochemical methods. The experimental section details the setup and methodology used to investigate the inactivation of Escherichia coli in various electrolyte solutions. Results and discussion cover the comparison between two-electrode and three-electrode configurations, the influence of different electrolytes on disinfection efficiency, and the identification and quantification of reactive oxygen species, particularly hydroxyl radicals, generated during the process.

Chapter 3: Electrochemical Detection and Quantification of Praziquantel

This chapter explores the development of electrochemical methods for detecting and quantifying praziquantel, an important antiparasitic drug, in water samples. The chapter begins with an overview of the environmental concerns related to pharmaceutical contaminants and the need for sensitive and reliable detection methods. It then describes the optimization of a voltametric technique for praziquantel analysis and compares its performance with gas chromatography-mass spectrometry (GC-MS). The chapter concludes with a discussion on the potential applications of the developed method in environmental monitoring and pharmaceutical quality control.

Chapter 4: Towards Organic CO_2 Batteries

This chapter investigates the electrochemical properties of quinones and their potential applications in CO_2 reduction and energy storage. The experimental section details the controlled potential electrolysis studies of various quinones under inert and CO_2 atmospheres. Results and discussion cover the mechanisms of quinone-CO_2 interactions, the stability of reduced quinone species, and the feasibility of using quinones in CO_2-based energy storage systems.

Chapter 5: Probing the Supramolecular Interactions of Electrochemically Reduced Vitamin B_2 with CO_2 in Non-Aqueous Media

This chapter focuses on the electrochemical behavior of riboflavin (vitamin B_2) and its interactions with CO_2. The chapter begins with an introduction to the biological significance of riboflavin and its potential as a bio-inspired redox mediator. It then describes the electrochemical studies conducted to elucidate the mechanisms of riboflavin reduction in the presence of CO_2. The results section presents findings from cyclic voltammetry, controlled potential electrolysis, spectroscopic analyses, and molecular orbital analysis providing insights into the formation of riboflavin-CO_2 complexes and their implications for CO_2 reduction processes.

Chapter 6: Conclusions and Future Perspectives

The final chapter synthesizes the key findings from the preceding chapters, highlighting the contributions of this thesis to the field of electrochemistry and its applications. It discusses the implications of the research for water treatment technologies, pharmaceutical analysis, and CO_2 utilization strategies. The chapter concludes by outlining future research directions and potential applications of

the developed electrochemical methods in addressing environmental and energy challenges.

Throughout the thesis, each chapter is structured to include a targeted introduction, detailed experimental procedures, comprehensive results and discussion, and specific conclusions. This organization allows for a thorough examination of each research topic while maintaining a cohesive narrative that demonstrates the versatility and potential of analytical electrochemistry in addressing critical global challenges.

References

(1) Rafiee, M.; Mayer, M. N.; Punchihewa, B. T.; Mumau, M. R. Constant Potential and Constant Current Electrolysis: An Introduction and Comparison of Different Techniques for Organic Electrosynthesis. *The Journal of Organic Chemistry* **2021**, Publisher: American Chemical Society, DOI: 10.1021/acs.joc.1c01391.

(2) Atkins, P., *Concepts in Physical Chemistry*; Royal Society of Chemistry: 2024.

(3) Barker, G. C.; Gardner, A. W. Pulse polarography. *Fresenius' Zeitschrift für analytische Chemie* **1960**, *173*, 79–83.

(4) Lovrić, M. In *Electroanalytical Methods*; Springer, Berlin, Heidelberg: 2005, pp 111–136.

(5) Kokoskarova, P.; Stojanov, L.; Najkov, K.; Ristovska, N.; Ruskovska, T.; Skrzypek, S.; Mirceski, V. Square-wave voltammetry of human blood serum. *Scientific Reports* **2023**, *13*, Publisher: Nature Publishing Group, 8485.

(6) Adam, V.; Mikelova, R.; Hubalek, J.; Hanustiak, P.; Beklova, M.; Hodek, P.; Horna, A.; Trnkova, L.; Stiborova, M.; Zeman, L.; Kizek, R. Utilizing of Square Wave Voltammetry to Detect Flavonoids in the Presence of Human Urine. *Sensors* **2007**, *7*, Number: 10 Publisher: Molecular Diversity Preservation International, 2402–2418.

(7) Trindade, M. A. G.; Boldrin Zanoni, M. V. Square-Wave Voltammetry Applied to the Analysis of the Dye Marker, Solvent Blue 14, in Kerosene and Fuel Alcohol. *Electroanalysis* **2007**, *19*, _eprint: https://analyticalsciencejournals-onlinelibrary-wiley-com.remotexs.ntu.edu.sg/doi/pdf/10.1002/elan.200703964, 1901–1907.

(8) Bain, R.; Johnston, R.; Mitis, F.; Chatterley, C.; Slaymaker, T. Establishing Sustainable Development Goal Baselines for Household Drinking Water, Sanitation and Hygiene Services. *Water* **2018**, *10*, Number: 12 Publisher: Multidisciplinary Digital Publishing Institute, 1711.

(9) Nhamo, G.; Nhemachena, C.; Nhamo, S. Is 2030 too soon for Africa to achieve the water and sanitation sustainable development goal? *Science of The Total Environment* **2019**, *669*, 129–139.

(10) Zhang, X. et al. Urban drought challenge to 2030 sustainable development goals. *Science of The Total Environment* **2019**, *693*, 133536.

(11) Diaz-Elsayed, N.; Rezaei, N.; Guo, T.; Mohebbi, S.; Zhang, Q. Wastewater-based resource recovery technologies across scale: A review. *Resources, Conservation and Recycling* **2019**, *145*, 94–112.

(12) Hube, S.; Wu, B. Mitigation of emerging pollutants and pathogens in decentralized wastewater treatment processes: A review. *Science of The Total Environment* **2021**, *779*, 146545.

(13) Paul, R.; Kenway, S.; Mukheibir, P. How scale and technology influence the energy intensity of water recycling systems-An analytical review. *Journal of Cleaner Production* **2019**, *215*, 1457–1480.

(14) Clematis, D.; Panizza, M. Electrochemical oxidation of organic pollutants in low conductive solutions. *Current Opinion in Electrochemistry* **2021**, *26*, 100665.

(15) Mousset, E. Interest of micro-reactors for the implementation of advanced electrocatalytic oxidation with boron-doped diamond anode for wastewater treatment. *Current Opinion in Electrochemistry* **2022**, *32*, 100897.

(16) McBeath, S. T.; English, J. T.; Wilkinson, D. P.; Graham, N. J. D. Circumneutral electrosynthesis of ferrate oxidant: An emerging technology for small, remote and decentralised water treatment applications. *Current Opinion in Electrochemistry* **2021**, *27*, 100680.

(17) Sandoval, M. A.; Calzadilla, W.; Salazar, R. Influence of reactor design on the electrochemical oxidation and disinfection of wastewaters using boron-doped diamond electrodes. *Current Opinion in Electrochemistry* **2022**, *33*, 100939.

(18) Wang, J.; Zhuan, R. Degradation of antibiotics by advanced oxidation processes: An overview. *Science of The Total Environment* **2020**, *701*, 135023.

(19) Hu, Z.; Cai, J.; Song, G.; Tian, Y.; Zhou, M. Anodic oxidation of organic pollutants: Anode fabrication, process hybrid and environmental applications. *Current Opinion in Electrochemistry* **2021**, *26*, 100659.

(20) Ganiyu, S. O.; Martínez-Huitle, C. A.; Oturan, M. A. Electrochemical advanced oxidation processes for wastewater treatment: Advances in formation and detection of reactive species and mechanisms. *Current Opinion in Electrochemistry* **2021**, *27*, 100678.

(21) Dos Santos, A. J.; Kronka, M. S.; Fortunato, G. V.; Lanza, M. R. V. Recent advances in electrochemical water technologies for the treatment of antibiotics: A short review. *Current Opinion in Electrochemistry* **2021**, *26*, 100674.

(22) Rodríguez-Narváez, O. M.; Picos, A. R.; Bravo-Yumi, N.; Pacheco-Alvarez, M.; Martínez-Huitle, C. A.; Peralta-Hernández, J. M. Electrochemical oxidation technology to treat textile wastewaters. *Current Opinion in Electrochemistry* **2021**, *29*, 100806.

(23) Trellu, C.; Olvera Vargas, H.; Mousset, E.; Oturan, N.; Oturan, M. A. Electrochemical technologies for the treatment of pesticides. *Current Opinion in Electrochemistry* **2021**, *26*, 100677.

(24) Huang, D.; Wang, K.; Niu, J.; Chu, C.; Weon, S.; Zhu, Q.; Lu, J.; Stavitski, E.; Kim, J.-H. Amorphous Pd-Loaded Ti4O7 Electrode for Direct Anodic Destruction of Perfluorooctanoic Acid. *Environmental Science & Technology* **2020**, *54*, Publisher: American Chemical Society, 10954–10963.

(25) Lee, J.; Son, A.; Ko, Y.-J.; Shin, M.-J.; Kim, W. S.; Choi, J. W.; Lee, J.; Hong, S. W. Investigation of titanium mesh as a cathode for the electro-Fenton process: consideration of its practical application in wastewater treatment. *Environmental Science: Water Research & Technology* **2020**, *6*, Publisher: The Royal Society of Chemistry, 1627–1637.

(26) Sirés, I.; Brillas, E. Upgrading and expanding the electro-Fenton and related processes. *Current Opinion in Electrochemistry* **2021**, *27*, 100686.

(27) Nidheesh, P. V.; Trellu, C.; Vargas, H. O.; Mousset, E.; Ganiyu, S. O.; Oturan, M. A. Electro-Fenton process in combination with other advanced oxidation processes: Challenges and opportunities. *Current Opinion in Electrochemistry* **2023**, *37*, 101171.

(28) Salazar-Banda, G. R.; Santos, G. d. O. S.; Duarte Gonzaga, I. M.; Dória, A. R.; Barrios Eguiluz, K. I. Developments in electrode materials for wastewater treatment. *Current Opinion in Electrochemistry* **2021**, *26*, 100663.

(29) Pointer Malpass, G. R.; de Jesus Motheo, A. Recent advances on the use of active anodes in environmental electrochemistry. *Current Opinion in Electrochemistry* **2021**, *27*, 100689.

(30) Bergmann, H. Electrochemical disinfection – State of the art and tendencies. *Current Opinion in Electrochemistry* **2021**, *28*, 100694.

(31) Lévesque, S.; Graham, T.; Bejan, D.; Lawson, J.; Zhang, P.; Dixon, M. An electrochemical advanced oxidation process (EAOP) for the inactivation of Rhizoctonia solani in fertigation solutions. *Canadian Journal of Plant Science* **2020**, *100*, Publisher: NRC Research Press, 415–424.

(32) Chen, Y.-d.; Duan, X.; Zhou, X.; Wang, R.; Wang, S.; Ren, N.-q.; Ho, S.-H. Advanced oxidation processes for water disinfection: Features, mechanisms and prospects. *Chemical Engineering Journal* **2021**, *409*, 128207.

(33) Brillas, E.; Garcia-Segura, S.; Skoumal, M.; Arias, C. Electrochemical incineration of diclofenac in neutral aqueous medium by anodic oxidation using Pt and boron-doped diamond anodes. *Chemosphere* **2010**, *79*, 605–612.

(34) Zambrano, J.; Min, B. Electrochemical treatment of leachate containing highly concentrated phenol and ammonia using a Pt/Ti anode at different current densities. *Environmental Technology & Innovation* **2020**, *18*, 100632.

(35) Jiang, Y.; Zhao, H.; Liang, J.; Yue, L.; Li, T.; Luo, Y.; Liu, Q.; Lu, S.; Asiri, A. M.; Gong, Z.; Sun, X. Anodic oxidation for the degradation of organic pollutants: Anode materials, operating conditions and mechanisms. A mini review. *Electrochemistry Communications* **2021**, *123*, 106912.

(36) Long, F.; Ghani, D.; Huang, R.; Zhao, C. Versatile electrode materials applied in the electrochemical advanced oxidation processes for wastewater treatment: A systematic review. *Separation and Purification Technology* **2025**, *354*, 128725.

(37) Andrews, P. A summary of the efficacy of praziquantel against schistosomes in animal experiments and notes on its mode of action. *Arzneimittel-Forschung* **1981**, *31*, 538–541.

(38) Bader, C.; Starling, D. E.; Jones, D. E.; Brewer, M. T. Use of praziquantel to control platyhelminth parasites of fish. *Journal of Veterinary Pharmacology and Therapeutics* **2019**, *42*, _eprint: https://onlinelibrary.wiley.com/doi/pdf/10.1111/jvp.127 139–153.

(39) Thomas, C. M.; Timson, D. J. The Mechanism of Action of Praziquantel: Six Hypotheses. *Current Topics in Medicinal Chemistry* **2018**, *18*, 1575–1584.

(40) Cioli, D.; Pica-Mattoccia, L. Praziquantel. *Parasitology Research* **2003**, *90*, S3–S9.

(41) Frohberg, H. Results of toxicological studies on praziquantel. *Arzneimittel-Forschung* **1984**, *34*, 1137–1144.

(42) Norbury, L. J.; Shirakashi, S.; Power, C.; Nowak, B. F.; Bott, N. J. Praziquantel use in aquaculture – Current status and emerging issues. *International Journal for Parasitology: Drugs and Drug Resistance* **2022**, *18*, 87–102.

(43) Santos, A. L.; Takeuchi, R. M.; Stradiotto, N. R. Electrochemical, Spectrophotometric and Liquid-Chromatographic Approaches for Analysis of Tropical Disease Drugs. *Current Pharmaceutical Analysis*, *5*, 69–88.

(44) Aydin, E. B.; Aydin, M.; Sezginturk, M. K. Biosensors in Drug Discovery and Drug Analysis. *CURRENT ANALYTICAL CHEMISTRY* **2019**, *15*, Num Pages: 18 Place: Sharjah Publisher: Bentham Science Publ Ltd Web of Science ID: WOS:000473758500009, 467–484.

(45) Gouveia, F.; Bicker, J.; Goncalves, J.; Alves, G.; Falcao, A.; Fortuna, A. Liquid chromatographic methods for the determination of direct oral anticoagulant drugs in biological samples: A critical review. *ANALYTICA CHIMICA ACTA* **2019**, *1076*, Num Pages: 14 Place: Amsterdam Publisher: Elsevier Web of Science ID: WOS:000471599900002, 18–31.

(46) Nannou, C.; Ofrydopoulou, A.; Evgenidou, E.; Heath, D.; Heath, E.; Lambropoulou, D. Analytical strategies for the determination of antiviral drugs in the aquatic environment. *TRENDS IN ENVIRONMENTAL ANALYTICAL CHEMISTRY* **2019**, *24*, Num Pages: 15 Place: Amsterdam Publisher: Elsevier Web of Science ID: WOS:000500597900005, e00071.

(47) Qriouet, Z.; Qmichou, Z.; Bouchoutrouch, N.; Mahi, H.; Cherrah, Y.; Sefrioui, H. Analytical Methods Used for the Detection and Quantification of Benzodiazepines. *JOURNAL OF ANALYTICAL METHODS IN CHEMISTRY* **2019**, *2019*, Num Pages: 11 Place: London Publisher: Hindawi Ltd Web of Science ID: WOS:000486399900001, 2035492.

(48) Acquavia, M. A.; Foti, L.; Pascale, R.; Nicolo, A.; Brancaleone, V.; Cataldi, T. R.; Martelli, G.; Scrano, L.; Bianco, G. Detection and quantification of Covid-19 antiviral drugs in biological fluids and tissues. *TALANTA* **2021**, *224*, Num Pages: 17 Place: Amsterdam Publisher: Elsevier Web of Science ID: WOS:000600787800077, 121862.

(49) Fu, E.; Khederlou, K.; Lefevre, N.; Ramsey, S. A.; Johnston, M. L.; Wentland, L. Progress on Electrochemical Sensing of Pharmaceutical Drugs in Complex Biofluids. *CHEMOSENSORS* **2023**, *11*, Num Pages: 24 Place: Basel Publisher: MDPI Web of Science ID: WOS:001056972600001, 467.

(50) Saleem, M.; Hanif, M.; Rafiq, M.; Ali, A.; Raza, H.; Kim, S. J.; Lu, C. Recent Development on Sensing Strategies for Small Molecules Detections. *JOURNAL OF FLUORESCENCE* **2023**, Num Pages: 33 Place: New York Publisher: Springer/Plenum Publishers Web of Science ID: WOS:001060207900001, DOI: 10.1007/s10895-023-03387.

(51) Devaka, N. V. S. K.; Rao, V. M. Chromatographic Quantification of Ivermectin and Pranziquantel in the Tablets Using Stability Indicating RP-HPLC Method. *Pharmaceutical Sciences* **2019**, *25*, Number: 3 Publisher: Tabriz University of Medical Sciences, 254–261.

(52) Eason, T.; Ramirez, G.; Clulow, A. J.; Salim, M.; Boyd, B. J. Revisiting the Dissolution of Praziquantel in Biorelevant Media and the Impact of Digestion of Milk on Drug Dissolution. *Pharmaceutics* **2022**, *14*, 2228.

(53) Baralla, E.; Varoni, M. V.; Nieddu, M.; Demontis, M. P.; Merella, P.; Burreddu, C.; Garippa, G.; Boatto, G. Determination of Praziquantel in Sparus aurata L. after Administration of Medicated Animal Feed. *Animals* **2020**, *10*, Number: 3 Publisher: Multidisciplinary Digital Publishing Institute, 528.

(54) Ding, T.-Y.; Shu, X.-G.; Xiong, R.-P.; Qiu, J.-L.; Li, L.; He, L.-M. Simultaneous determination of praziquantel and its main metabolites in the tissues of black goats and their residue depletion. *Food Additives & Contaminants: Part A* **2022**, *39*, Publisher: Taylor & Francis _eprint: https://doi.org/10.1080/19440049.2022.2032 666–677.

(55) Teng, F.; Ji, J.; Yang, Y.; Wang, H. A useful quantitative model for determining the optical purity of praziquantel enantiomers based on near infrared spectroscopy with partial least squares. *Journal of Near Infrared Spectroscopy* **2022**, *30*, Publisher: SAGE Publishing, 246–253.

(56) Meier, H.; Blaschke, G. Capillary electrophoresis-mass spectrometry, liquid chromatography-mass spectrometry and nanoelectrospray-mass spectrometry of praziquantel metabolites. *Journal of Chromatography. B, Biomedical Sciences and Applications* **2000**, *748*, 221–231.

(57) Rizk, M.; Belal, F.; Ibrahim, F.; Ahmed, S.; El-Enany, N. M. Voltammetric Determination of Praziquantel in Tablets and Biological Fluids. *Arzneimittelforschung* **2001**, *51*, Publisher: Editio Cantor Verlag, 673–678.

(58) Ghoneim, M. M.; Mabrouk, M. M.; Tawfik, A. Direct determination of praziquantel in pharmaceutical formulations and human plasma by cathodic adsorptive stripping differential-pulse voltammetry. *Journal of Pharmaceutical and Biomedical Analysis* **2002**, *30*, 1311–1318.

(59) Radi, a.-e.; Hassanein, A. Indirect determination of praziquantel in human serum by cathodic adsorptive stripping voltammetry. *Chemia Analityczna* **2001**, *46*, 561–567.

(60) Robards, K.; Ryan, D., *Principles and Practice of Modern Chromatographic Methods*, Google-Books-ID: 0OFSEAAAQBAJ; Academic Press: 2021; 532 pp.

(61) Ahmad Dar, A.; Sangwan, P.; Kumar, A. Chromatography: An important tool for drug discovery. *Journal of Separation Science* **2020**, *43*, _eprint: https://onlinelibrary.wiley.com/doi/pdf/10.1002/jssc.201900656, 105–119.

(62) Ferrari, A. G.-M.; Carrington, P.; J. Rowley-Neale, S.; E. Banks, C. Recent advances in portable heavy metal electrochemical sensing platforms. *Environmental Science: Water Research & Technology* **2020**, *6*, Publisher: Royal Society of Chemistry, 2676–2690.

(63) De Faria, L. V.; Lisboa, T. P.; Campos, N. d. S.; Alves, G. F.; Matos, M. A. C.; Matos, R. C.; Munoz, R. A. A. Electrochemical methods for the determination of antibiotic residues in milk: A critical review. *Analytica Chimica Acta* **2021**, *1173*, 338569.

(64) Atmospheric Monthly In Situ CO2 Data - Mauna Loa Observatory, Hawaii Context Object: url_ver=Z39.88-2004&ctx_ver=Z39.88-2004&rft_val_fmt=info%3Aofi%2Ffmt%3Ak
+Mauna+Loa+Observatory%2C+Hawaii&rft.date=1958+to+present&rft.date=2017&rft.language

(65) Morice, C. P.; Kennedy, J. J.; Rayner, N. A.; Winn, J. P.; Hogan, E.; Killick, R. E.; Dunn, R. J. H.; Osborn, T. J.; Jones, P. D.; Simpson, I. R. An Updated Assessment of Near-Surface Temperature Change From 1850: The HadCRUT5 Data Set. *Journal of Geophysical Research: Atmospheres* **2021**, *126*, e2019JD032361.

(66) Hauck, J.; Zeising, M.; Le Quéré, C.; Gruber, N.; Bakker, D. C. E.; Bopp, L.; Chau, T. T. T.; Gürses, Ö.; Ilyina, T.; Landschützer, P.; Lenton, A.; Resplandy, L.; Rödenbeck, C.; Schwinger, J.; Séférian, R. Consistency and Challenges in the Ocean Carbon Sink Estimate for the Global Carbon Budget. *Frontiers in Marine Science* **2020**, *7*, 571720.

(67) Hauck, J.; Landschützer, P.; Mayot, N.; Jersild, A. Global Carbon Budget 2023, surface ocean fugactiy of CO2 (fCO2) and air-sea CO2 flux of individual global ocean biogechemical models and surface ocean fCO2-based data-products, 2023.

(68) Kim, Y.; Tanaka, K.; Matsuoka, S. Environmental and economic effectiveness of the Kyoto Protocol. *PLoS ONE* **2020**, *15*, e0236299.

(69) Dooley, K. et al. Ethical choices behind quantifications of fair contributions under the Paris Agreement. *Nature Climate Change* **2021**, *11*, Publisher: Nature Publishing Group, 300–305.

(70) Ntiamoah, A.; Ling, J.; Xiao, P.; Webley, P. A.; Zhai, Y. CO2 Capture by Temperature Swing Adsorption: Use of Hot CO2-Rich Gas for Regeneration. *Industrial & Engineering Chemistry Research* **2016**, *55*, Publisher: American Chemical Society, 703–713.

(71) Scott, A. Sucking carbon dioxide from air in Iceland Section: COVER STORY, `https://cendigitalmagazine.acs.org/2024/06/03/sucking-carbon-dioxide-from-air-in-iceland-2/content.html` (accessed 06/04/2024).

(72) Matter, J. M. et al. Rapid carbon mineralization for permanent disposal of anthropogenic carbon dioxide emissions. *Science* **2016**, *352*, Publisher: American Association for the Advancement of Science, 1312–1314.

(73) Renfrew, S. E.; Starr, D. E.; Strasser, P. Electrochemical Approaches toward CO2 Capture and Concentration. *ACS Catalysis* **2020**, *10*, Publisher: American Chemical Society, 13058–13074.

(74) Ranjan, R.; Olson, J.; Singh, P.; Lorance, E. D.; Buttry, D. A.; Gould, I. R. Reversible Electrochemical Trapping of Carbon Dioxide Using 4,4'-Bipyridine That Does Not Require Thermal Activation. *The Journal of Physical Chemistry Letters* **2015**, *6*, Publisher: American Chemical Society, 4943–4946.

(75) Singh, P.; Rheinhardt, J. H.; Olson, J. Z.; Tarakeshwar, P.; Mujica, V.; Buttry, D. A. Electrochemical Capture and Release of Carbon Dioxide Using a Disulfide–Thiocarbonate Redox Cycle. *Journal of the American Chemical Society* **2017**, *139*, Publisher: American Chemical Society, 1033–1036.

(76) Appel, A. M.; Newell, R.; DuBois, D. L.; Rakowski DuBois, M. Concentration of Carbon Dioxide by Electrochemically Modulated Complexation with a Binuclear Copper Complex. *Inorganic Chemistry* **2005**, *44*, Publisher: American Chemical Society, 3046–3056.

(77) Comeau Simpson, T.; Durand, R. R. Reactivity of carbon dioxide with quinones. *Electrochimica Acta* **1990**, *35*, 1399–1403.

(78) Kang, J. S.; Kim, S.; Hatton, T. A. Redox-responsive sorbents and mediators for electrochemically based CO2 capture. *Current Opinion in Green and Sustainable Chemistry* **2021**, *31*, 100504.

(79) Barlow, J. M.; Clarke, L. E.; Zhang, Z.; Bím, D.; Ripley, K. M.; Zito, A.; Brushett, F. R.; Alexandrova, A. N.; Yang, J. Y. Molecular design of redox carriers for electrochemical CO $_2$ capture and concentration. *Chemical Society Reviews* **2022**, *51*, 8415–8433.

(80) Barlow, J. M.; Yang, J. Y. Oxygen-Stable Electrochemical CO $_2$ Capture and Concentration with Quinones Using Alcohol Additives. *Journal of the American Chemical Society* **2022**, *144*, 14161–14169.

(81) Diederichsen, K. M.; Liu, Y.; Ozbek, N.; Seo, H.; Hatton, T. A. Toward solvent-free continuous-flow electrochemically mediated carbon capture with high-concentration liquid quinone chemistry. *Joule* **2022**, *6*, 221–239.

(82) Li, X.; Zhao, X.; Liu, Y.; Hatton, T. A.; Liu, Y. Redox-tunable Lewis bases for electrochemical carbon dioxide capture. *Nature Energy* **2022**, *7*, Number: 11 Publisher: Nature Publishing Group, 1065–1075.

(83) Simeon, F.; Stern, M. C.; Diederichsen, K. M.; Liu, Y.; Herzog, H. J.; Hatton, T. A. Electrochemical and Molecular Assessment of Quinones as CO2-Binding Redox Molecules for Carbon Capture. *The Journal of Physical Chemistry C* **2022**, *126*, Publisher: American Chemical Society, 1389–1399.

(84) Choi, G. H.; Song, H. J.; Lee, S.; Kim, J. Y.; Moon, M.-W.; Yoo, P. J. Electrochemical direct CO2 capture technology using redox-active organic molecules to achieve carbon-neutrality. *Nano Energy* **2023**, *112*, 108512.

(85) Mizen, M. B.; Wrighton, M. S. Reductive Addition of CO 2 to 9,10-Phenanthrenequinone. *Journal of The Electrochemical Society* **1989**, *136*, Publisher: IOP Publishing, 941.

(86) Scovazzo, P.; Poshusta, J.; DuBois, D.; Koval, C.; Noble, R. Electrochemical Separation and Concentration of ¡1% Carbon Dioxide from Nitrogen. *Journal of The Electrochemical Society* **2003**, *150*, Publisher: IOP Publishing, D91.

(87) Suwannasom, N.; Kao, I.; Pruß, A.; Georgieva, R.; Bäumler, H. Riboflavin: The Health Benefits of a Forgotten Natural Vitamin. *International Journal of Molecular Sciences* **2020**, *21*, Number: 3 Publisher: Multidisciplinary Digital Publishing Institute, 950.

(88) Olfat, N.; Ashoori, M.; Saedisomeolia, A. Riboflavin is an antioxidant: a review update. *British Journal of Nutrition* **2022**, *128*, Publisher: Cambridge University Press, 1887–1895.

(89) Walsh, C. Flavin coenzymes: at the crossroads of biological redox chemistry. *Accounts of Chemical Research* **1980**, *13*, Publisher: American Chemical Society, 148–155.

(90) Bruice, T. C. Oxygen-Flavin Chemistry. *Israel Journal of Chemistry* **1984**, *24*, _eprint: https://onlinelibrary.wiley.com/doi/pdf/10.1002/ijch.198400008, 54–61.

(91) Ghisla, S.; Massey, V. Mechanisms of flavoprotein-catalyzed reactions. *European Journal of Biochemistry* **1989**, *181*, _eprint: https://onlinelibrary.wiley.com/doi/pdf/10.1033.1989.tb14688.x, 1–17.

(92) Niemz, A.; Imbriglio, J.; Rotello, V. M. Model Systems for Flavoenzyme Activity: One- and Two-Electron Reduction of Flavins in Aprotic Hydrophobic Environments. *Journal of the American Chemical Society* **1997**, *119*, Publisher: American Chemical Society, 887–892.

(93) Tan, S. L. J.; Webster, R. D. Electrochemically Induced Chemically Reversible Proton-Coupled Electron Transfer Reactions of Riboflavin (Vitamin B2). *Journal of the American Chemical Society* **2012**, *134*, Publisher: American Chemical Society, 5954–5964.

(94) Lovander, M. D.; Lyon, J. D.; Parr, D. L.; Wang, J.; Parke, B.; Leddy, J. Critical Review—Electrochemical Properties of 13 Vitamins: A Critical Review and Assessment. *Journal of The Electrochemical Society* **2018**, *165*, Publisher: IOP Publishing, G18.

(95) Bui, A. T.; Hartley, N. A.; Thom, A. J. W.; Forse, A. C. Trade-Off between Redox Potential and the Strength of Electrochemical CO2 Capture in Quinones. *The Journal of Physical Chemistry C* **2022**, *126*, Publisher: American Chemical Society, 14163–14172.

(96) Li, C. J.; Ziller, J. W.; Barlow, J. M.; Yang, J. Y. Aqueous Electrochemical and pH Studies of Redox-Active Guanidino Functionalized Aromatics for CO2 Capture. *ACS Organic & Inorganic Au* **2024**, *4*, Publisher: American Chemical Society, 387–394.

(97) Li, X.; Zhao, X.; Zhang, L.; Mathur, A.; Xu, Y.; Fang, Z.; Gu, L.; Liu, Y.; Liu, Y. Redox-tunable isoindigos for electrochemically mediated carbon capture. *Nature Communications* **2024**, *15*, Publisher: Nature Publishing Group, 1175.

(98) Massen-Hane, M.; Diederichsen, K. M.; Hatton, T. A. Engineering redox-active electrochemically mediated carbon dioxide capture systems. *Nature Chemical Engineering* **2024**, *1*, Publisher: Nature Publishing Group, 35–44.

Chapter 2

Feasibility study of electrochemical *Escherichia coli* inactivation using platinized titanium electrodes

2.1 Abstract

This chapter explores the feasibility of using platinized titanium electrodes for the electrochemical inactivation of *Escherichia coli* (*E. coli*) in water, aiming to develop an efficient and sustainable water disinfection method. The study focuses on elucidating the mechanisms underlying the disinfection process and identifying the key factors influencing the inactivation efficiency.

A comparative analysis between three-electrode and two-electrode configurations revealed the superiority of the three-electrode system in achieving higher current throughput, a critical factor in effective water purification processes. The inactivation of *E. coli* in various electrolyte solutions followed a logarithmic decay pattern, with no significant differences observed among the electrolytes tested, except for sodium chloride (NaCl). The enhanced bactericidal activity in the presence of NaCl was attributed to the generation of chlorine species.

The comparison of deactivation efficacy between potentiostatic and galvanostatic modes revealed that the inactivation velocity of *E. coli* is more influenced by the applied current than the potential. The identification and quantification of hydroxyl radicals generated during water electrolysis were successfully achieved through the analysis of dimethyl sulfoxide (DMSO) decomposition using proton nuclear magnetic resonance (^{1}H$-$NMR) spectroscopy. The findings underscore the crucial role of hydroxyl radicals in the electrochemical inactivation of *E. coli*, with a strong correlation observed between the quantity of hydroxyl radicals generated and the degree of bacterial inactivation achieved.

This study demonstrates the feasibility of using platinized titanium electrodes for the effective inactivation of *E. coli* in water through electrochemical processes. The insights gained into the mechanisms of disinfection, the influence of different electrolytes, and the role of hydroxyl radicals contribute to a better understanding of the electrochemical water treatment process. These findings can guide the optimization of electrochemical disinfection systems for enhanced bacterial inactivation efficiency and the development of practical applications in water treatment technologies.

2.2 Introduction

Water disinfection is crucial for preventing the spread of waterborne diseases. Traditional methods, such as chlorination, have been widely used for this purpose. However, these chemical treatment methods have several drawbacks, including the formation of harmful byproducts and the potential for creating chlorine-resistant pathogens. Electrochemical water disinfection has emerged as a promising alternative, offering the ability to generate powerful oxidants, such as hydroxyl radicals, in situ without the use of harmful chemicals.[1]

Recent studies have attributed the enhanced disinfection efficacy of electrochemical processes to the generation of reactive oxygen species (ROS), such as hydroxyl radicals ($OH^{\bullet}$), ozone, and hydrogen peroxide, during water electrolysis.[2] These ROS are particularly effective when generated directly in the electrolyzer rather than in an externally generated oxidant solution. For example, the high redox potential of $OH^{\bullet}$ (E_0 = 2.7 V vs. saturated calomel electrode (SCE)) allows it to compensate for its short-lived nature in advanced oxidation technologies.[3] However, most previous studies have not successfully demonstrated the clear role of these oxidants due to the simultaneous production of chlorine in their experimental designs, leaving the disinfecting nature of these oxidants unclear.

This chapter focuses on investigating the disinfecting nature of an electrochemical disinfection system, including without generating chlorine by employing a chloride-free phosphate buffer medium as the electrolyte in some studies. The roles of individual ROS, including $OH^{\bullet}$, ozone, and hydrogen peroxide, in the disinfection process are systematically examined. Additionally, factors affecting the disinfection efficiency, such as current density (or applied voltage), the presence of radical scavengers, initial bacterial population, and electrode cleaning, are also investigated. *E. coli* was used as an indicator bacterium, and platinized titanium electrodes, for both the anode and the cathode were chosen for the electrochemical disinfection studies due to their chemical stability.

The feasibility of using platinized titanium electrodes for inactivating *E. coli* K-12 bacteria in relatively low ionic strength media similar to found in surface water used for drinking was assessed. The process efficiency for the removal of *E. coli* was evaluated under optimized conditions, providing insights into the mechanisms of electrochemical disinfection and the potential for its application in water treatment.

The findings of this study will contribute to the development of effective, sustainable, and environmentally friendly water disinfection methods.

2.3 Materials and methods

The experiments were conducted using an electrochemical cell under potentiostatic or galvanostatic control in two-electrode or three-electrode arrangements. The disinfection efficiency was assessed by measuring the reduction in *E. coli* microbial populations in the treated water.

2.3.1 Chemicals and reagents

All the reagents were of analytical grade and were used as received without further purification. The water used for preparation of *E. coli* suspension and electrolyte solution was distilled and deionised by an ELGA Purelab option-Q to ensure the exclusion of chloride ions from the electrolytic solution (for experiments in the absence of chloride). Dimethyl sulfoxide, sodium carbonate, sodium chloride, sodium dihydrogen phosphate and sodium sulphate were procured from Sigma-Aldrich. Stock solutions of electrolyte with different concentrations were prepared by dissolving appropriate amount of electrolyte in ultrapure water before subsequent serial dilutions.

2.3.2 Electrolysis instrumentation and procedure

Electrolysis was carried out using a computer-controlled Eco-Chemie Autolab PGSTAT302N potentiostat, employing either a three-electrode or two-electrode configuration. Experiments were performed at a constant temperature of 22(2) °C, under conditions of either constant potential or constant current. A 50 mL beaker served as the electrolytic cell.

2.3.3 Comparison study between two-electrode and three-electrode arrangement

Most experiments were carried out in either a two-electrode undivided or three-electrode undivided cell, with platinized titanium electrodes as cathode and anode, and Ag/AgCl reference electrode in a 50 mL beaker. The platinized titanium electrode was cut into a 2 × 2 cm sized plate (0.010 inches thickness, surface area, 4 cm cm) from a 10 × 10 cm platinized titanium screen (the Fuel Cell Store, USA). An Ag/AgCl reference electrode (Metrohm, Switzerland) was filled with 3 mol L^{-1} KCl as the reference electrolyte. All the potential values measured in this study are reported relative to the Ag/AgCl reference electrode. All electrochemical experiments were performed using a potentiostat-galvanostat (Eco-Chemie Autolab PGSTAT302N, Metrohm, Switzerland).

2.3.3.1 Two-Electrode Configuration

The two-electrode system consisted of two 2 cm × 2 cm platinum mesh electrodes serving as working and counter electrodes. The electrodes were positioned parallel to each other at a fixed distance of 0.5 cm in a 50 mL beaker. The reference and auxiliary leads from the potentiostat were connected to the counter electrode. The system contained 40 mL of electrolyte solution inoculated with a predetermined concentration of *E. coli*.

2.3.3.2 Three-Electrode Configuration

The three-electrode arrangement utilized the same platinum mesh electrodes as the working and counter electrodes, with the addition of an Ag/AgCl reference electrode (Metrohm Pte Ltd). The reference electrode was positioned 0.5 cm from the working electrode to minimize solution resistance effects. The working and counter electrodes maintained the same spatial configuration as in the two-electrode configuration.

Prior to each experiment, all electrodes underwent thorough cleaning with ultra-pure water followed by complete drying to ensure reproducible surface conditions.

2.3.4 Preparation and analysis of *E. coli*

E. coli K12, obtained from Nanyang Environment and Water Research Institute (NEWRI), was first pre-cultured by inoculating a single colony in 5 mL sterile LB Miller broth, then incubated at 35 °C for 24 hours with agitation at 130 rpm. This pre-culture was subsequently inoculated into 100 mL LB Miller broth and grown under identical conditions. Prior to each experimental run, the *E. coli* culture was diluted to achieve the desired concentration for use as the electrolyte solution.

2.3.5 Electrochemical inactivation of *E. coli*

Prior to all the experiments, the electrodes are washed with 70% ethanol and ultrapure water to remove any deposits or absorbed dead cells. The volume of the solution treated in each experiment was 50 mL and the solution was stirred (500 rpm) during the experiments using a Teflon coated magnetic stirrer bar. The *E. coli* culture was freshly prepared with 0.1 mL of the *E. coli* culture and was diluted in 50 mL electrolyte solution for disinfection experiments. The concentration of *E. coli* was not identical in all experiments, due to fluctuations in the concentration of *E. coli* in the culture. As an approximation, *E. coli* culture freshly prepared in the lab was diluted and the concentration of *E. coli* in the diluted solutions was measured. Based on these results, the initial concentration of *E. coli* in most experiments in this work was estimated at 1.0×10^6 CFU/mL.

2.3.6 Viable *E. coli* cells counting by plating

The viability of *E. coli* was assessed by quantifying colony-forming units (CFU) through a serial dilution and plating method. At designated time points, aliquots of the culture were collected and serially diluted to obtain countable bacterial concentrations. Diluted samples were then spread onto Nutrient agar plates and incubated at 37 °C for 24 hours to facilitate the development of visible colonies. Each colony theoretically represents a single viable bacterium from the original sample. Post-incubation, colonies were enumerated, and the results expressed as $log(N/N_0)$, where N_0 denotes the initial colony count at 0 hours and N signifies the colony count at subsequent time intervals. This approach provides a reliable

estimation of the viable *E. coli* population, acknowledging that not all bacteria in the sample may successfully proliferate into a visible colony.

2.3.7 Monitoring of hydroxyl radicals

Hydroxyl radicals generated during electrolysis were analyzed by monitoring the conversion of dimethyl sulfoxide to dimethyl sulfone and detected by quantitative ^{1}H-NMR spectroscopy. Prior to the experiment, 1.0 µL of DMSO was added into 40 mL of electrolyte solution and passed through the three-electrode electrolysis protocol without added *E. coli*. In each timepoint, 0.5 mL of the electrolyte solution was sampled and stored for ^{1}H-NMR experiment. NMR experiments were performed on Bruker Avance 400 MHz or JEOL JNM-ECA 400 MHz spectrometers. All NMR data were processed and analyzed using Mestrenova software.

2.4 Results and discussion

2.4.1 Preliminary studies of electrolysis of tap water

Initial investigations utilized cyclic voltammetry to determine the onset potentials for electrolysis in the electrolyte solutions. Given the low conductivity of tap water, cyclic voltammetry was also conducted on tap water supplemented with 0.1 mol L^{-1} $NaHCO_3$. Figure 2.1 illustrates the voltammetric results with a significantly higher current generated in the spiked tap water due to the increased concentration of ions.

The electrolysis of water at neutral pH, as described by (2.1) and (2.2), involves the reduction of water to hydrogen gas and hydroxide ions at the cathode (negative electrode) and the oxidation of water to oxygen gas and hydrogen ions at the anode (positive electrode). These reactions generate an electric current, the magnitude of which increases with applied potential or overpotential, leading to a greater production of oxygen gas, hydrogen gas, acid, and base.

In a three-electrode setup, the minimum potential needed to oxidize tap water is approximately 1.9 V vs Ag/AgCl (3 mol L^{-1} KCl), as illustrated in Fig. 2.1. To

maximize bacterial inactivation, our study employed an overpotential to enhance the production of disinfecting agents.

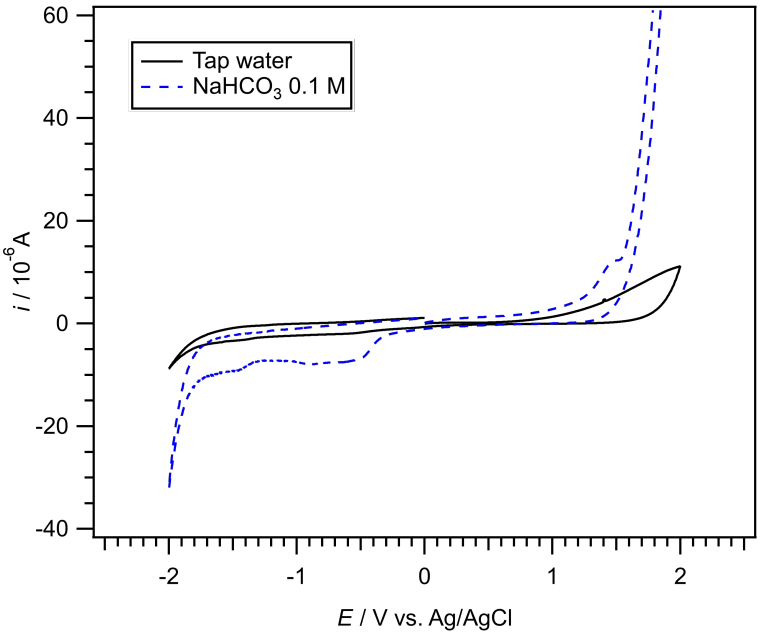

FIGURE 2.1: Cyclic voltammogram of tap water (solid black line) and 0.1 mol L^{-1} $NaHCO_3$ (dashed blue line). The scan was performed from 0 V to 2 V and -2 V, consecutively.

EQUATION 2.1: Water reduction equation in neutral conditions

$$2\,H_2O\,(l) + 2\,e^- \longrightarrow H_2\,(g) + 2\,OH^-\,(aq) \tag{2.1}$$

EQUATION 2.2: Water oxidation equation in neutral conditions

$$2\,H_2O\,(l) \longrightarrow 4\,e^- + 4\,H^+\,(aq) + O_2\,(g) \tag{2.2}$$

However, recognizing the potential limitations inherent, especially the detrimental potential drop, we proposed a mitigation strategy by adjusting the solution's conductivity via the introduction of additional electrolytes into the simulated tap water. Although the ultimate objective is to purify water without supplemental electrolytes, understanding their role in microbial inactivation, particularly in organisms like *E. coli*, was deemed essential. This necessity stems from tap water's low conductivity, attributable to its minimal ion content. The hypothesis was that enhancing conductivity through electrolyte addition would facilitate higher currents, thereby accelerating the generation of disinfecting agents and the subsequent

inactivation of microorganisms. This led to an investigative study examining the impacts of various electrolytes.

2.4.2 Inactivation of *E. coli* by platinized titanium electrode water electrolysis

2.4.2.1 General overview

Building on previous research and considering cost-effectiveness, platinized titanium was selected as a substitute for platinum. Given the limited existing research on bacterial inactivation using electrolyzed platinized titanium, particularly regarding the influence of different electrolytes, this study offers novel insights into *E. coli* inactivation under such conditions.

Utilizing platinized titanium for both working and auxiliary electrodes, the inactivation of *E. coli* was investigated in various electrolyte media, employing both potentiostatic (constant potential) and galvanostatic (constant current) modes. The advantages and disadvantages of each mode will be explored further. To assess *E. coli* inactivation, viable cell counts were determined using the plate counting method.

2.4.2.2 Comparing the deactivation efficacy between different electrolytes with similar ionic strength in two-electrode operations

The deactivation of *E. coli* in various electrolyte solutions was investigated to elucidate the influence of different anions on the inactivation process. The electrolytes chosen for this study were sodium chloride (NaCl), sodium bicarbonate ($NaHCO_3$), sodium sulfate (Na_2SO_4), and sodium dihydrogen phosphate (NaH_2PO_4), each prepared at similar ionic strengths to ensure comparability. These electrolytes were chosen because they are commonly found in potable water supplies.

To investigate the influence of electrolyte composition and ionic strength on the potential and current throughput of the electrolytic water treatment system, a series of experiments were conducted by applying a constant potential of 6 V across the electrodes, as illustrated in Fig. 2.2. The results indicate that, for a given

ionic strength, the choice of electrolyte did not significantly impact the current throughput. At an ionic strength of 10 mM, the current density averaged between 30 and 50 A m^{-2} across the various electrolytes tested. When the ionic strength was reduced to 1 mM, the average current density decreased to less than 10 A m^{-2}, irrespective of the electrolyte used. These findings suggest that ionic strength plays a more significant role in determining the current throughput of the electrolytic system than the specific electrolyte composition, within the range of electrolytes investigated in this study.

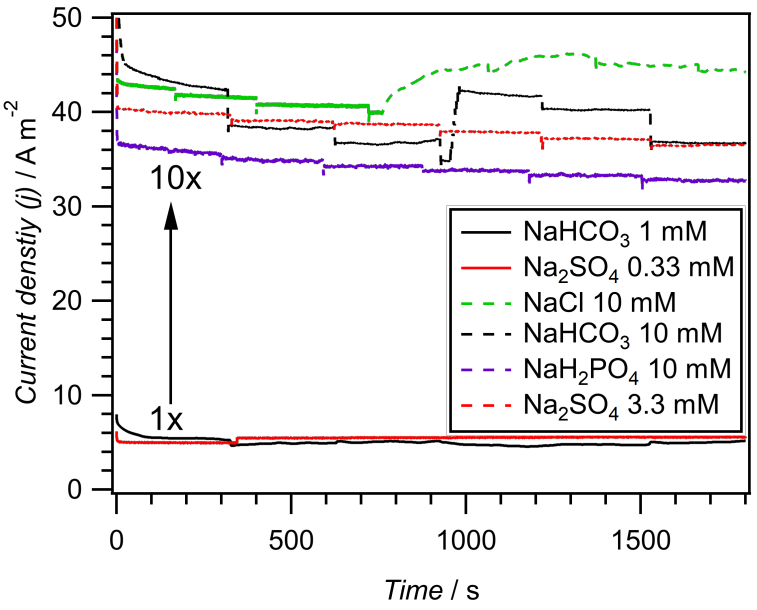

FIGURE 2.2: Current throughput over time for various electrolytes at different ionic strengths under a constant applied potential of 6 V. The current response is primarily dependent on the ionic strength, with electrolytes at 10 mmol L^{-1} ($NaCl$, Na_2SO_4, $NaHCO_3$, and NaH_2PO_4) and those at lower ionic strengths ($NaHCO_3$ and Na_2SO_4 at 1 mmol L^{-1}).

The inactivation kinetics of *E. coli* followed a logarithmic decay pattern, as evidenced by the linear relationship between the logarithm of the viable CFU ml^{-1} and treatment time (Fig. 2.3). This trend was consistent across the three electrolytes tested ($NaHCO_3$, NaH_2PO_4, and Na_2SO_4) at ionic strengths of 1 mmol L^{-1}. The logarithmic decay suggests that the inactivation process adheres to first-order kinetics, with the rate of bacterial deactivation proportional to the remaining active population.

Notably, the inactivation efficiency was comparable among the three electrolytes, despite their different chemical compositions. However, additional tests using

sodium chloride (NaCl) as the electrolyte resulted in a 6-log scale deactivation of the E. coli in the first 10 minutes (the data are not included in Fig. 2.2 as the concentrations drop to zero within 10 minutes so are not clearly represented on a logarithmic scale). The distinct efficacy using Cl^- as the electrolyte anion can be attributed to the generation of chlorine species during the electrolysis process. Chlorine is a well-known disinfectant that enhances the bactericidal activity of the system. When sodium chloride undergoes electrolysis, chloride ions (Cl^-) are oxidized at the anode, forming chlorine(Cl_2), hypochlorous acid (HOCl) and hypochlorite ions (OCl^-), which are potent antimicrobial agents. The presence of these chlorine species in the NaCl electrolyte solution contributes to the increased inactivation of *E. coli* compared to other electrolytes.

This observation indicates that the primary factor governing the inactivation process is the electrochemical generation of bactericidal species, such as reactive oxygen species (ROS) and other oxidants, rather than the specific electrolyte used. The electrolytes containing carbonate (HCO_3^-), phosphate ($H_2PO_4^-$), and sulfate (SO_4^{2-}) anions exhibited similar *E. coli* inactivation rates, as demonstrated by the parallel lines in Fig. 2.3. These anions do not directly contribute to the formation of bactericidal species during electrolysis. Instead, their primary function is to maintain the ionic strength and conductivity of the solution, ensuring efficient operation of the electrochemical cell.

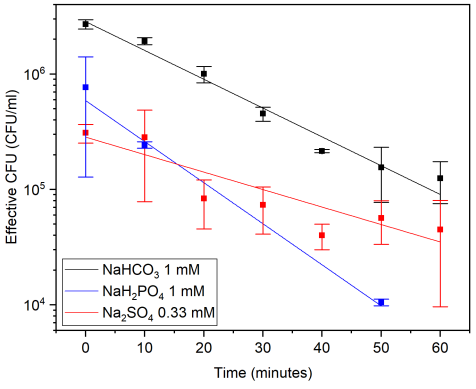

FIGURE 2.3: Inactivation kinetics of E. coli in the presence of different electrolytes ($NaHCO_3$, NaH_2PO_4, and Na_2SO_4) at ionic strengths of 1 mmol L^{-1} by applying constant current of 10 mA across two electrodes setting.

The effect of ionic strength on the inactivation kinetics of *E. coli* was further

investigated using $NaHCO_3$ as the electrolyte. As depicted in Fig. 2.4, the inactivation efficiency significantly improved when the ionic strength was increased from 1 mmol L^{-1} to 10 mmol L^{-1}. At 1 mmol L^{-1} ionic strength, a 1-log reduction in *E. coli* concentration was achieved after 60 minutes of treatment, while at 10 mmol L^{-1}, a 2-log reduction was observed within 20 minutes. Interestingly, at an ionic strength of 100 mmol L^{-1}, no appreciable inactivation was detected throughout the experimental duration.

To elucidate this phenomenon, the potential at the working electrode was examined for each ionic strength condition. At 1 mmol L^{-1} ionic strength, the potential exceeded 10 V (the upper limit of the instrument), while at 10 mmol L^{-1}, the average potential was approximately 6.5 V. In contrast, at 100 mmol L^{-1} ionic strength, the average potential was only 3 V. The lower potential observed at 100 mmol L^{-1} is likely insufficient to drive the water electrolysis reactions ((2.1) and (2.2)), resulting in diminished inactivation efficacy compared to the higher potentials attained at 1 mmol L^{-1} and 10 mmol L^{-1} ionic strengths. These findings support our hypothesis that the generation of reactive oxygen species (ROS) at the electrode surfaces is the primary contributor to *E. coli* inactivation, irrespective of the anion type.

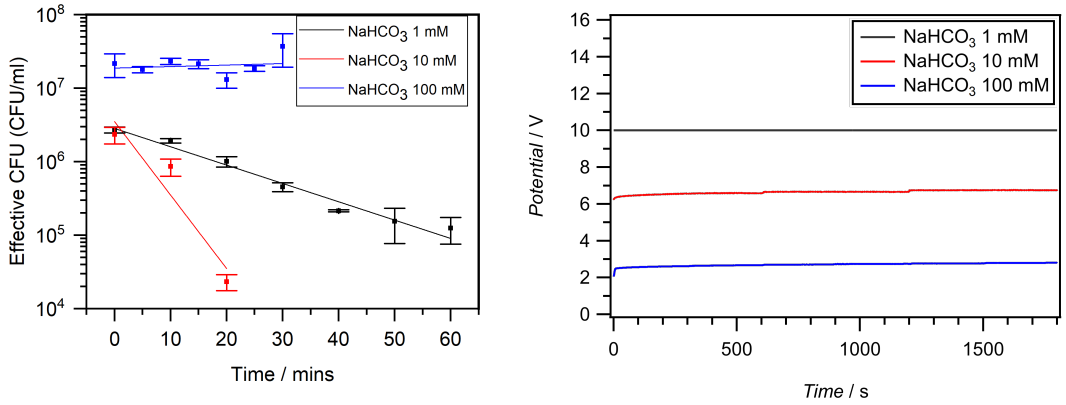

FIGURE 2.4: (Left) Inactivation kinetics of *E. coli* in the presence of $NaHCO_3$ electrolyte at various ionic strengths (1 mmol L^{-1}, 10 mmol L^{-1}, and 100 mmol L^{-1}) at the constant current of 10 mA in two-electrode configuration. (Right) Potentials at the working electrode as a function of time (chronopotentiometry) for $NaHCO_3$ electrolyte at different ionic strengths (1 mmol L^{-1}, 10 mmol L^{-1}, and 100 mmol L^{-1}) at the constant current of 10 mA.

The absence of a significant correlation between the anion type (except for NaCl) and *E. coli* inactivation suggests that the primary inactivation mechanism is not contingent upon the specific anion present. Instead, the deactivation process

appears to be governed by factors such as the generation of ROS at the electrode surface. ROS, including hydroxyl radicals ($OH^{\bullet}$), hydrogen peroxide (H_2O_2), and superoxide anions ($O_2^{\bullet -}$), are produced during water electrolysis and possess potent antimicrobial properties. The consistent inactivation patterns observed across various electrolytes indicate that the ROS-mediated inactivation mechanism is predominant and independent of the anion type. Additional explanations for *E. coli* deactivation include localized pH changes at the electrode surface due to water electrolysis and direct electroporation of the bacterial cells at the electrode surface, leading to cell membrane damage and lysis.

2.4.2.3 Achieving higher current throughout via three-electrode operation

This section delves into the comparative analysis between three-electrode and two-electrode configurations in the electrochemical treatment of water, emphasizing the superiority of the former in achieving higher current throughput, a critical factor in effective water purification processes. Electrolysis experiments were conducted using both configurations in water having similar ionic concentrations to that found in typical potable water, and the resultant currents at varying applied potentials were meticulously compared. Both configurations exhibited a consistent trend: an escalation in potential led to an increased current, conforming to Ohm's law. However, the three-electrode arrangement outperformed its two-electrode counterpart by generating substantially higher currents at equivalent potentials.

The enhanced performance of the three-electrode system is attributed to the potentiostat's ability to compensate for the voltage drop across the solution resistance (iR drop). While both configurations experience this voltage drop due to solution resistance, the three-electrode arrangement, coupled with the potentiostat's negative feedback circuitry, actively corrects for these losses. The reference electrode provides a stable potential reference point, allowing the potentiostat to adjust the applied voltage to maintain the desired potential at the working electrode despite solution resistance effects. In contrast, the two-electrode system lacks this compensation mechanism, resulting in an effective potential at the working electrode that is lower than the applied potential due to uncompensated solution resistance. The placement of the reference electrode near the working electrode helps minimize the resistance between these electrodes, enabling more accurate potential control.

Fig. 2.5 shows the current throughput through the chronoamperometry graph of 10 mmol L^{-1} $NaHCO_3$ at constant 6 V applied potential with respect to the counter electrode and Ag/AgCl reference electrode, in two-electrode and three-electrode arrangement, respectively. The average current throughput of the three-electrode arrangement is much higher at 110 mA, while the two-electrode arrangement shows moderate current throughput at 18 mA.

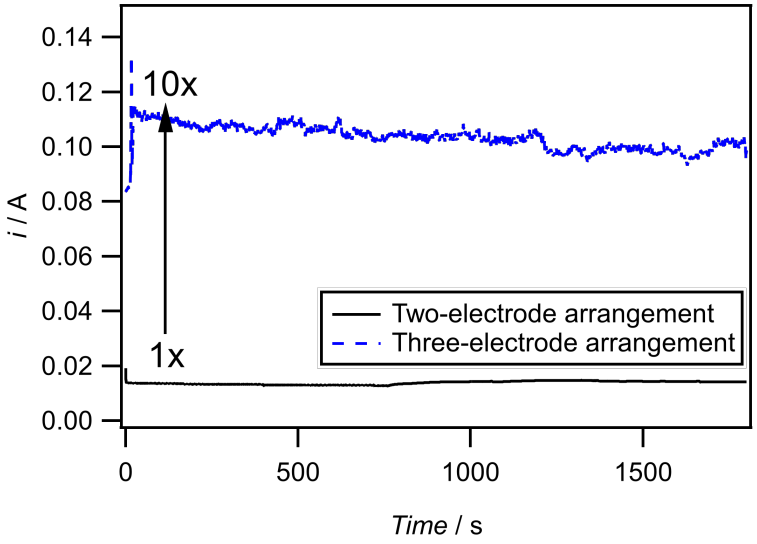

FIGURE 2.5: Chronoamperometry graph of 10 mM $NaHCO_3$ at 6 V applied potential with respect to the counter electrode (black solid line, two-electrode arrangement) and with respect to Ag/AgCl reference electrode (blue dashed line, three-electrode arrangement).

To investigate the impact of the higher current throughput in three-electrode systems on water treatment efficacy, the *E. coli* inactivation performance of the three-electrode arrangement was compared to that of the two-electrode arrangement mentioned in the Section 2.4.2.2. Fig. 2.6 presents representative experiments of *E. coli* inactivation in $NaHCO_3$ and Na_2SO_4 solutions at constant ionic strength and applied potential. In the three-electrode arrangements, every experiment achieved a 6-log reduction in *E. coli* within the first 5 minutes (Fig. 2.6, top), and even a 1-log reduction within the first minute (Fig. 2.6, bottom). This is an improvement over two-electrode configuration which only achieve modest 2-log reduction over 20 minutes (Fig. 2.4 (Left), red line). An examination of the chronoamperometry and chronopotentiometry data reveals a much higher current throughput (50 to 100 mA) in the three-electrode settings compared to the two-electrode settings. This observation leads to the hypothesis that the inactivation efficacy is a function of

the applied current, with higher currents resulting in more rapid and extensive bacterial inactivation.

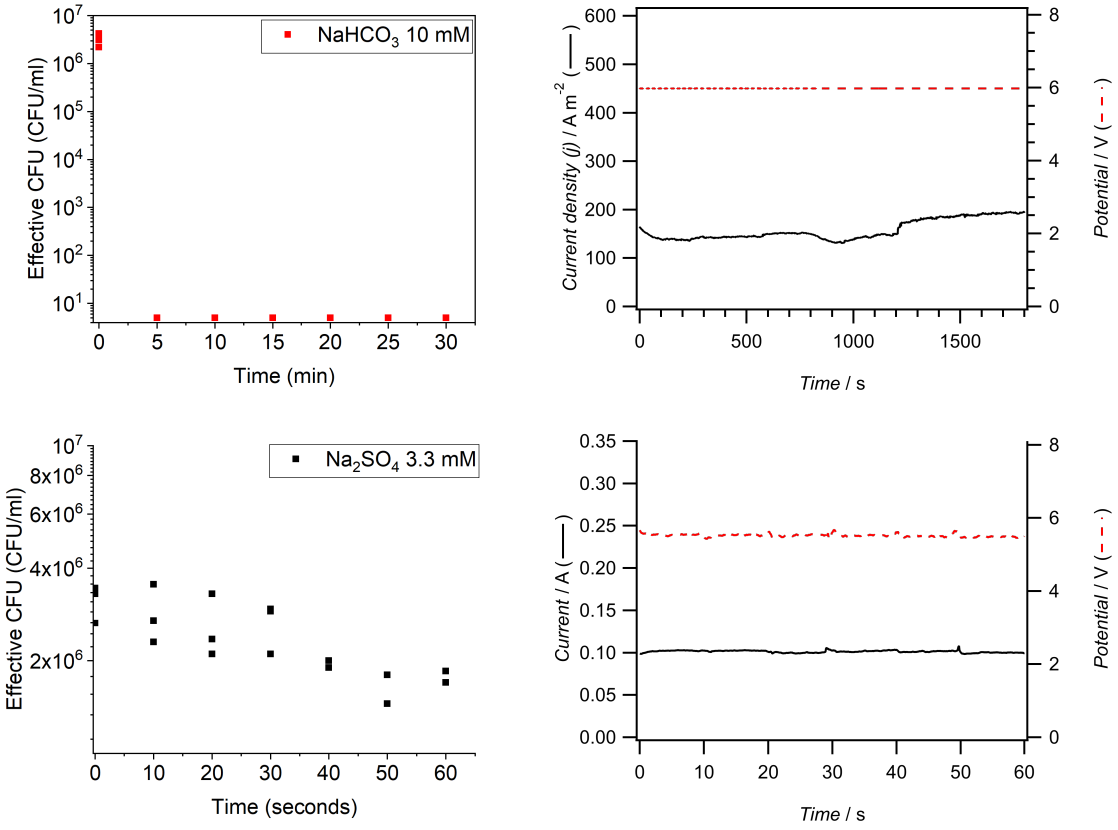

FIGURE 2.6: (Left) Inactivation kinetics of *E. coli* in the presence of $NaHCO_3$ and Na_2SO_4 at 10 mmol L^{-1} ionic strength at the constant applied potential of 6 V with respect to the Ag/AgCl reference electrode in three-electrode setup. (Right) Chronoamperometry (black solid line) and chronopotentiometry (red dashed line) of the same experiment.

2.4.3 Identification and quantification of hydroxyl radical generated from water electrolysis in three-electrode operations

The electrochemical inactivation of *E. coli* is a complex process that involves the generation of various oxidants during water electrolysis. Among these oxidants, hydroxyl radicals ($OH^{\bullet}$) are considered to play a pivotal role in the bacterial inactivation process. To better understand the mechanisms underlying electrochemical disinfection, it is essential to identify and quantify the oxidants generated, particularly the $OH^{\bullet}$ radicals.

The hypothesis of $OH^{\bullet}$ formation was a central focus of this study, investigating its role in the electrochemical inactivation process. Hydroxyl radicals are a highly reactive species with a short lifetime, making their direct detection challenging. To overcome this obstacle, an indirect approach was employed, utilizing the decomposition of dimethyl sulfoxide (DMSO) as a probe for $OH^{\bullet}$ quantification.

Nuclear magnetic resonance (NMR) spectroscopy was employed for the precise measurement of the sulfone formation. NMR is a powerful analytical technique that provides detailed structural information and enables the quantification of specific compounds in a mixture. The electrolyte solution containing DMSO was subjected to electrochemical treatment, and the samples were collected at various time intervals for NMR analysis.

DMSO is known to react selectively with $OH^{\bullet}$, and the resulting ^{1}H-NMR peaks were confirmed to be dimethyl sulfone as a stable product.[4] By monitoring the formation of the sulfone, it was possible to indirectly quantify the $OH^{\bullet}$ generated during the electrochemical process. Fig. 2.7 shown the time-dependent change of DMSO to dimethyl sulfone ($DMSO_2$) over the experiment timescale.

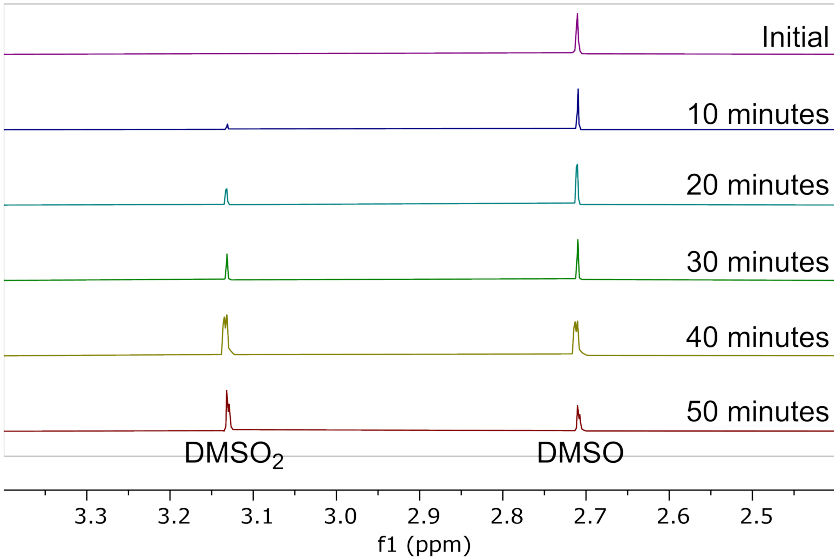

FIGURE 2.7: ^{1}H-NMR spectra of DMSO and dimethyl sulfone ($DMSO_2$) over time for the electrolysis of 10 mM $NaHCO_3$ under galvanostatic mode at 30 mA. The original concentration of DMSO prior the electrolysis being 3.5×10^{-4} mol L^{-1}.

The reaction between DMSO and $OH^{\bullet}$ was reported to be under first-order kinetics with respect to DMSO and $OH^{\bullet}$.[5] The derivation used in this chapter is as follows

$$Reaction\ rate = -\frac{d[DMSO]}{dt} = k[DMSO][\mathrm{OH}^\bullet] \tag{2.3}$$

Assuming [$\mathrm{OH}^\bullet$] produced (concentration of $\mathrm{OH}^\bullet$ produced) is constant over the experiment time, then

$$\frac{d[DMSO]}{[DMSO]} = -k[\mathrm{OH}^\bullet]dt \tag{2.4}$$

And integrate of both sides of the equation to obtain

$$ln\frac{[DMSO]_t}{[DMSO]_0} = -k[\mathrm{OH}^\bullet]t \tag{2.5}$$

A plot the ratio between $[DMSO]_t$ (concentration of DMSO at time t) and $[DMSO]_0$ (initial concentration of DMSO) over time (seconds) gives a slope of $-k[\mathrm{OH}^\bullet]$, with the kinetic constant (k) between DMSO and $\mathrm{OH}^\bullet$ reported to be $7.1 \times 10^9\,\mathrm{L\,mol^{-1}\,s^{-1}}$.[5,6] The correlation between time and the natural logarithm of DMSO concentrations is shown in Fig. 2.8.

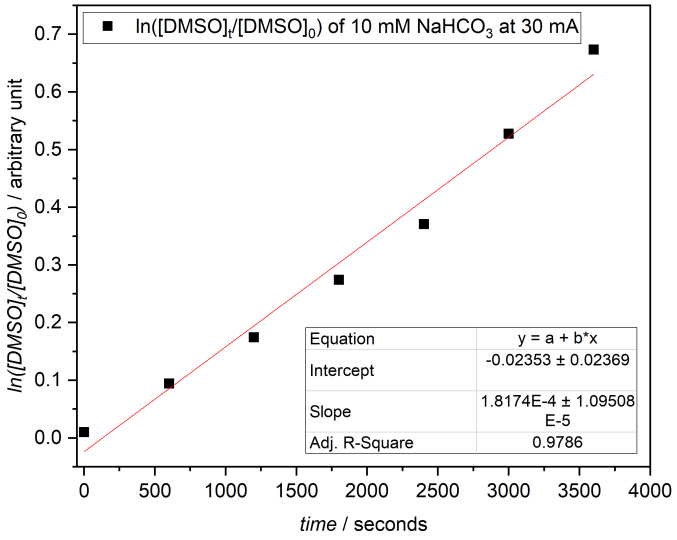

FIGURE 2.8: Correlation graph between natural log of the concentration of DMSO over time for electrolysis of 10 mmol $\mathrm{L^{-1}}$ $NaHCO_3$ under galvanostatic mode at 30 mA.

The NMR spectra of the treated samples revealed the presence of the sulfone, confirming the generation of $OH^{\bullet}$ during the electrochemical process. The intensity of the DMSO signal was found to decrease with treatment time, indicating a higher concentration of $OH^{\bullet}$ being produced. By comparing the degradation of DMSO signal intensity over time, it was possible to quantify the $OH^{\bullet}$ generated. The calculated $OH^{\bullet}$ concentration (ranging from 1×10^{-14} to 5×10^{-14} mol L^{-1}), was comparable to previous other quantification methods using fluorescence compounds.[7,8] To further investigate the factors influencing $OH^{\bullet}$ generation, the relationship between the applied current and the $OH^{\bullet}$ concentration was examined across different electrolytes, as shown in Fig. 2.9. The results suggest that the choice of electrolyte does not have a strong effect on the generation of $OH^{\bullet}$ during the electrochemical water treatment process. This finding implies that the applied current is the primary factor governing the production of $OH^{\bullet}$, regardless of the specific electrolyte used.

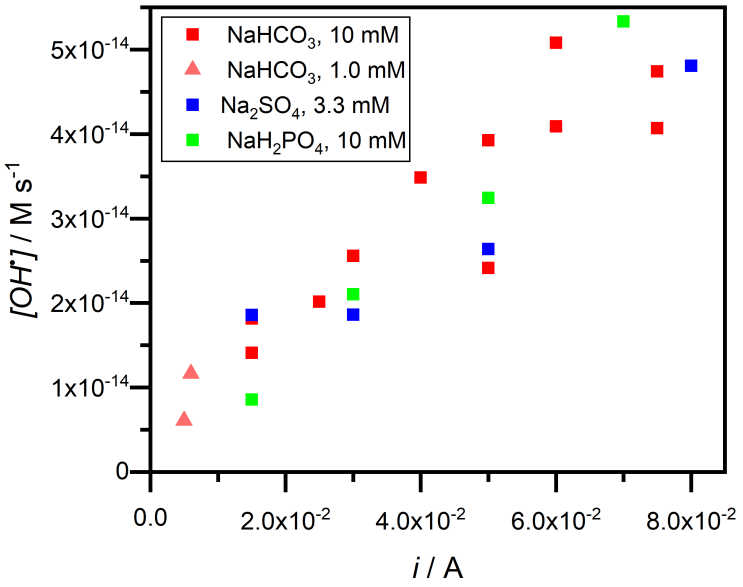

FIGURE 2.9: Correlation graph between calculated $OH^{\bullet}$ concentrations and applied current for various electrolyte types and concentrations.

The NMR analysis confirmed the presence of $OH^{\bullet}$ and suggested potential relationships between hydroxyl radical generation and *E. coli* inactivation. The data indicated a positive correlation between the quantity of $OH^{\bullet}$ generated and bacterial inactivation rates, where samples with higher measured $OH^{\bullet}$ concentrations generally showed faster inactivation of *E. coli* cells.

Other oxidant species, including hydrogen peroxide (H_2O_2) and ozone (O_3), may also play important roles in the inactivation process. While this study focused primarily on $OH^\bullet$, future work could investigate the relative contributions of these additional oxidants and potential synergistic effects in bacterial inactivation.

In summary, the analysis of DMSO decomposition using NMR spectroscopy enabled successful identification and quantification of $OH^\bullet$ generated during water electrolysis. The findings suggest $OH^\bullet$ may be an important factor in the electrochemical inactivation of *E. coli*. This improved understanding of potential disinfection mechanisms could help inform the optimization of electrochemical treatment systems, although further research is needed to fully elucidate the relative importance of different oxidant species.

2.4.4 Comparative analysis of platinized titanium electrode longevity and cost against alternative materials

This section presents a comprehensive comparison of various electrode materials for water treatment applications, analyzing their properties, advantages, and limitations against platinized titanium electrodes. The mechanism of water treatment typically involves initial water discharge at anode active sites (M), producing adsorbed hydroxyl radicals ($M(OH^\bullet)_{ads}$). These radicals facilitate organic pollutant destruction in aqueous solutions, competing with side reactions that form dioxygen, as described by Comninellis.[9] Electrodes can be categorized as either active or non-active based on their mechanism of action during electrochemical oxidation processes.[9] Active anodes involve surface changes during oxidation, with oxygen atoms forming covalent bonds with the anode surface. In contrast, non-active electrodes maintain surface stability and function primarily as electron transfer sites without direct participation in anodic oxidation reactions. Non-active anodes, such as boron-doped diamond, Ti_4O_7 and noble metals electrode (such as platinized titanium used in this work), are particularly efficient in advanced oxidation processes due to their capacity to generate hydroxyl radicals and secondary oxidants.[10,11]

The criteria used to determine the electrode longevity include:

- Physical stability and resistance to mechanical wear

- Chemical stability and corrosion resistance
- Maintenance of disinfection efficacy over time
- Operational lifespan under standard conditions

2.4.4.1 Alternative electrode materials

Pure platinum electrodes These electrodes exhibit excellent electrical conductivity and remarkable catalytic capabilities with superior corrosion resistance. Their low oxygen evolution potential makes them particularly effective for water treatment applications, as demonstrated by Brillas et al. in dichlophenac mineralization studies.[12] However, their high cost and low abundance limit widespread adoption.

Boron-doped diamond (BDD) electrodes BDD electrodes offer superior stability compared to conventional diamond electrodes and demonstrate high electrocatalytic activity with excellent chemical durability. While they exhibit the highest overpotential and require minimal maintenance, their complex preparation through chemical vapor deposition and associated costs restrict large-scale implementation.[13]

Mixed metal oxide (MMO) electrodes MMO electrodes present an economical alternative to BDD electrodes, offering enhanced stability compared to graphite electrodes and suitability for high current density applications. However, their stability and longevity characteristics do not match BDD standards.[13]

Graphite/carbon-based electrodes These electrodes feature extensive surface area and strong adsorption characteristics at relatively low cost. Their primary limitations include susceptibility to surface oxidation and scaling effects.[13]

Titanium suboxide electrodes While titanium dioxide exhibits poor conductivity, substoichiometric titanium oxide demonstrates enhanced conductivity. Magneli phase titanium has proven stable as an anode material, utilizing higher oxygen

evolution potential for hydroxyl radical production. These electrodes can be fabricated through various methods including CVD, coating, magnetron sputtering, and sol-gel processes.

Platinized titanium electrodes These electrodes combine platinum's benefits with titanium's structural integrity, offering high electrical conductivity, mechanical strength, and non-toxicity. Research by Zambrano and Min has demonstrated their effectiveness in phenol oxidation, with increased COD removal at higher current densities. They show particular promise for treating low biodegradability effluents and toxic materials.[14]

2.4.5 Scalability and integration with renewable energy sources

The development of effective water treatment systems requires careful consideration of scale and complexity. Traditional approaches to water treatment typically fall into two categories: point-of-use systems for small-scale applications and centralized facilities for large-scale industrial treatment. While large-scale systems employ comprehensive multi-step processes including coagulation, flocculation, sedimentation, and advanced filtration to achieve potable water standards, small-scale systems often rely on simpler, passive treatment methods such as basic filtration and precipitation.[15]

Small-scale water treatment systems for remote applications face unique challenges. These include limited resource availability, energy constraints, and the risk of compromised water quality when simplifying treatment processes.[16] Current research highlights a significant gap in developing systems that can produce high-quality potable water while maintaining a small footprint and minimal resource requirements.[17] The development of such systems is particularly crucial for remote communities without access to centralized water treatment infrastructure.

Electrochemical water treatment methods offer a promising solution to these challenges. These systems can effectively eliminate pathogens and chemical contaminants without requiring additional reactive chemicals or high-pressure conditions. However, several engineering challenges must be addressed,[18–21] including:

- Electrode fouling and degradation
- Power control requirements
- System robustness across varying water qualities
- Optimal electrode configuration and placement

The findings from this study suggest that a three-electrode system utilizing platinized titanium electrodes could provide a viable solution for small-scale water treatment. The replacement of conventional two-electrode power supplies with miniaturized potentiostats enables effective bacterial inactivation even with readily available electrode materials. This approach offers several advantages for remote applications:

- Improved control over the treatment process through precise potential regulation
- Efficient operation at low electrolyte concentrations
- Compatibility with renewable energy sources
- Simple maintenance through easily replaceable electrodes

The potential integration with renewable energy sources, such as solar panels or small-scale wind turbines, makes this system particularly suitable for remote locations lacking reliable grid power. Furthermore, the system's ability to operate effectively with minimal infrastructure requirements addresses many of the challenges typically associated with remote water treatment applications.

These findings contribute to bridging the research gap between large-scale water treatment facilities and small-scale point-of-use systems, offering a potential pathway for providing safe drinking water in remote or resource-limited settings. Future development should focus on optimizing system design for specific deployment scenarios and further evaluating long-term performance under varied environmental conditions.

2.5 Conclusion

In this chapter, the feasibility of using platinized titanium electrodes for the electrochemical inactivation of *Escherichia coli* in water was investigated. The study aimed to elucidate the mechanisms underlying the disinfection process and identify the key factors influencing the inactivation efficiency.

The inactivation of *E. coli* in various electrolyte solutions followed a logarithmic decay pattern, with no significant differences observed among the electrolytes tested, except for sodium chloride. The enhanced bactericidal activity in the presence of NaCl was attributed to the generation of chlorine species. The consistent inactivation patterns across various ionic strengths and bacterial concentrations suggest that the primary mechanism of deactivation is ROS-mediated and independent of the specific anion present in the electrolyte.

The comparative analysis between three-electrode and two-electrode configurations revealed the superiority of the three-electrode system in achieving higher current throughput, a critical factor in effective water purification processes. The enhanced performance of the three-electrode system was attributed to its significantly lower internal resistance, facilitated by the inclusion of a reference electrode with a stable potential.

The identification and quantification of hydroxyl radicals generated during water electrolysis were successfully achieved through the analysis of DMSO decomposition using NMR spectroscopy. The findings underscore the crucial role of hydroxyl radicals in the electrochemical inactivation of *E. coli*. A strong correlation was observed between the quantity of hydroxyl radicals generated and the degree of bacterial inactivation achieved.

In conclusion, this study demonstrated the feasibility of using platinized titanium electrodes for the effective inactivation of *E. coli* in water through electrochemical processes. The insights gained into the mechanisms of disinfection, the influence of different electrolytes, and the role of hydroxyl radicals contribute to a better understanding of the electrochemical water treatment process. These findings have several potential practical applications, particularly in small-scale water treatment systems for remote communities. The demonstrated effectiveness at low electrolyte concentrations suggests possible implementation in treating natural water sources

without chemical additives, while the rapid disinfection rates observed in the three-electrode system could be valuable for point-of-use water purification devices.

However, several limitations of this study should be acknowledged. The experiments were conducted under controlled laboratory conditions using a single bacterial strain, and real-world applications would need to address more complex microbial communities and varying water qualities. Additionally, while the study demonstrated effective bacterial inactivation, it did not address the removal of other potential contaminants such as viruses, protozoa, or chemical pollutants. The scalability of the three-electrode system, while promising in terms of performance, may face practical challenges in field implementation due to the complexity of maintaining reference electrode stability in continuous operation.

Experiments in three-electrode mode indicate that fast disinfection is feasible even at low electrolyte concentrations, meaning that electrochemical disinfection may be carried out in natural waters without the need of added electrolytes under potentiostatic or galvanostatic control. This finding has particular relevance for developing portable water treatment systems, though further research is needed to optimize the design for practical deployment.

Additionally, while this study demonstrated effectiveness against *E. coli* as a model organism, future research should examine the system's performance with more complex microbial communities. This could include testing against mixed bacterial populations commonly found in natural water sources, as well as investigating the system's efficacy using real potable water samples spiked with various microorganisms. Such studies would better reflect real-world conditions and provide valuable insights into the system's practical effectiveness. Particular attention should be paid to potential variations in disinfection efficiency across different bacterial species, as well as any selective pressure that might arise during the treatment process. This expanded testing would help validate the technology's applicability for real-world water treatment scenarios and identify any limitations or necessary modifications for treating diverse microbial populations.

References

(1) Tonanon, P.; Webster, R. D. Recent electrode and electrolyte choices for use in small scale water treatment applications—A short review. *Current Opinion in Electrochemistry* **2023**, *38*, 101211.

(2) Chaplin, B. P. The Prospect of Electrochemical Technologies Advancing Worldwide Water Treatment. *Accounts of Chemical Research* **2019**, *52*, Publisher: American Chemical Society, 596–604.

(3) Deng, Y.; Zhao, R. Advanced Oxidation Processes (AOPs) in Wastewater Treatment. *Current Pollution Reports* **2015**, *1*, Company: Springer Distributor: Springer Institution: Springer Label: Springer Number: 3 Publisher: Springer International Publishing, 167–176.

(4) Westwood, S. Rapport BIPM-2018/04: Internal Standard Reference Data for qNMR: Dimethyl sulfone. **2018**.

(5) Dorfman, L. M.; Adams, G. E. In Edition: 0 Report Number: NBS NSRDS 46, National Bureau of Standards: Gaithersburg, MD, 1973, NBS NSRDS 46.

(6) Panganamala, R. V.; Sharma, H. M.; Heikkila, R. E.; Geer, J. C.; Cornwell, D. G. Role of hydroxyl radical scavengers dimethyl sulfoxide, alcohols and methional in the inhibition of prostaglandin biosynthesis. *Prostaglandins* **1976**, *11*, 599–607.

(7) Tai, C.; Xiao, C.; Zhao, T.; Wu, L.; Han, D. Determination of hydroxyl radicals photochemically generated in surface waters under sunlight by high performance liquid chromatography with fluorescence detection. *Analytical Methods* **2014**, *6*, Publisher: The Royal Society of Chemistry, 8193–8199.

(8) Wang, B.; Shi, H.; Habteselassie, M. Y.; Deng, X.; Teng, Y.; Wang, Y.; Huang, Q. Simultaneous removal of multidrug-resistant *Salmonella enterica* serotype typhimurium, antibiotics and antibiotic resistance genes from water by electrooxidation on a Magnéli phase Ti4O7 anode. *Chemical Engineering Journal* **2021**, *407*, 127134.

(9) Comninellis, C. Electrocatalysis in the electrochemical conversion/combustion of organic pollutants for waste water treatment. *Electrochimica Acta* **1994**, *39*, 1857–1862.

(10) Comninellis, C.; Kapalka, A.; Malato, S.; Parsons, S. A.; Poulios, I.; Mantzavinos, D. Advanced oxidation processes for water treatment: advances and trends for R&D. *Journal of Chemical Technology & Biotechnology* **2008**, *83*, _eprint: https://scijournals-onlinelibrary-wiley-com.remotexs.ntu.edu.sg/doi/pdf/10.1002/jctb.1873 769–776.

(11) Fu, R.; Zhang, P.-S.; Jiang, Y.-X.; Sun, L.; Sun, X.-H. Wastewater treatment by anodic oxidation in electrochemical advanced oxidation process: Advance in mechanism, direct and indirect oxidation detection methods. *Chemosphere* **2023**, *311*, 136993.

(12) Brillas, E.; Garcia-Segura, S.; Skoumal, M.; Arias, C. Electrochemical incineration of diclofenac in neutral aqueous medium by anodic oxidation using Pt and boron-doped diamond anodes. *Chemosphere* **2010**, *79*, 605–612.

(13) Jiang, Y.; Zhao, H.; Liang, J.; Yue, L.; Li, T.; Luo, Y.; Liu, Q.; Lu, S.; Asiri, A. M.; Gong, Z.; Sun, X. Anodic oxidation for the degradation of organic pollutants: Anode materials, operating conditions and mechanisms. A mini review. *Electrochemistry Communications* **2021**, *123*, 106912.

(14) Zambrano, J.; Min, B. Electrochemical treatment of leachate containing highly concentrated phenol and ammonia using a Pt/Ti anode at different current densities. *Environmental Technology & Innovation* **2020**, *18*, 100632.

(15) Diaz-Elsayed, N.; Rezaei, N.; Guo, T.; Mohebbi, S.; Zhang, Q. Wastewater-based resource recovery technologies across scale: A review. *Resources, Conservation and Recycling* **2019**, *145*, 94–112.

(16) Hube, S.; Wu, B. Mitigation of emerging pollutants and pathogens in decentralized wastewater treatment processes: A review. *Science of The Total Environment* **2021**, *779*, 146545.

(17) Paul, R.; Kenway, S.; Mukheibir, P. How scale and technology influence the energy intensity of water recycling systems-An analytical review. *Journal of Cleaner Production* **2019**, *215*, 1457–1480.

(18) Clematis, D.; Panizza, M. Electrochemical oxidation of organic pollutants in low conductive solutions. *Current Opinion in Electrochemistry* **2021**, *26*, 100665.

(19) Mousset, E. Interest of micro-reactors for the implementation of advanced electrocatalytic oxidation with boron-doped diamond anode for wastewater treatment. *Current Opinion in Electrochemistry* **2022**, *32*, 100897.

(20) McBeath, S. T.; English, J. T.; Wilkinson, D. P.; Graham, N. J. D. Circumneutral electrosynthesis of ferrate oxidant: An emerging technology for small, remote and decentralised water treatment applications. *Current Opinion in Electrochemistry* **2021**, *27*, 100680.

(21) Sandoval, M. A.; Calzadilla, W.; Salazar, R. Influence of reactor design on the electrochemical oxidation and disinfection of wastewaters using boron-doped diamond electrodes. *Current Opinion in Electrochemistry* **2022**, *33*, 100939.

Chapter 3

A comparison of the detection and quantification of Praziquantel via Electrochemical and Gas Chromatography Methods in Freshwater and Saltwater Samples

3.1 Abstract

Two new techniques for analyzing Praziquantel (PZQ), an effective antiparasitic drug used in fresh and saltwater aquariums, were optimized and compared. One method was based on voltammetry and one method used gas chromatography combined with mass spectrometry (GC-MS), although both procedures utilized the same sample pretreatment strategy for saltwater samples which involved the PZQ being quantitatively transferred into acetonitrile using solid phase extraction. GC-MS analysis led to lower limits of detection ($0.16\,\mu mol\,L^{-1}$) and quantification ($0.48\,\mu mol\,L^{-1}$) compared to voltammetry, although both methods gave acceptable quantification for levels of PZQ $> 2.5\,\mu mol\,L^{-1}$. GC-MS is preferred for the most accurate determination, but voltammetry may provide a cost-effective alternative for detecting PZQ where on-site testing is required.

3.2 Introduction

Praziquantel (PZQ), also known as 2-(cyclcohexylcarbonyl)-1,2,3,6,7,11b-hexahydro-4H-pyrazino [2,1a] isoquinolin-4-one, is a synthetic drug that was discovered by Bayer in the 1970s. It is one of the most commonly used anthelmintic drugs in medicine with strong efficacy against a broad range of cestodes (tapeworms) and trematodes (flukes).[1] The exact mechanism of its functionality is largely unknown, with the leading hypothesis suggesting that PZQ may have multiple pharmacologically relevant targets and the effects on these may synergize through protein-protein interactions to produce an overall detrimental effect on the parasite.[2] As PZQ is effective amongst a wide range of hosts, it has also found applications in veterinary science, especially in aquaculture.[3] With the wide consumption of PZQ, it would be beneficial to develop a method that could easily determine the PZQ content in aquatic environments rapidly and accurately.

The accurate detection and quantification of active pharmaceutical ingredients (APIs), PZQ included, represents critical aspects of analytical chemistry research, development, and quality control. Accurate API detection and quantification methods are essential in surveillance and regulatory compliance. In recent years, advancements in analytical techniques and instrumentation have led to more sophisticated and sensitive methods for API detection and quantification, contributing

significantly to analytical chemistry research. Previous review articles can be attributed to the different approaches of detection of API.[4–11] Recent studies have demonstrated successful API detection using carbon-based electrodes,[12,13] modified glassy carbon electrodes,[14] and screen-printed electrodes.[15–17] Previous review articles can be attributed to the different approaches of detection of API.

Various methods have been developed to determine the PZQ content in different matrices, including high performance liquid chromatography (HPLC),[18,19] liquid chromatography with tandem mass spectrometry (LC-MS/MS),[20,21] near infrared spectroscopy (NIS),[22] and capillary electrophoresis (CE).[23] Electrochemical methods are also attractive since they have simpler less expensive instrumentation that can be portable. However, although electrochemical methods offer good sensitivity and simpler instrumentation, they often suffer more interference problems than chromatography methods,[24–26] therefore, the exact method that is used will depend critically on the complexity of the sample matrix.

The electrochemistry of PZQ in aqueous solution was first studied by Rizk et al. using a dropping mercury electrode under basic conditions,[24] and it was proposed that PZQ underwent reduction at the carbonyl group. The authors applied this method to analyze spiked human urine and blood plasma without pretreatment and obtained near identical recoveries. Another study by Ghoneim, Mabrouk, and Tawfik proposed a single 2-electron irreversible reduction wave in acidic aqueous conditions.[25] The authors developed a voltammetric procedure based on cathodic adsorptive stripping differential-pulse voltammetry on a hanging mercury drop electrode. Separately, Radia and Hassanein proposed the indirect determination of praziquantel through nitration to produce more electroactive nitro-praziquantel derivatives.[26] This method also relied on the adsorptive nature of a hanging mercury drop electrode and differential-pulse techniques. Nevertheless, despite the development of various voltammetric detection methods for the determination of PZQ, the use of hanging mercury drop electrodes has largely been phased out due to safety and environmental concerns over mercury use.

While all the published reports on voltammetric studies conducted on PZQ were performed in aqueous solutions, preliminary work from the present laboratory found that PZQ undergoes a chemically irreversible oxidation wave on a glassy carbon (GC) electrode in acetonitrile (MeCN) at a relatively positive potential (*vide infra*). This discovery presented an opportunity to utilize MeCN for the analysis

medium, which offers a wide potential window for the determination of PZQ instead of relying solely on aqueous solutions and mercury-based electrodes, where the oxidative response cannot be observed due to the lesser usable potential window of water. Since PZQ is soluble in both aqueous solutions and organic solvents, the application of solid-phase extraction (SPE) for PZQ determination addressed the issue of the solvent background response in aqueous solutions.[27,28] Furthermore, this extraction method simultaneously eliminates water-soluble interferences present in the sample solution while achieving excellent selectivity. Hence, the present chapter focuses on investigating and optimizing a voltammetric method that employs MeCN as the solvent medium for the quantitative determination of PZQ extracted from fresh and saltwater samples and comparing the results with that from GC-MS analysis on the same SPE treated samples.

3.3 Materials and methods

3.3.1 Chemicals

PZQ (CRS Grade) was obtained from United State Pharmacopeia. MeCN and methanol used in all experiments were either high-performance liquid chromatography or analytical reagent grades. Purified water, with a resistivity $\geq 18\,\mathrm{M\Omega\,cm}$, was obtained from an ELGA Purelab Option-Q system. Tetrabutylammonium hexafluorophosphate (n-Bu_4NPF_6) was used as the supporting electrolyte for electrochemical experiments and was prepared following a literature procedure[29] by reacting equimolar amounts of aqueous solutions of n-Bu_4NOH (40%, Alfa Aesar) and HPF_6 (65%, Fluka), washing the white precipitate with water until the pH was neutral, recrystallizing three times from hot ethanol and drying under vacuum at 413 K for 6 h. Artificial saltwater was prepared by dissolving the correct amount of Blue Treasure™aquarium salt. Aquarium saltwater was obtained courtesy of S.E.A. aquarium, Singapore.

3.3.2 Sample preparation and PZQ extraction

Samples of PZQ dissolved in artificial freshwater and artificial saltwater were prepared by dissolving the correct solid amount of PZQ in aqueous solutions. Oasis

Hydrophilic-Lipophilic Balanced Copolymer (HLB) SPE cartridges (6 mL, 500 mg sorbent, 60 µm pore size) were used to extract PZQ from simulated solutions in a similar procedure used previously to extract caffeine[27] and capsaicinoids[28] from foods and beverages.[27,28] The 5-step extraction procedures involved conditioning, equilibrating, sample loading, washing, and eluting. The cartridge was conditioned with methanol (6 mL) and equilibrated with water (6 mL). The sample solution (100 mL) was loaded into the cartridge and subsequently washed with water (6 mL). MeCN (10 mL) was used to elute PZQ from the cartridge into a vial containing preweighed supporting electrolyte (388 mg). After each step, air was pushed through the cartridge to remove any excess solvent. The concentration of PZQ in the eluted solution was 10 times the sample solution through this process (verified by performing PZQ recovery tests on the PZQ procedure). The SPE protocol procedure and steps are summarized in Figure 3.1. For consistency, the GC-MS and electrochemical analysis of all samples was performed after they had undergone the SPE procedure, without the last step of preweighed supporting electrolyte..

3.3.3 Instrumentation

GC-MS analysis was performed on an Agilent 7890A gas chromatography system coupled with an Agilent 5975C mass spectrometer. A ZB-5MS Guardian (7HG-G010-11-GGA) column (30 m x 0.25 mm x 0.25 µm) was used for chromatography. Initial oven temperature of 50 °C was maintained for 1 min and then increased to 300 °C at a rate of 20 °C min^{-1} followed by holding at 300 °C for 5 min. The injection size was 2 µL in split (4:1) mode. Helium (high purity grade, 99.999%, Leeden National Oxygen) was used as the carrier gas (1.2 mL min^{-1}). The injector temperature was set at 200 °C, while the MS transfer line temperature was set at 280 °C. The MS source temperature was set to 230 °C and the MS quad temperature was set to 150 °C. The electron impact (EI) mode was set to 70 eV for sample ionization. The mass spectrometer acquisition parameter was set to SCAN mode (m/z: 20.00 – 350.00) for the preliminary analysis and SIM mode (m/z: 55.00, 83.10, 132.00, 145.00, 173.10, 181.10, 185.10, 201.10, and 312.20) for the quantification.

All voltammetric experiments were carried out using a Metrohm Autolab PG-STAT302N potentiostat controlled by NOVA software. Voltammetry experiments in MeCN were conducted in a three-electrode cell configuration. A 3 mm diameter

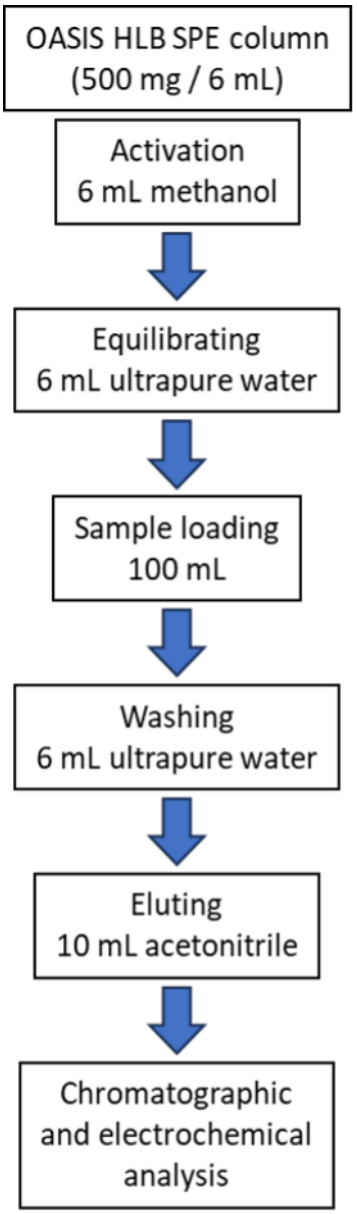

FIGURE 3.1: Solid-phase extraction protocol of PZQ in freshwater and saltwater

circular glassy carbon electrode was used as the working electrode, a platinum wire as the auxiliary electrode, and a miniature silver wire connected to the test solution via a salt bridge containing $0.5\,\mathrm{mol\,L^{-1}}$ n-Bu_4NPF_6 in MeCN was used as the reference electrode. voltammetric experiments were performed in MeCN containing $0.1\,\mathrm{mol\,L^{-1}}$ n-Bu_4NPF_6 as the supporting electrolyte at 22 °C in a Faraday cage. Potentials were calibrated using ferrocene (Fc) as the internal standard. Cyclic voltammograms (CVs) were obtained at a scan rate of $0.1\,\mathrm{V\,s^{-1}}$, while square-wave voltammograms (SWVs) were recorded with a pulse period of 25 Hz, potential step of 2 mV, and pulse amplitude of 50 mV which had been optimized to obtain the

best peak shape and peak height.

3.3.4 Validation and statistical analysis

To evaluate the effectiveness of both methods in quantifying PZQ from samples taken from both artificial freshwater and artificial saltwater sources, a comprehensive validation process was undertaken. This validation encompassed key parameters such as target specificity, linearity, detection limits, precision, repeatability, and accuracy. The GC-MS method was validated and established as the reference standard against which the electrochemical results were compared.

Given the intricacies of sample extraction, linearity assessments were conducted based on three replicates for the GC-MS method and seven replicates for the electrochemical method. The calibration curves were established using the internal standard method, where known concentration of the analyte is spiked, and subsequent measurements were taken. PZQ standard solutions were prepared from CRS grade PZQ obtained from United State Pharmacopeia to serve as the analytical standard. Each calibration point was analyzed in triplicate injection for the GC-MS method and measured seven independent times by the electrochemical method. The concentration levels used to construct the analytical curves was 1.6, 3.2, 6.4, 12.8, 19.1, 25.5, and 31.8 µmol L^{-1} for GC-MS method (0.5 – 10 ppm equivalent), and 5.0, 10.0, 15.0, 20.0, 25.0, and 30.0 µmol L^{-1} for electrochemical method. This ensured sufficient statistical sampling to reliably construct the standard addition calibration curves.

The determination of method detection and quantification limits relied on an ICH method based on standard deviation. The calibration curve enabled estimation of the minimum PZQ concentration that could be detected and quantified with acceptable accuracy. The detection limit was calculated to be 3.3 times the standard deviation of response over the slope of the calibration curve, and the quantification limit was calculated to be 10 times the standard deviation of the response over the slope of the calibration curve, based on the ICH Guideline: Validation of Analytical Procedures Q2(R1).[30] The precision was evaluated by calculating the pooled standard deviation across measurements, while accuracy was assessed by comparing the measured values to the declared concentrations of reference materials. Intermediate precision assessments were conducted over random experimental days.

Precision, accuracy, and intermediate precision measurements were carried out with three replicates for various concentration ranges (12.7 and 25.5 µmol L^{-1} for GC-MS method, and 10.0, 15.0, 20.0 µmol L^{-1} for electrochemical method), all performed by the same analyst on the same day within the same batch, thereby demonstrating within-run variation for routine applications.

To compare the performance of the GC-MS method and the electrochemical method, paired comparison of means between the results utilizing Student's t-test ($p<0.05$) and F-test at 15.0 µmol L^{-1} were employed as chosen methods for this assessment.[31]

3.4 Results and discussion

GC-MS is the most reliable and accurate quantification method for many low molecular weight species dissolved in organic media, so it was adopted as the gold standard identification and quantitative determination of PZQ in MeCN. The experimental mass fragmentation of praziquantel was identified to be m/z 55, 83.1, 132.1, 145, 173.1, 181.1, 185.1, 201.1, 312.2 and 99% matched with the National Institute of Standards and Technology (NIST) library,[32] as shown in Figure 3.2.

3.4.1 GC-MS optimization

The GC-MS procedure was optimized to obtain the target specification as shown in Table 3.1 . The specifications were established based on the International Conference on Harmonization of Technical Requirements For Registration Of Pharmaceuticals For Human Use – Validation Of Analytical Procedures: Text And Methodology (ICH Q2 (R2)).[30] GC-MS coupled with purge and trap was unable to directly extract the PZQ from the aquarium water matrix because PZQ is a non-volatile compound with a melting point around 135 °C. According to United States Environmental Protection Agency, volatile compounds are compounds that convert to vapor readily at normal atmospheric pressure and temperature. Typically, solid compounds with melting points below 70 °C are considered volatile.

Direct injection of the simulated saltwater containing PZQ was not considered because of the likely clogging of the GC inlet with the very high concentration soluble salts that would also harm the column. Hence, the sample extraction via

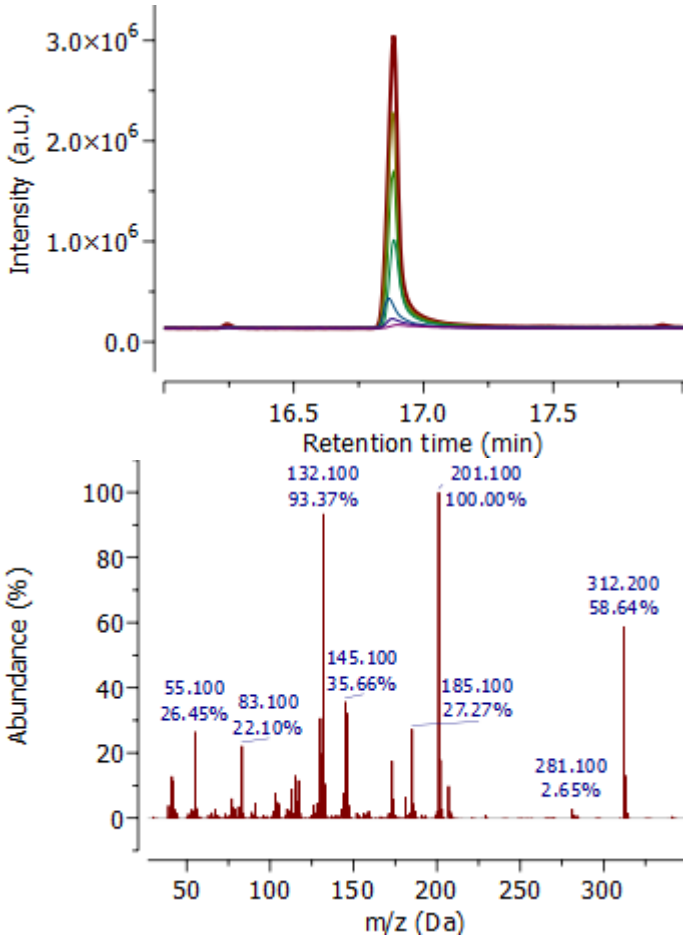

FIGURE 3.2: (top) Chromatograms obtained from samples containing different concentrations of PZQ in MeCN (16 µM, 32 µM, 64 µM, 0.13 mM, 0.19 mM, 0.25 mM, 0.32 mM). (top, Inset) Calibration plot of PZQ peak height with increasing concentration. (bottom) Mass spectrum obtained from the sample containing 0.32 mM PZQ.

the SPE treatment as shown in Figure 3.1 was adopted, enabling the GC-MS and electrochemical results to be directly compared. The column used is a mid-polar column, while a DB-Wax polar column that was also tested was found to be unable to detect PZQ from the extracts. An increase sample injection volume from 1 µL to 2 µL showed an increased sensitivity without traces of peak saturation.

3.4.2 Cyclic voltammetry and square wave voltammetry of PZQ

The electrochemical behavior of PZQ was initially explored in aqueous media. While PZQ exhibits limited solubility in water compared to organic solvents,[19] square

TABLE 3.1: Target specification for PZQ detection and quantification using GC-MS and electroanalysis method.

Specification parameters	Target value	GC-MS results	Electrochemistry results
Specificity	Absence of interference	No interference observed. The single peak has 99% similarity with the library data.	No interference observed.
Linearity	At least 0.95 coefficient of linearity	0.9902 for method calibration curve	0.9776 for method calibration curve
Limit of detection	Signal to noise = 3	MDL = 0.16 µmol L^{-1} and IDL = 0.32 µmol L^{-1}	MDL = 0.87 µmol L^{-1}
Limit of quantification	3 times signal to noise	MDL = 0.48 µmol L^{-1} and IDL = 0.72 µmol L^{-1}	MDL = 2.61 µmol L^{-1}
Precision	Within 5% standard deviation	Within 5% standard deviation	Within 5% standard deviation
Repeatability test	Within 5% relative standard deviation Within 95% confidence interval	SD and RSD are less than 5% at 95% confidence interval	SD and RSD are less than 5% at 95% confidence interval
Intermediate precision	Within 10% standard deviation Within 10% relative standard deivation Within 95% confidence interval	Pooled RSD at 95% confidence interval covering the whole working range is 7.70%	Pooled RSD at 95 % confidence interval covering the whole working range is 7.14%
Accuracy	80% to 120% of declared content	Between 84% to 108% across working range	Between 80% to 120% across the working range

MDL: Method Detection Limit; IDL: Instrument Detection Limit; MQL: Method Quantification Limit; IQL: Instrument Quantification Limit

wave voltammetry enabled its successful detection. As shown in Figure 3.3, a distinct oxidation peak for PZQ was observed at 0.175 V vs. Ag/AgCl in phosphate buffer solution (PBS). Further investigation revealed that the detectability of PZQ is pH dependent. Notably, lower pH values resulted in an increased peak current (δ current), as illustrated in Figure 3.4. This suggests that pH influences the electrochemical oxidation process of PZQ.

Nevertheless, although PZQ could be detected in aqueous PBS buffer, it was found that artificial seawater samples suffered from major interference due to the oxidation of chloride, resulting in poor electrochemical quantification. Therefore, electrochemical experiments were shifted towards organic solvents where PZQ exhibit good solubility, suitable for electrochemical analysis. Acetonitrile was chosen due to its wide potential window and high dielectric properties. In addition, the n-Bu_4NPF_6 electrolyte was selected for its compatibility with the wide potential window and

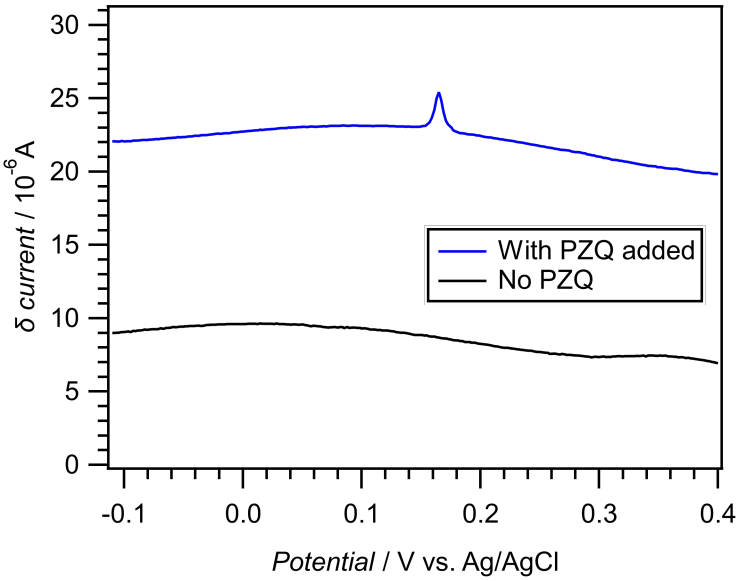

FIGURE 3.3: Square wave voltammogram obtained from samples containing 16 µmol L^{-1} (5 ppm) of PZQ (blue) compared to blank (black) in pH 5 citrate buffer

its inert nature, and it is commonly used in non-aqueous electrochemistry experiments. Notably, previous studies that investigated PZQ in aqueous solutions recommended the use of a high-density mercury drop electrode (HDME) for better surface cleanliness.[24–26]

In the initial experimental phase, the oxidation of 1 mM PZQ in acetonitrile containing 0.1 mol L^{-1} n-Bu_4NPF_6 was examined on glassy carbon electrodes. Glassy carbon electrodes were chosen for their electrochemical inertness and the broad potential window they offer in acetonitrile. PZQ exhibited a chemically irreversible oxidation wave, as illustrated in Figure 3.5, occurring at a relatively positive potential of 1.6 V vs. Fc/Fc^+ (where Fc = ferrocene).

3.4.3 Electrochemical detection of PZQ

To demonstrate the sensitivity of SWV for PZQ using the oxidation peak at 1.6 V vs. Fc/Fc+, experiments were conducted covering a concentration range of 25 µM to 0.25 mM, which is similar to the PZQ concentrations added to aquarium water (Figure 3.6). At these lower PZQ concentrations, additional very broad peaks were also detected at less positive potentials (ca. 0.4 – 0.8 V vs. Fc/Fc+), but these did not scale uniformly with concentration and were possibly associated with

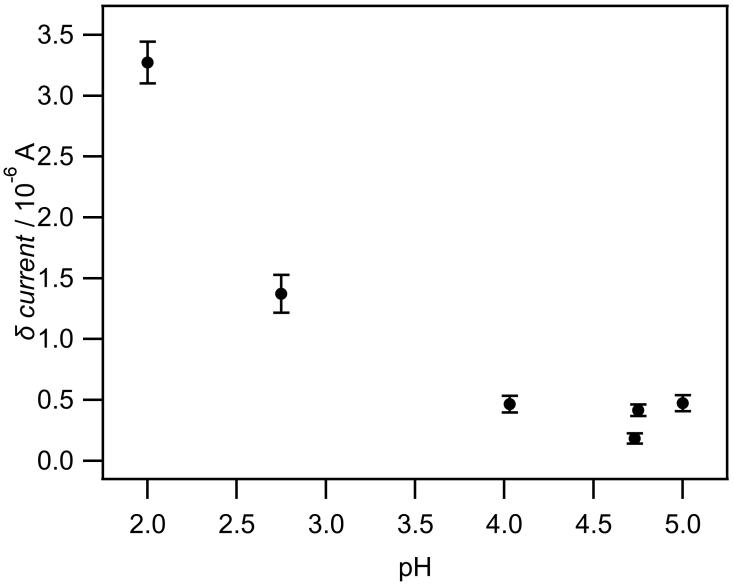

FIGURE 3.4: Baseline-substracted δ current obtained from square wave voltammograms of 1 ppm PZQ in PBS buffer at different pH. Error bar obtained from 5 replicates.

weak adsorption responses and so were not used for quantification purposes. A linear relationship was observed for the anodic peak at 1.6 V vs. Fc/Fc+ within the range of 25 µM to 0.3 mM, with a good coefficient of determination (R^2) of 0.991, as shown in the inset of Figure 3.6. The repeatability of the method was demonstrated by a standard deviation of approximately 6% for seven replicates performed between 50 µM and 0.3 mM, indicating excellent consistency within the 50 µM to 0.3 mM range.

3.4.4 Matrix effects and interference studies

The effectiveness of the SPE protocol in eliminating potential matrix interferences was validated by analyzing PZQ in various water samples including ultrapure water, tap water, simulated saltwater, and real saltwater samples. The results showed excellent agreement across all matrices, demonstrating the robustness of the method. This consistent performance can be attributed to the selective nature of the SPE protocol, which effectively removes interfering ions and retains only the organic compounds of interest before elution with acetonitrile.

The HLB SPE cartridge's dual-phase chemistry allows for:

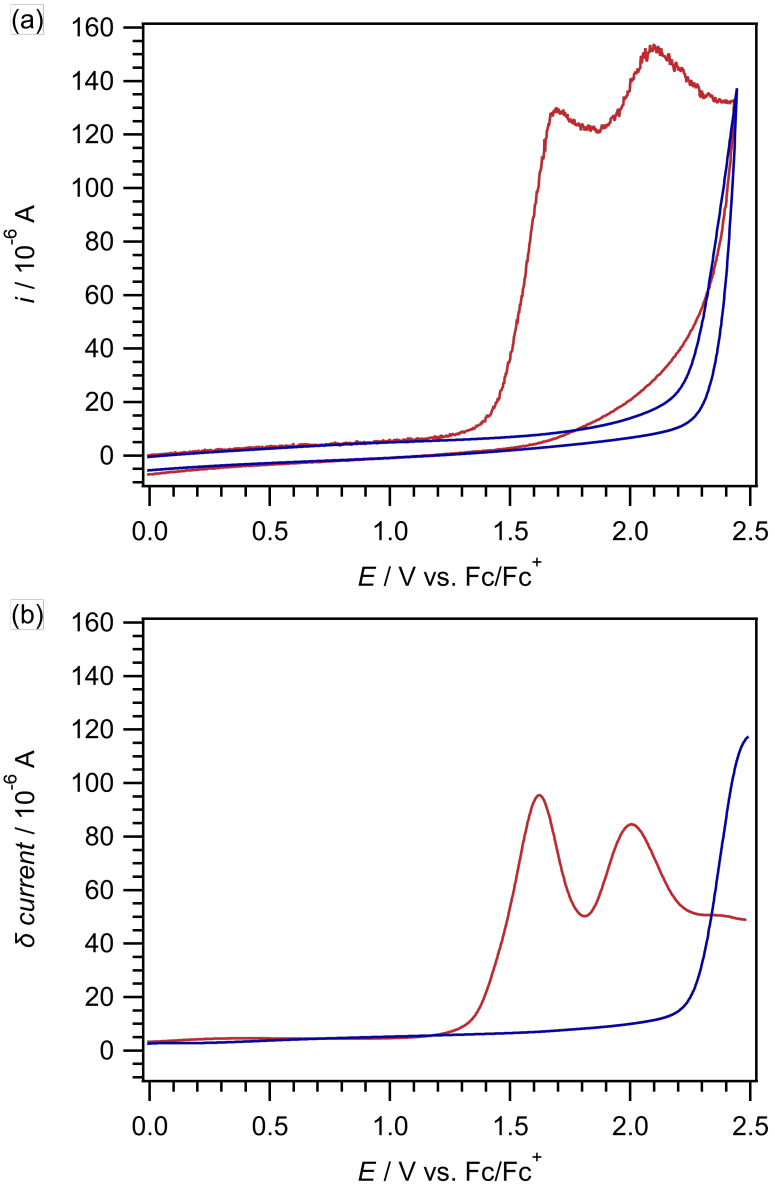

FIGURE 3.5: (a) Cyclic voltammogram obtained from samples containing 0.1 mol L^{-1} PZQ in MeCN (red) compared to blank (blue) (b) Square wave voltammogram obtained from samples containing 1 µmol L^{-1} PZQ in MeCN (red) compared to blank (blue).

- Retention of PZQ through hydrophobic interactions while aqueous matrix components pass through
- Complete removal of potentially interfering ions during the washing step
- Selective elution of PZQ in acetonitrile, providing a clean sample matrix for both GC-MS and voltammetric analysis

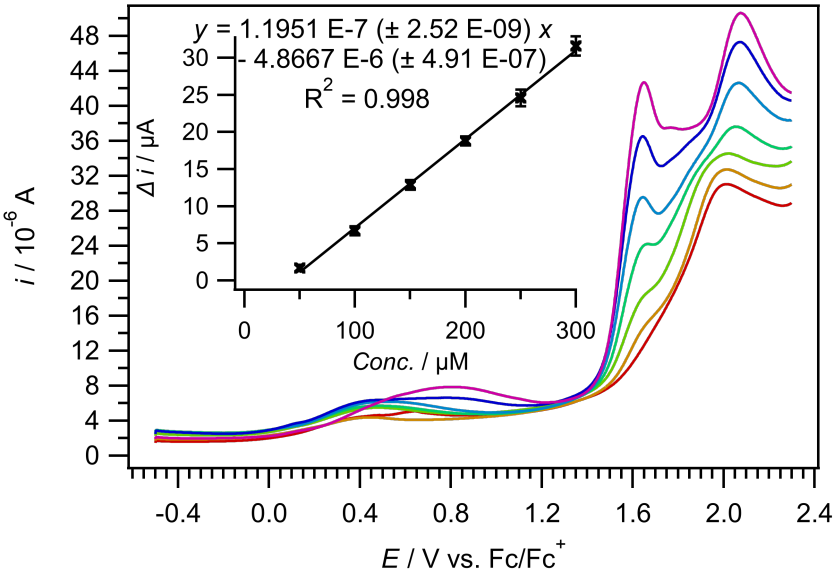

FIGURE 3.6: Square wave voltammogram of increasing concentration of PZQ on glassy carbon electrode in MeCN (0 µM, 25 µM, 50 µM, 0.1 mM, 0.15 mM, 0.20 mM, 0.25 mM). (Inset) Calibration plot of PZQ peak height with increasing concentration. Standard deviations marked for each concentration were obtained from 7 replicates.

Recovery studies across different water matrices showed consistent results within 84.3% to 108.0%, indicating that common ions present in various water sources do not impact the analytical performance. This validates the effectiveness of the sample preparation strategy in producing interference-free samples suitable for both analytical methods.

3.4.5 Evaluation of method agreement through statistical analysis

It is important to note that the concentrations reported in this section reflect the original sample concentrations before SPE preconcentration, while the concentrations mentioned in previous sections refer to neat samples in acetonitrile. Through our SPE protocol, samples were concentrated by a factor of 10 (100 mL sample to 10 mL final volume), allowing for enhanced detection sensitivity. Therefore, while the statistical comparison was performed at 15.0 µM (referring to original sample concentration), the actual measurements were conducted at 150 µM after preconcentration. This concentration factor should be considered when comparing different sections of this study.

Statistical analysis is performed to compare the performance of the voltammetric and GC-MS methods, specifically the accuracy of PZQ quantification. Paired Student's t-test are used to evaluate whether there is a significant difference between the mean PZQ concentrations quantified by each method at a spiked level of 15 µM. The mean concentration found was 14.583 ± 0.836 µM for GC-MS and 15.317 ± 0.594 µM for the electrochemical method. The t-test result (t=1.907) was less than the critical value at the 5% significance level (t=2.447), indicating no significant difference between the means.

An F-test was also performed to compare the variances of the results obtained by each method. The F-test result (F=2.027) was less than the critical value at the 5% significance level (F=4.28), suggesting no significant difference in variance between the two methods. Both analyses indicate comparable results, as is given in Table 3.2.

TABLE 3.2: Precision and accuracy data for the determination of PZQ by the proposed GC-MS method and electroanalysis method

	GC-MS method		Electrochemical method	
PZQ 15 µM	Conc. found (µM)	% found	Conc. found (µM)	% found
$\bar{x} \pm S.D.$	14.583 ± 0.836	97.22 ± 5.74	15.317 ± 0.594	102.11 ± 3.88
t-test				1.907 (2.447)
F-test				2.027 (4.280)

The values shown in parenthesis are the tabulated t-test and F-test values at p = 0.05.[31]

Overall, the statistical analysis demonstrates strong agreement between the proposed voltammetric method and the established GC-MS technique for PZQ quantification. No significant differences are found between the methods in terms of accuracy or precision at a 95% confidence level. This supports the validity of the voltammetric method as a more convenient and cost-effective alternative to GC-MS for detecting PZQ in water samples.

3.4.6 SPE coupled to voltammetry compared to non-SPE direct voltammetric determination of PZQ

While both GC-MS and voltammetric methods have demonstrated suitable analytical performance for PZQ detection, each technique offers distinct advantages

and limitations that make them appropriate for different applications. To aid in method selection, Table 3.3 presents a comparison of key operational parameters between GC-MS and voltammetric detection. The comparison considers practical aspects such as equipment costs, analysis time, detection capabilities, portability, maintenance requirements, and operator training needs.

The data show that while GC-MS offers superior detection limits and is well-suited for regulatory compliance testing and research laboratories, voltammetric detection provides advantages in terms of cost, speed, and portability that make it particularly suitable for routine monitoring and field applications. These complementary strengths suggest that the choice between methods should be guided by specific analytical requirements, resource availability, and intended application rather than purely analytical performance metrics.

TABLE 3.3: Cost-benefit analysis comparison between GC-MS and voltammetry detection of PZQ

Parameter	GC-MS	Voltammetric Detection
Equipment Cost	High ($50,000+)	Low ($5,000-15,000)
Analysis Time	20-30 min/sample	5-10 min/sample
Detection Limit	0.32 µmol	0.87 µmol
Field Deployment	Not portable	Portable
Maintenance	Complex, expensive	Simple, inexpensive
Operator Training	Advanced (1-2 weeks)	Basic (2-3 days)

Best For:
GC-MS: Regulatory compliance, research labs
Voltammetry: Routine monitoring, field testing

To quantify PZQ in real samples, an SPE technique was employed to extract PZQ from salt and freshwater aqueous sample solutions, followed by elution using MeCN. This change in solvent medium, from aqueous to organic, enabled the retention of PZQ while removing unwanted water-soluble interferences and insoluble non-polar compounds. This extraction process allowed for the quantification of the sample using both electroanalytical and GC-MS methods. The SPE procedure exhibited satisfactory percentage recoveries ranging from 84.3% to 108.0% when measured using GC-MS, and these results were consistent with the voltammetric findings (Table 3.1)

Comparing the advantages of using SPE coupled with GC-MS and SPE coupled with voltammetric methods for PZQ determination in MeCN, to directly injecting

the samples into GC-MS or using voltammetric methods without any extraction procedures, several points can be discussed.

- Detection limit: SPE coupled with the GC-MS method provides smaller detection limits than SPE coupled with voltammetric methods (Table 3.1), although SPE-coupled detection can be used to lower the detection limits by concentrating the sample (injecting more solution through the SPE cartridges, as described in this chapter). It is important to note that the PZQ dosing range in an aquarium setting typically falls between 2.5 to 5.0 ppm (8.0 to 16.0 µM), necessitating sample preconcentration when employing voltammetric methods for measuring aquarium samples.

- Cost of methodology: While the absolute costs are difficult to assess between studies, it is expected that electrochemical methods are more economical than GC-MS methods, both in terms of equipment and reagents.

- Ease of operation: Previously reported voltammetric analysis of PZQ was typically done in aqueous solution while relying on hanging drop mercury electrodes. While reducing the complication of sample preparation, the use of mercury electrodes has increasingly been phased out due to toxicity and environmental concerns. The presented method relies on SPE to allow the electrochemical detection to be performed on a glassy carbon electrode.

3.5 Conclusions

This chapter introduces two methods for quantifying PZQ in water samples: GC-MS and voltammetric analysis, facilitated by the SPE sample preparation. Through SPE, PZQ present in aquarium samples can be efficiently extracted into the organic medium, MeCN. This process effectively eliminates water-soluble interferences and insoluble non-polar compounds. The voltammetric method for PZQ detection demonstrates comparable accuracy to the results obtained from GC-MS. Moreover, the extraction procedure is straightforward, while the detection process is convenient and cost-effective compared to GC-MS.

References

(1) Bader, C.; Starling, D. E.; Jones, D. E.; Brewer, M. T. Use of praziquantel to control platyhelminth parasites of fish. *Journal of Veterinary Pharmacology and Therapeutics* **2019**, *42*, _eprint: https://onlinelibrary.wiley.com/doi/pdf/10.1111/jvp.12735, 139–153.

(2) Thomas, C. M.; Timson, D. J. The Mechanism of Action of Praziquantel: Six Hypotheses. *Current Topics in Medicinal Chemistry* **2018**, *18*, 1575–1584.

(3) Norbury, L. J.; Shirakashi, S.; Power, C.; Nowak, B. F.; Bott, N. J. Praziquantel use in aquaculture – Current status and emerging issues. *International Journal for Parasitology: Drugs and Drug Resistance* **2022**, *18*, 87–102.

(4) Santos, A. L.; Takeuchi, R. M.; Stradiotto, N. R. Electrochemical, Spectrophotometric and Liquid-Chromatographic Approaches for Analysis of Tropical Disease Drugs. *Current Pharmaceutical Analysis*, *5*, 69–88.

(5) Aydin, E. B.; Aydin, M.; Sezginturk, M. K. Biosensors in Drug Discovery and Drug Analysis. *CURRENT ANALYTICAL CHEMISTRY* **2019**, *15*, Num Pages: 18 Place: Sharjah Publisher: Bentham Science Publ Ltd Web of Science ID: WOS:000473758500009, 467–484.

(6) Gouveia, F.; Bicker, J.; Goncalves, J.; Alves, G.; Falcao, A.; Fortuna, A. Liquid chromatographic methods for the determination of direct oral anticoagulant drugs in biological samples: A critical review. *ANALYTICA CHIMICA ACTA* **2019**, *1076*, Num Pages: 14 Place: Amsterdam Publisher: Elsevier Web of Science ID: WOS:000471599900002, 18–31.

(7) Nannou, C.; Ofrydopoulou, A.; Evgenidou, E.; Heath, D.; Heath, E.; Lambropoulou, D. Analytical strategies for the determination of antiviral drugs in the aquatic environment. *TRENDS IN ENVIRONMENTAL ANALYTICAL CHEMISTRY* **2019**, *24*, Num Pages: 15 Place: Amsterdam Publisher: Elsevier Web of Science ID: WOS:000500597900005, e00071.

(8) Qriouet, Z.; Qmichou, Z.; Bouchoutrouch, N.; Mahi, H.; Cherrah, Y.; Sefrioui, H. Analytical Methods Used for the Detection and Quantification of Benzodiazepines. *JOURNAL OF ANALYTICAL METHODS IN CHEMISTRY* **2019**, *2019*, Num Pages: 11 Place: London Publisher: Hindawi Ltd Web of Science ID: WOS:000486399900001, 2035492.

(9) Acquavia, M. A.; Foti, L.; Pascale, R.; Nicolo, A.; Brancaleone, V.; Cataldi, T. R.; Martelli, G.; Scrano, L.; Bianco, G. Detection and quantification of Covid-19 antiviral drugs in biological fluids and tissues. *TALANTA* **2021**, *224*, Num Pages: 17 Place: Amsterdam Publisher: Elsevier Web of Science ID: WOS:000600787800077, 121862.

(10) Fu, E.; Khederlou, K.; Lefevre, N.; Ramsey, S. A.; Johnston, M. L.; Wentland, L. Progress on Electrochemical Sensing of Pharmaceutical Drugs in Complex Biofluids. *CHEMOSENSORS* **2023**, *11*, Num Pages: 24 Place: Basel Publisher: MDPI Web of Science ID: WOS:001056972600001, 467.

(11) Saleem, M.; Hanif, M.; Rafiq, M.; Ali, A.; Raza, H.; Kim, S. J.; Lu, C. Recent Development on Sensing Strategies for Small Molecules Detections. *JOURNAL OF FLUORESCENCE* **2023**, Num Pages: 33 Place: New York Publisher: Springer/Plenum Publishers Web of Science ID: WOS:001060207900001, DOI: 10.1007/s10895-023-03387.

(12) David, I. G.; Buleandra, M.; Popa, D. E.; Cheregi, M. C.; David, V.; Iorgulescu, E. E.; Tartareanu, G. O. Recent Developments in Voltammetric Analysis of Pharmaceuticals Using Disposable Pencil Graphite Electrodes. *Processes* **2022**, *10*, Number: 3 Publisher: Multidisciplinary Digital Publishing Institute, 472.

(13) Erşan, T.; Dilgin, D. G.; Kumrulu, E.; Kumrulu, U.; Dilgin, Y. Voltammetric Determination of Favipiravir Used as an Antiviral Drug for the Treatment of Covid-19 at Pencil Graphite Electrode. *Electroanalysis* **2023**, *35*, _eprint: https://analyticalsciencejournals-onlinelibrary-wiley-com.remotexs.ntu.edu.sg/doi/pdf/10.10 e202200295.

(14) Eldin, G. M. G.; Khalifa, M. E.; Munshi, A. M.; Aldawsari, A. M.; El-Metwaly, N. M. Determining nadifloxacin in pharmaceutical formulations using novel differential pulse voltammetric approach. *Microchemical Journal* **2021**, *163*, 105942.

(15) Clares, P.; Pérez-Ràfols, C.; Serrano, N.; Díaz-Cruz, J. M. Voltammetric Determination of Active Pharmaceutical Ingredients Using Screen-Printed Electrodes. *Chemosensors* **2022**, *10*, Number: 3 Publisher: Multidisciplinary Digital Publishing Institute, 95.

(16) Alberto, E.; Bastos-Arrieta, J.; Pérez-Ràfols, C.; Serrano, N.; Silvia Díaz-Cruz, M.; Manuel Díaz-Cruz, J. Voltammetric determination of sulfamethoxazole using commercial screen-printed carbon electrodes. *Microchemical Journal* **2023**, *193*, 109125.

(17) Cortés, K.; Triviño, J. J.; Arancibia, V. Simultaneous voltammetric determination of acetylsalicylic acid, caffeine and paracetamol in pharmaceutical formulations using screen-printed carbon electrode. *Electroanalysis* **2023**, *35*, _eprint: https://analyticalsciencejournals-onlinelibrary-wiley-com.remotexs.ntu.edu.sg/doi/pdf/10.1002/elan.202200484, e202200484.

(18) Devaka, N. V. S. K.; Rao, V. M. Chromatographic Quantification of Ivermectin and Pranziquantel in the Tablets Using Stability Indicating RP-HPLC Method. *Pharmaceutical Sciences* **2019**, *25*, Number: 3 Publisher: Tabriz University of Medical Sciences, 254–261.

(19) Eason, T.; Ramirez, G.; Clulow, A. J.; Salim, M.; Boyd, B. J. Revisiting the Dissolution of Praziquantel in Biorelevant Media and the Impact of Digestion of Milk on Drug Dissolution. *Pharmaceutics* **2022**, *14*, 2228.

(20) Baralla, E.; Varoni, M. V.; Nieddu, M.; Demontis, M. P.; Merella, P.; Burreddu, C.; Garippa, G.; Boatto, G. Determination of Praziquantel in Sparus aurata L. after Administration of Medicated Animal Feed. *Animals* **2020**, *10*, Number: 3 Publisher: Multidisciplinary Digital Publishing Institute, 528.

(21) Ding, T.-Y.; Shu, X.-G.; Xiong, R.-P.; Qiu, J.-L.; Li, L.; He, L.-M. Simultaneous determination of praziquantel and its main metabolites in the tissues of black goats and their residue depletion. *Food Additives & Contaminants: Part A* **2022**, *39*, Publisher: Taylor & Francis _eprint: https://doi.org/10.1080/19440049.2022.2032380, 666–677.

(22) Teng, F.; Ji, J.; Yang, Y.; Wang, H. A useful quantitative model for determining the optical purity of praziquantel enantiomers based on near infrared spectroscopy with partial least squares. *Journal of Near Infrared Spectroscopy* **2022**, *30*, Publisher: SAGE Publishing, 246–253.

(23) Meier, H.; Blaschke, G. Capillary electrophoresis-mass spectrometry, liquid chromatography-mass spectrometry and nanoelectrospray-mass spectrometry of praziquantel metabolites. *Journal of Chromatography. B, Biomedical Sciences and Applications* **2000**, *748*, 221–231.

(24) Rizk, M.; Belal, F.; Ibrahim, F.; Ahmed, S.; El-Enany, N. M. Voltammetric Determination of Praziquantel in Tablets and Biological Fluids. *Arzneimittelforschung* **2001**, *51*, Publisher: Editio Cantor Verlag, 673–678.

(25) Ghoneim, M. M.; Mabrouk, M. M.; Tawfik, A. Direct determination of praziquantel in pharmaceutical formulations and human plasma by cathodic adsorptive stripping differential-pulse voltammetry. *Journal of Pharmaceutical and Biomedical Analysis* **2002**, *30*, 1311–1318.

(26) Radi, a.-e.; Hassanein, A. Indirect determination of praziquantel in human serum by cathodic adsorptive stripping voltammetry. *Chemia Analityczna* **2001**, *46*, 561–567.

(27) Chan, K. K.; Webster, R. D. Solid Phase Extraction – Voltammetric Coupled Detection of Caffeine in Acetonitrile. *Electroanalysis* **2016**, *28*, _eprint: https://analyticalsciencejournals.onlinelibrary.wiley.com/doi/pdf/10.1002/elan.201500383, 516–522.

(28) Chan, K. K.; Hamid, M. S. B.; Webster, R. D. Quantification of capsaicinoids in chillies by solid-phase extraction coupled with voltammetry. *Food Chemistry* **2018**, *265*, 152–158.

(29) Kissinger, P.; Heineman, W. R., *Laboratory Techniques in Electroanalytical Chemistry, Second Edition, Revised and Expanded*, Google-Books-ID: AwuTx14Ro2UC; CRC Press: 1996; 1014 pp.

(30) EMA ICH Q2(R2) Validation of analytical procedures - Scientific guideline, European Medicines Agency `https://www.ema.europa.eu/en/ich-q2r2-validation-analytical-procedures-scientific-guideline` (accessed 08/03/2023).

(31) Harris, D. C.; Lucy, C. A., *Quantitative chemical analysis*, Ninth edition, OCLC: 915084423; W.H. Freeman & Company: New York, 2016; 1 p.

(32) Wallace, W. E. Mass Spectra. *NIST Chemistry WebBook, NIST Standard Reference Database Number 69* **2014**, Last Modified: 2020-06-12T12:22-04:00.

Chapter 4

Towards organic CO_2 batteries

4.1 Abstract

This chapter investigates the unique electrochemical properties of quinones and their potential applications in CO_2 reduction and energy storage. The primary focus is on elucidating the behavior of quinones during controlled potential electrolysis (CPE) experiments under inert and CO_2 atmospheres, assessing their viability for energy storage, optimizing conditions for reversible electrochemical cycling, and investigating their stability and decomposition pathways.

Preliminary studies revealed that weakly complexing quinones exhibit a positive shift in the second reduction wave under CO_2, while strongly complexing quinones display a complete merging of the first and second reduction waves. Attempts to use quinones as organocatalysts for the electrocarboxylation of styrene were unsuccessful, leading to a redirection of efforts towards understanding the binding of CO_2 to quinones for battery applications.

CPE experiments demonstrated that reduced quinones are sensitive to further reactions via adventitious impurities present in aprotic solvents, with attempts leading to decomposition. The use of organic oxidants, such as phenylene diamines, in the counter chamber helped to alleviate this issue. The chemical reversibility of quinone redox processes was found to be better under CO_2 than under Ar, likely due to the positive shift in the second reduction potential under CO_2. However, reduction under CO_2 followed by Ar purging led to irreversible decomposition, contrary to previous findings.

The impact of proton/hydrogen sources on the cyclic voltammograms of quinones was also investigated. Trifluoroethanol and diethylmalonate successfully shifted the reduction potentials of naphthoquinone and tetrachlorobenzoquinone to more positive values, increasing the stability of the reduced quinones-CO_2 adduct. However, acidification of reduced quinone species did not yield the desired formate or methanol products.

A prototype battery was constructed based on the two-electron reduction and two-electron oxidation of naphthoquinone. While the charging reaction proceeded well, the charge release efficiency was limited to 40%. Preliminary tests suggest that a CO_2 oxidation atmosphere enables more charge release than Ar.

This chapter highlights the potential of quinones as CO_2-binding redox molecules for carbon capture and energy storage applications. However, challenges such as oxidative instability, modest charge release efficiency, and discrepancies in the stability of reduced quinone species under different conditions need to be addressed. Further research is necessary to optimize quinone-based systems and elucidate the underlying mechanisms governing their behavior.

4.2 Introduction

The escalating levels of atmospheric carbon dioxide (CO_2) and its profound impact on climate change have driven the exploration of innovative strategies for mitigating its environmental effects.[1] One promising avenue involves leveraging CO_2 as a resource in chemical processes, aligning with the broader quest for sustainable energy technologies. Among advanced energy storage systems, redox flow batteries (RFBs) stand out for their scalability and ability to independently tune energy and power capacities, making them particularly suited for large-scale applications. Within this context, organic redox-active compounds such as quinones have emerged as compelling candidates due to their abundance, affordability, and structural adaptability, positioning them at the forefront of efforts to develop efficient and cost-effective energy storage solutions.[2]

Quinones, renowned for their exceptional redox properties, hold significant potential for revolutionizing energy storage, particularly in redox flow batteries (RFBs).[2] Their structural flexibility and reliance on earth-abundant elements make them ideal for designing scalable and low-cost systems.[3] Moreover, the unique reactivity of reduced quinones with CO_2 opens up possibilities for integrating energy storage with CO_2 utilization, converting it into valuable chemical products.[4] However, challenges persist in optimizing their performance under controlled potential electrolysis (CPE) conditions, including issues with chemical stability, reversible transformations, and operational efficiency during charging and discharging cycles. Additional obstacles such as pH-dependent solubility, oxidative stability, and limited operational voltage further highlight the need for innovative approaches like molecular engineering and tailored electrolyte formulations to unlock the full potential of quinone-based energy systems.

Tam et al. investigated the electrocatalytic behavior of similar quinones in acetonitrile solutions.[5] The study focused on the reversible binding of CO_2 to the reduced forms of quinones ($Q^{\bullet -}/Q^{2-}$) and the subsequent release of CO_2 or $CO_2^{\bullet -}$ under an argon atmosphere. Using cyclic voltammetry (CV) and CPE, the authors observed that the two one-electron reduction processes of quinones merged into a single two-electron process in the presence of CO_2, indicating the formation of a complex $[Q(CO_2)_n]^{2-}$ The binding of CO_2 was found to be chemically reversible, as evidenced by the regeneration of the original quinone species upon purging with Ar. The study also employed UV-vis spectroscopy to characterize the quinone species and their complexes with CO_2, confirming the reversible nature of the binding process. The finding of this study is the basis of this chapter as we aim to extend the applicability of this process further.

This project aims to address these knowledge gaps by elucidating the processes quinones undergo during CPE under inert and CO_2 atmospheres, assessing the viability of quinone-based energy storage systems, optimizing conditions for reversible electrochemical cycling, and investigating quinone stability and decomposition pathways. The potential impacts of this research are potentially far-reaching, as it will contribute to the development of fundamental knowledge of quinone electrochemistry under different reactive atmospheres, provide a basis for potential grid-scale quinone-based redox flow battery systems, and offer a strategy to store intermittent renewable energy sources through CO_2 utilization. Moreover, this project presents a novel approach that merges energy storage and CO_2 conversion motivations, paving the way for innovative solutions to address the pressing challenges of sustainable energy management and climate change mitigation.

4.3 Materials and methods

4.3.1 Materials

The supporting electrolyte, tetrabutylammonium hexafluorophosphate (n-Bu_4NPF_6), was synthesized by reacting equimolar 40% aqueous n-Bu4NOH with 65% aqueous HPF_6. The precipitate was washed with water, recrystallized thrice from hot ethanol, and vacuum dried at 140 °C for 24 hours.[6] Electrochemical solutions were prepared by adding acetonitrile (Merck) and n-Bu_4NPF_6 to activated 3 Å molecular

sieves (Fluka) that had been vacuum dried at 250 °C for 6 hours. The acetonitrile/electrolyte mixture was stored under nitrogen in a glass vacuum syringe for at least 36 hours prior to use.[7] Quinone reagents were commercially obtained from Sigma-Aldrich and used as received.

4.3.2 Electrochemical measurements

Cyclic voltammetry (CV) was performed using an Eco Chemie Autolab PGSTAT302N potentiostat in a three-electrode cell configuration. The working electrode was a 1-mm diameter planar glassy carbon (GC) disk (eDAQ). The counter electrode was a platinum wire (Metrohm). A silver wire isolated by a salt bridge containing 0.5 M n-Bu_4NPF_6/acetonitrile served as a miniature reference electrode (eDAQ). Test solutions contained 1-2 mM analyte in 0.1 M n-Bu_4NPF_6/acetonitrile and were deoxygenated with argon for 5 minutes prior to measurement. Experiments were conducted at 22 °C inside a Faraday cage. The GC electrode was polished with 0.3 µm alumina slurry on a Buehler Ultra-pad, rinsed with water and acetone, and dried between measurements. Measured redox potentials were referenced to the ferrocene/ferrocenium (Fc/Fc^+) couple added as an internal standard.

Controlled potential electrolysis (CPE) was conducted in a two-compartment cell divided by a sintered glass frit (porosity no. 5, 1.0 µm to 1.7 µm pores). Twin cylindrical GC electrodes (34.4 cm^2 area each) served as the working and counter electrodes in separate compartments. A silver wire reference isolated by a 0.5 M n-Bu_4NPF_6/acetonitrile salt bridge was positioned near the working electrode. Each compartment contained 30 mL of 0.1 M n-Bu_4NPF_6/acetonitrile electrolyte and was deaerated and stirred by bubbling with argon. The number of electrons transferred (n) was determined by measuring the charge passed (Q) and applying Faraday's law:

$$n = \frac{Q}{N_A F} \tag{4.1}$$

where N_A is moles of analyte electrolyzed, and F is Faraday's constant (96 485 C mol^{-1}).

4.3.3 Rationale for Reagent Selection

Acetonitrile was chosen as the solvent for its compatibility with organic and inorganic species, high dielectric constant, and wide electrochemical window (up to 6.1 V depending on electrolyte and water content).[8] Glassy carbon served as the electrode material due to its wide potential range, high chemical resistance, and large overpotential for solvent breakdown compared to platinum.[8] Zito and Yang (2024) explored the impact of different electrolyte cations on the reduction potential and CO_2 binding affinity of quinones in acetonitrile solutions.[9] The study focused on two key properties of quinone-based redox carriers for electrochemical CO_2 capture and concentration (eCCC): the reduction potential required to activate the carrier and the CO_2 binding constant. The authors investigated the effects of various alkylammonium and alkali/alkaline earth metal cations on these properties. They found that the choice of electrolyte cation can significantly influence the reduction potential of quinones, with shorter-chained alkylammonium cations leading to more positive reduction potentials. However, the CO_2 binding affinity was not significantly affected by the choice of electrolyte cation. The study also revealed that the interaction between alkali and alkaline earth metal cations and quinones can inhibit CO_2 binding due to strong interactions with the anionic oxygen of the quinone. Based on this outcome, n-Bu_4NPF_6 was selected as supporting electrolyte for its excellent solubility, high conductivity, and lack of interference.

4.4 Results and discussion

4.4.1 Preliminary studies on electrochemistry of quinones

In the absence of CO_2, 1,4-cyclohexadienediones (p-quinones) exhibit two well-separated reduction waves in aprotic electrolyte solutions. The first wave is attributed to the reduction of the neutral quinone (Q) to form the semiquinone radical anion ($Q^{\bullet -}$), while the second wave represents the further reduction of the semiquinone to form the aromatic dianion (Q^{2-}). The electrochemical behavior of the first wave was typically characterized as reversible, indicating a rapid electron transfer process. In contrast, the second wave displayed quasi-reversible kinetics, suggesting a slower electron transfer rate. The relative positions of the two reduction

potentials followed the expected trend, with the second electron transfer occurring at a more negative potential than the first. This observation can be rationalized by considering the electrostatic repulsion experienced by the incoming electron during the second reduction step. The semiquinone radical anion, bearing a negative charge, presents a higher energy barrier for the second electron transfer compared to the initial reduction of the neutral quinone. Consequently, the second reduction process requires electrons with greater reducing power to overcome the increased electrostatic repulsion.

Previous studies by Hatton et al. and Hofer et al. classified para-quinones into two classes depending on their interactions with CO_2 and how it affected their redox properties in aprotic organic solvents: weakly complexing (those that shows only weak interaction with CO_2) and strongly complexing (those that showed stronger interaction with CO_2).[10,11] Subsequent analysis by Yayuan et al. through molecular dynamics and DFT studies highlighted the correlation between CO_2 binding strength and the reaction rate.[12] Cyclic voltametric studies of quinones in the presence of CO_2 revealed distinct behaviors depending on the strength of the quinone-CO_2 interaction. For quinones exhibiting weak coordination, the introduction of CO_2 resulted in a positive shift of the second reduction wave, indicative of the formation of a complex between the dianion quinone and CO_2. Notably, no evidence of complex formation was observed between the semiquinone radical anion and CO_2. In contrast, quinones displaying strong complexation tendencies exhibited a merging of the first and second reduction waves, suggesting a concerted two-electron transfer process at the potential of the first reduction. The oxidation and dissociation of CO_2 from the reduced quinone species followed either an electrochemical-chemical (EC) or a chemical-electrochemical (CE) mechanism, contingent upon the sweep rate employed in the cyclic voltametric experiments. This mechanistic distinction highlights the intricate interplay between the electrochemical reduction and the chemical complexation processes, emphasizing the importance of kinetic considerations in understanding the behavior of quinone-CO_2 systems.

The CV data for dichlorodicyanobenzoquinone (no interaction with CO_2), tetrachlorobenzoquinone (weak interaction with CO_2), duroquinone, naphthoquinone and menadione (strong interaction with CO_2) are shown in Fig. 4.1 to Fig. 4.5, respectively.[10]

Dichlorodicyanobenzoquinone has no observed change in the voltammogram when cycling between argon and CO_2 atmosphere, indicating that the reduced state of dichlorodicyanobenzoquinone has no supramolecular interaction with CO_2 (Fig. 4.1). This can be attributed to the lower (more positive) reduction potential of dichlorodicyanobenzoquinone. Yang et al. reported on the linear relationship between reduction potential and CO_2-binding constant,[13] so that quinones with more negative reduction potentials undergo stronger interactions with CO_2. Therefore, in order for the quinone to bind strongly with CO_2 in solution state and the effects to be observable with voltammetry (via the shot in voltametric wave), the quinone requires a reduction potential of -1.1 V vs Fc/Fc+.[13] Thus, dichlorodicyanobenzoquinone with its relatively low reduction potential does not appear to undergo significant molecular binding with CO_2.

Tetrachlorobenzoquinone exhibits a 0.1 V positive shift in reduction potential for the second reduction process in a CO_2 atmosphere compared to in an argon atmosphere, as well as a change in the peak shape for the reverse oxidation process of the second reduction peak (Fig. 4.2). Hatton et al. described the behavior of tetrachlorobenzoquinone and this class as "weakly complexing quinones" (quinones that exhibit a positive shift only in the second reduction potential under the CO2 atmosphere).[10] Scheme 4.1 shows the interaction pathway between CO2 and weakly complexing quinones during the reduction process (dark blue arrow). For weakly complexing quinones, the reduction process is separated into two sequential steps, the first reduction (E_1^{red}) from quinone (Q) to quinone radical anion ($Q^{\bullet -}$), and the second reduction (E_2^{red}) from $Q^{\bullet -}$ to quinone dianion (Q^{2-}), before subsequent coordination with CO_2.

Duroquinone, naphthoquinone, and menadione exhibit substantial shifts in the second reduction potential to an almost-merging or merging between the first and second reduction processes. Hatton et al. described the behavior of these three quinones as "strongly complexing quinones" (quinones that exhibit a merging between first and second reduction potentials).[10] Scheme 4.1 shows the interaction pathway between CO_2 and strongly complexing quinones during the reduction process (dark green arrows). For strongly complexing quinones, the reduction process merges into one peak: two-electron reduction with simultaneous complexation with CO_2 to generate the dianion.

Zito et al. (2022) combined computational and experimental approaches to design quinone derivatives for electrochemical CO_2 capture and concentration (eCCC).[14] They used density functional theory (DFT) calculations to predict these properties for a vast library of substituted benzoquinones. The computational model was validated against experimental data, and molecular orbital analysis revealed key insights into the relationship between quinone structure, reduction potential, and CO_2 binding affinity. The authors found a linear relationship between the reduction potential and CO_2 binding affinity of quinone derivatives, suggesting that improving one property may negatively impact the other.

In this chapter, the attention was focused mainly on tetrachlorobenzoquinone (Fig. 4.2) and naphthoquinone (Fig. 4.4) as representative species for weakly complexing and strongly complexing quinones, respectively.

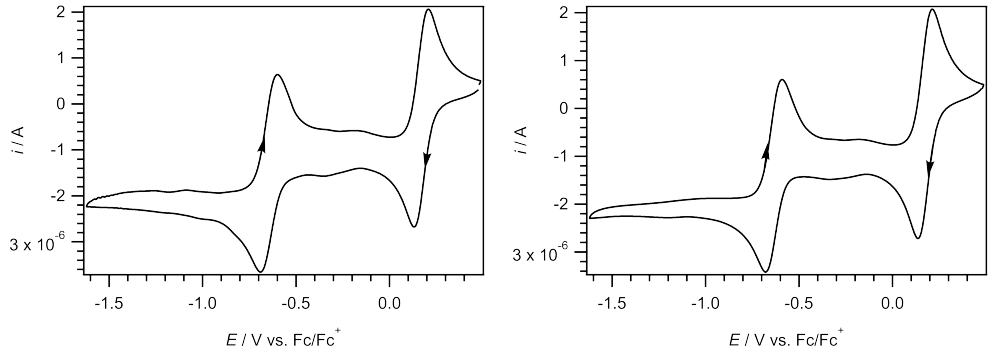

FIGURE 4.1: Cyclic voltammograms of 2 mM dicyanodichlorobenzoquinone in 0.1 M n-Bu_4NPF_6/MeCN recorded using a 1-mm diameter planar GC disk electrode at 0.1 $V\ s^{-1}$ (Left) under Ar and (Right) under CO_2 atmosphere.

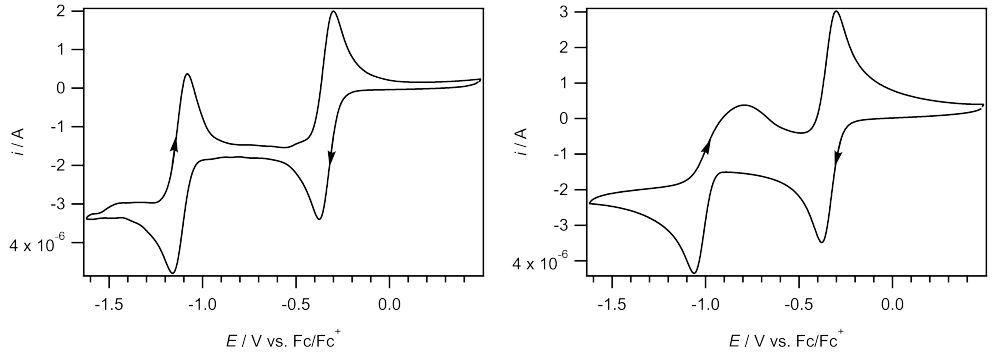

FIGURE 4.2: Cyclic voltammograms of 2 mM tetrachlorobenzoquinone in 0.1 M n-Bu_4NPF_6/MeCN recorded using a 1-mm diameter planar GC disk electrode at 0.1 $V\ s^{-1}$ (Left) under Ar and (Right) under CO_2 atmosphere.

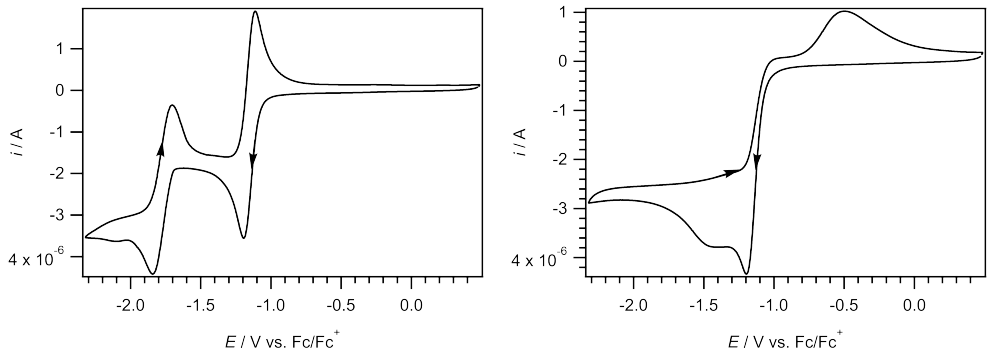

FIGURE 4.3: Cyclic voltammograms of 2 mM duroquinone in 0.1 M n-Bu_4NPF_6/MeCN recorded using a 1-mm diameter planar GC disk electrode at 0.1 $V\ s^{-1}$ (Left) under Ar and (Right) under CO_2 atmosphere.

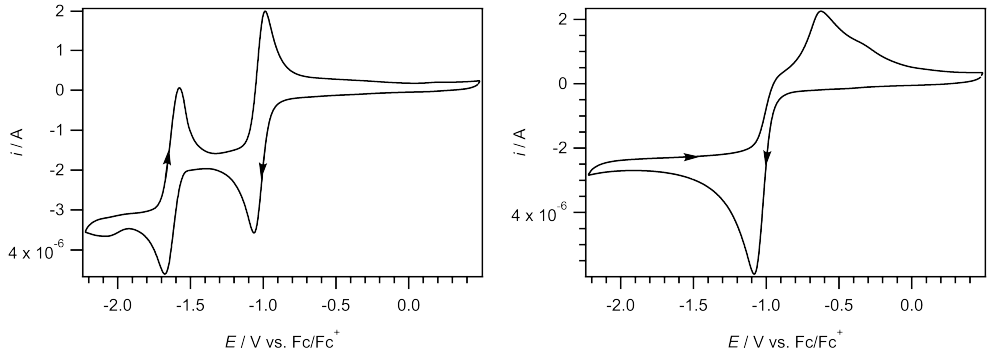

FIGURE 4.4: Cyclic voltammograms of 2 mM naphthoquinone in 0.1 M n-Bu_4NPF_6/MeCN recorded using a 1-mm diameter planar GC disk electrode at 0.1 $V\ s^{-1}$ (Left) under Ar and (Right) under CO_2 atmosphere.

4.4.2 Controlled potential electrolysis of quinones

Controlled potential electrolysis (CPE) experiments were conducted to assess the reversibility and stability of the redox processes under long time scales (minutes to hours). It was observed under a CO_2 atmosphere that when the reduction step was performed first, followed by re-oxidation of the reduced species, the starting material could be at least partly regenerated (depending on the exact quinone) indicating stability of the reduced species over hours timescales.

Fig. 4.6 (black line) is the cyclic voltammogram of naphthoquinone under an argon atmosphere (before electrolysis). The dashed blue line in Fig. 4.6 is the cyclic voltammogram that was obtained after naphthoquinone had been bulk reduced under a CO_2 atmosphere by two-electrons and then reoxidised by electrolysis (also under a CO_2 atmosphere), and then the solution again purged with argon to remove

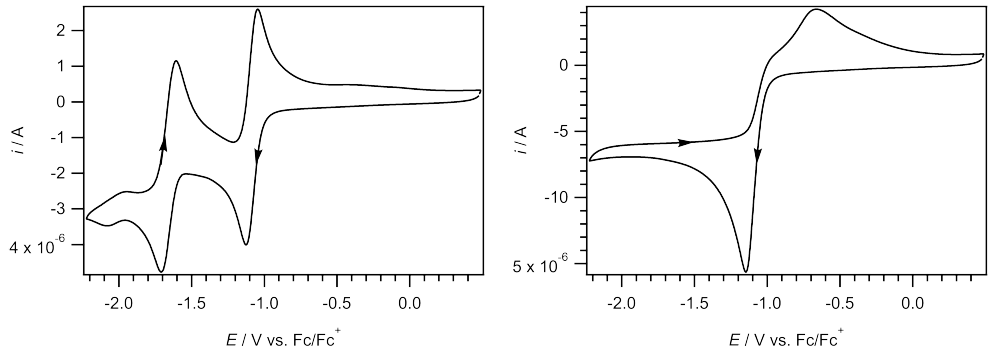

FIGURE 4.5: Cyclic voltammograms of 2 mM menadione in 0.1 M n-Bu_4NPF_6/MeCN recorded using a 1-mm diameter planar GC disk electrode at 0.1 $V\ s^{-1}$ (Left) under Ar and (Right) under CO_2 atmosphere.

the CO_2. An extra voltammetric peak was observed in the dashed blue trace, suggesting that the bulk reduced quinone has undergone reactions with CO2 over the electrolysis timescale possibly at the free sp^2C-H site, and so could not be completely reoxidised back to the starting material.

Fig. 4.7 shows cyclic voltammograms of duroquinone under an argon atmosphere (before electrolysis) and after bulk electrolysis under a CO_2 atmosphere to first exhaustively reduce the compound and then to exhaustively reoxidise the reduced solution. In this case, an extra peak was not observed in the CV at the completion of the entire CPE reactions, possibly because duroquinone does not have a freesp^2C-H bond available for side reaction. Noting that the position of the second reduction peak is substantially shifted possibly due to the presence of trace water seeping in the voltametric cell during the electrolysis timescale (hours), which results in the second reduction wave moving towards the first reduction wave due to a hydrogen-bonding mechanism of the reduced quinone with water molecules. The effect of water content on quinone electrochemistry in aprotic organic solvents has been extensively reported.[7,15,16]

Rocha-Ortiz et al. (2020) investigated the electrochemical behavior of disperse red 60 (DR60), an anthraquinone dye, in acetonitrile solutions.[17] The study focused on the interactions of the reduced forms of DR60 with water and molecular oxygen (O_2). Using cyclic voltammetry, the authors observed two one-electron reduction processes for DR60, forming an anion radical and then a dianion. The first reduction process was found to be influenced by the presence of water, suggesting hydrogen bonding interactions between the anion radical and water molecules. Additionally,

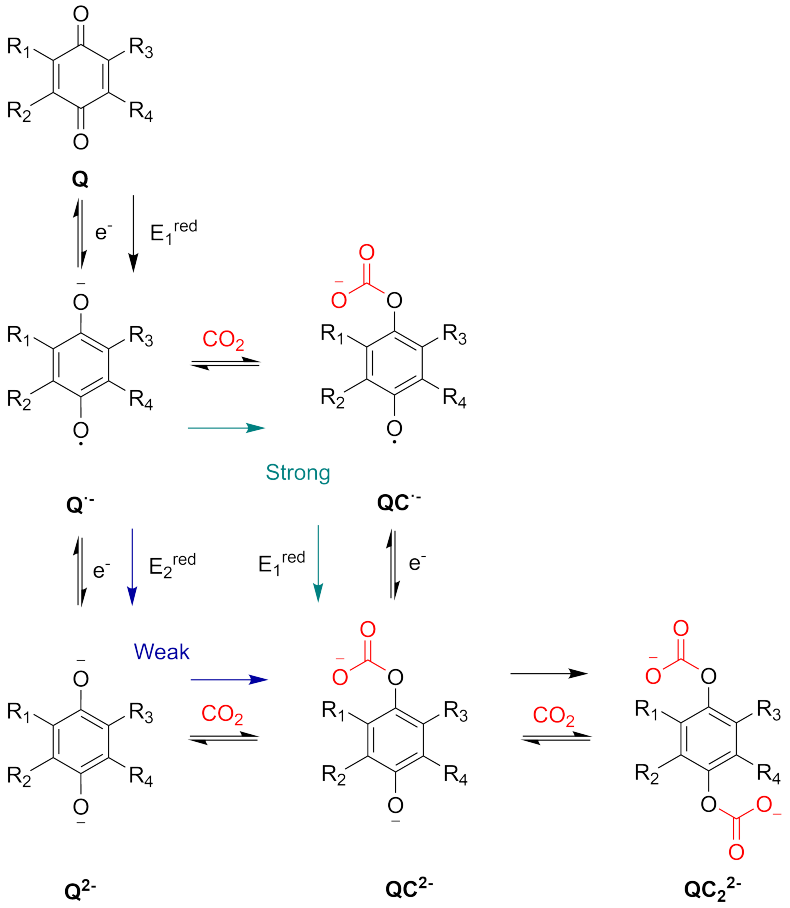

SCHEME 4.1: Mechanism for the interaction between CO_2 with weakly and strongly coordinating quinones during reduction process.

the presence of O_2 led to a homogeneous electron transfer reaction between the anion radical of DR60 and O_2, as evidenced by changes in the voltametric response and color of the solution. The study also examined the reduction of O_2 in the presence of DR60 and found that the superoxide intermediate formed during O_2 reduction undergoes association steps with water molecules. The authors estimated the equilibrium constant for the homogeneous electron transfer reaction between DR60 and O_2, indicating a slight preference for the forward reaction. Similar experiments with 9,10-anthraquinone (AQ) confirmed the occurrence of the homogeneous electron transfer reaction with O_2, and the presence of superoxide is suspected to cause an irreversible decomposition leading to the changing peak shape. We expected a similar interaction could be the cause of change in voltametric response in Fig. 4.6 and Fig. 4.7.

However, when the order of electrolysis was reversed, so that an exhaustive oxidative electrolysis was carried out first, preceding the exhaustive reverse reduction, it was

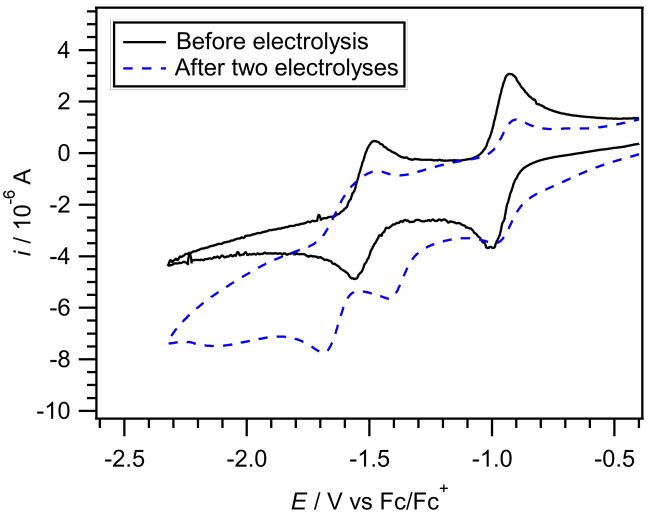

FIGURE 4.6: Cyclic voltammograms of naphthoquinone in acetonitrile under an argon atmosphere before (solid black line) the compound had been exhaustively reduced in an electrolysis cell under a CO_2 atmosphere and after (dashed blue line) the reduced solution had been exhaustively reoxidised (also under a CO_2 atmosphere).

noticed that there was a significant degradation in the electrochemical response for the quinone. Fig. 4.8 shows the results from an experiment where naphthoquinone was oxidized under constant current electrolysis (CCE) conditions, forcing the transfer of two-electrons from the system under electrolysis timescale (hours). As an oxidation peak was not originally observed in the CV, the CCE was used instead of CPE to forcefully apply current into the solution system. The loss of features in the cyclic voltammogram were observed after the bulk oxidation (Fig. 4.8). This led to the hypothesize that the application of a positive potential to the solution containing the quinone leads to its decomposition or further interaction with electrolyte and/or solvent, potentially through oxidative pathways that irreversibly alter the molecular structure marking the loss of voltammogram features. The reason for conducting this experiment was to test the quinones' stability under oxidizing conditions present in a flow battery and are discussed in more detail in Section 4.4.4

Interestingly, it was discovered that the chemical reversibility of the quinone redox processes were enhanced under electrolysis conditions when the experiments were conducted entirely under a CO_2 atmosphere compared to when an Ar atmosphere was used for recording the CVs. Fig. 4.9 shows experiments where the whole redox process (two-electron CPE reduction, followed by two-electron CPE reoxidation) appeared almost completely reversible (less the shift in reduction potential previously

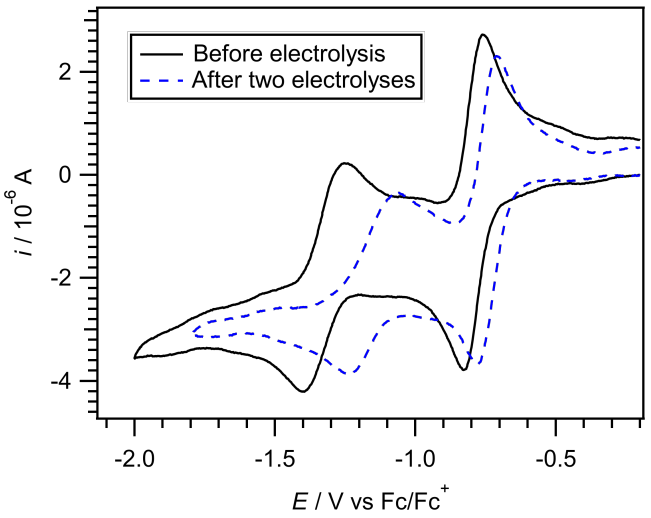

FIGURE 4.7: Cyclic voltammograms of duroquinone in acetonitrile under an argon atmosphere before (solid black line) the compound had been exhaustively reduced in an electrolysis cell under a CO_2 atmosphere and after (dashed blue line) the reduced solution had been exhaustively reoxidised (also under a CO_2 atmosphere).

stated due to the ingress of trace water). It is proposed that this improved reversibility can be attributed to the positive shift in the second reduction potential observed under CO_2. In the presence of CO_2, the reduction of quinone to its dianion form occurs at a less negative potential compared to the potential required for the two-electron reduction under Ar. This positive shift in potential likely minimizes the occurrence of side reactions and decomposition pathways, thereby contributing to the enhanced reversibility of the system under CO_2.

When the reduction of the naphthoquinone was carried out under CO_2 and the fully reduced solution was subsequently purged with Ar, it was found that this process led to the regeneration of the starting material. Fig. 4.10 shows the result when naphthoquinone was reduced under CO_2 (dashed blue line) and then purged with argon (dashed red line). The CV after the reduced quinone was purged under Ar is shown in the dashed red line, whose features resemble those of the starting CV shown in the solid black line. This observation suggests that purging the reduced solution with argon results in the CO_2 (two molecules) being released from the quinone as $CO_2^{\bullet -}$ (the carboxylate radical anion) and the quinone converting back to its neutral form.

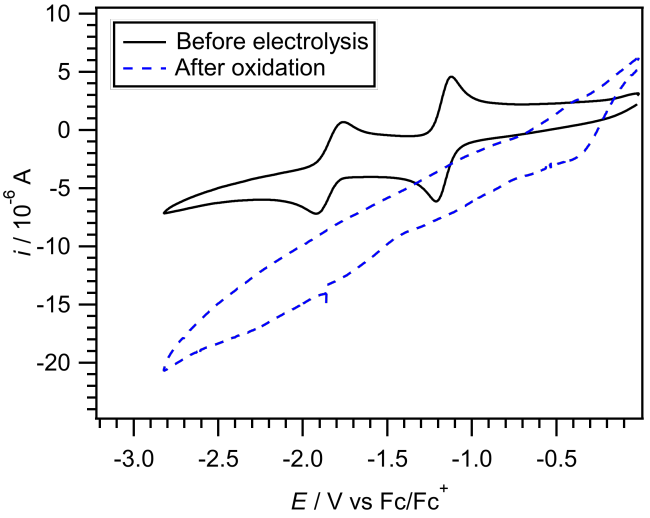

FIGURE 4.8: Cyclic voltammograms of duroquinone in acetonitrile under an argon atmosphere before (solid black line) the compound had been exhaustively reduced in an electrolysis cell under an argon atmosphere and after (dashed blue line) the reduced solution had been exhaustively reoxidised (also under an argon atmosphere).

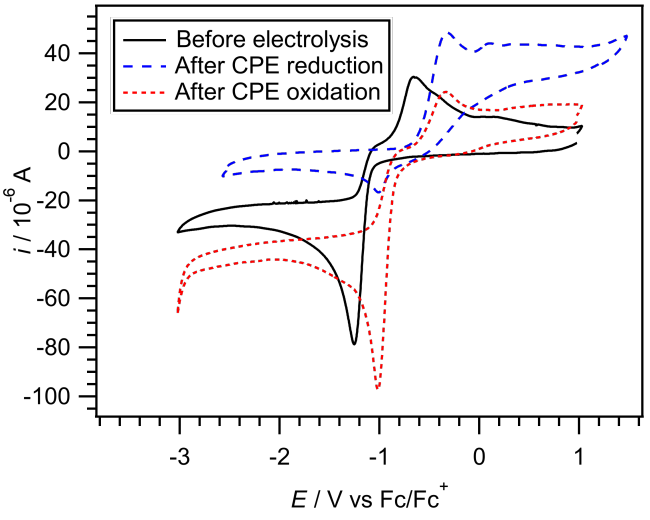

FIGURE 4.9: Cyclic voltammogram of naphthoquinone prior to electrolysis (solid black line), after CPE reduction (dashed blue line), and after CPE reoxidation (dashed red line).

4.4.3 Impact of proton/hydrogen sources on cyclic voltammograms of quinones

Due to the chemical instability of many reduced quinones under electrolysis conditions, attempts were made to improve their lifetimes by lowering their reduction

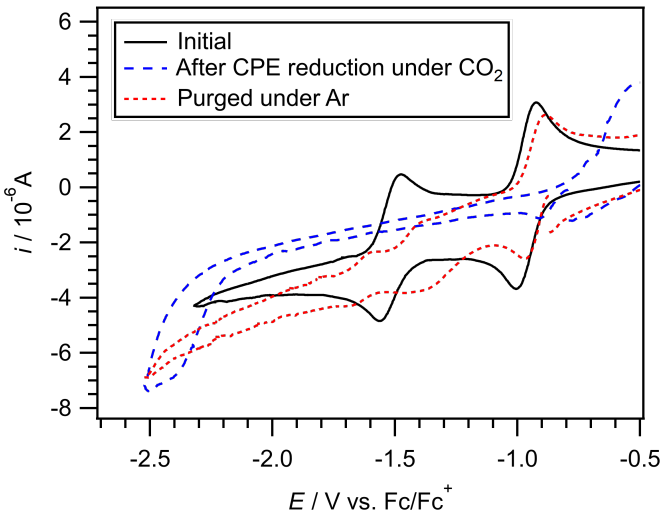

FIGURE 4.10: Cyclic voltammogram of naphthoquinone prior to electrolysis (solid black line), after CPE reduction under CO_2 atmosphere(dashed blue line), and after purging the solution under argon atmosphere (dashed red line).

potentials with the use of hydrogen-bonding additives, similar to the procedure proposed by Barlow and Yang on oxygen-stable quinone redox systems.[13] The motivation was to circumvent the potential for oxygen reduction, which can hinder the efficiency of CO_2 reduction catalysts.

The intermolecular hydrogen-bonding interactions mediated by alcohols have been shown to significantly influence the redox behavior of these compounds.[13,18] Specifically, hydrogen-bond donors can induce a positive shift in the second reduction potential of quinones while leaving the first reduction potential unaffected, as observed in tetrachlorobenzoquinone.[13] This phenomenon is particularly relevant when considering the chemical reactivity of quinone dianions with CO_2, which results in the irreversible formation of aryl carbonate species, rather than the weak CO_2 bound species that is preferred for CO_2 removal processes from solution. The presence of hydrogen-bond donors can stabilize the negatively charged oxygen atoms in both the quinone dianion and the quinone-CO_2 adduct through reversible interactions, leading to a more positive shift in the second reduction potential. Importantly, these hydrogen-bonding interactions can be fine-tuned by selecting alcohol additives with appropriate pKa values, offering a versatile approach to modulating the electrochemical properties of quinones.

In this section, our attention was focused on tetrachlorobenzoquinone as it was previously demonstrated the capability of tolerating oxygen in the presence of

alcohol as additives.[13] It was observed that the addition of 2,2,2-trifluoroethanol, a strong hydrogen bond donor, caused the most significant shift in the second reduction potential of tetrachlorobenzoquinone (Fig. 4.11 (b)), while not having a pronounced effect in hydrogen-bond acceptor such as urea (Fig. 4.11 (d)).

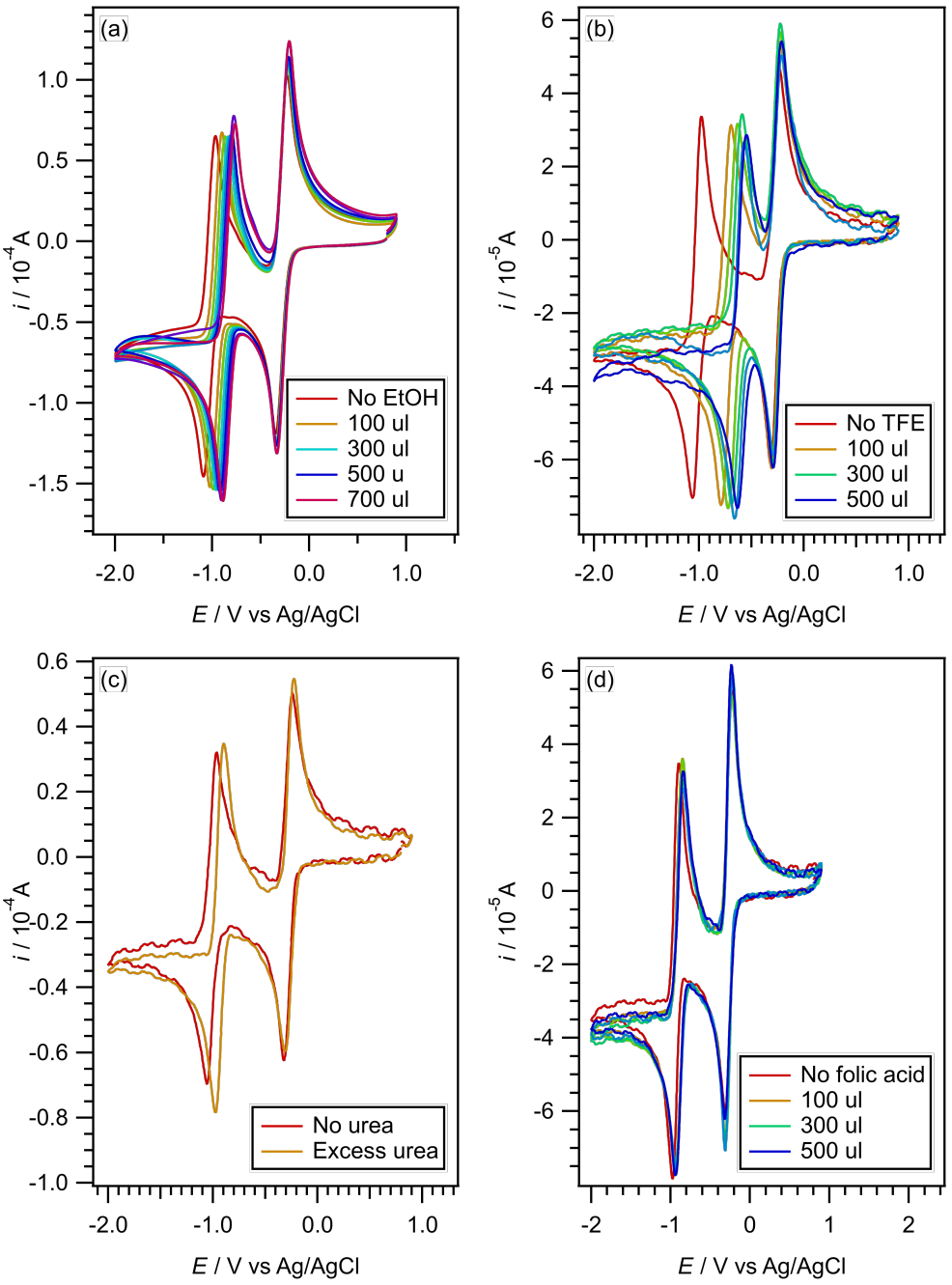

FIGURE 4.11: Cyclic voltammogram of naphthoquinone before (Solid red line) and after (Colored lines) adding additives to the solution.

Shi et al. investigated the impact of hydrogen bonding, protonation, and proton-coupled electron transfer (PCET) on the reduction potential of naphthoquinone.[18]

They found that hydrogen bonding with TFE and protonation with TFA could shift the reduction potential of naphthoquinone to more positive values, but the resulting reduced species had different stabilities. The hydrogen-bonded naphthoquinone dianion was less stable than the protonated dihydroquinone. DEM, a weak acid, exhibited a combination of hydrogen bonding and protonation effects, leading to a larger cell potential and excellent stability of the reduced quinone. Our finding in Section 4.4.3 corresponds are well supported by this work.

Building upon these findings, we attempted to modify the reduction potential of naphthoquinone and tetrachlorobenzoquinone using additives that function as hydrogen-bond donors, such as trifluoroethanol or diethylmalonate. The efforts were successful in shifting the reduction potential to more positive values, thereby increasing the stability of the reduced quinones-CO_2 adduct. This positive shift in reduction potential is crucial for enhancing the efficiency and selectivity of the CO_2 reduction process, as it helps to prevent the undesired reduction of oxygen and promotes the formation of the desired CO_2 reduction products.

In addition to exploring hydrogen-bond donors, we also investigated the acidification of reduced quinone species in a CO_2 environment using various proton sources. Our objective was to determine whether the acidification process could lead to the formation of valuable products such as formate or methanol, which are derived from the reduction of CO_2. However, our experiments, confirmed by ^{13}C-NMR analysis, revealed that the acidification of reduced quinone species did not yield the desired acidified CO_2 products. This finding suggests that the reduction of CO_2 using quinone-based catalysts may proceed through alternative mechanisms or require different reaction conditions to achieve the formation of formate or methanol.

4.4.4 Possibility of using reduced quinones in the presence of dissolved gases as redox flow batteries

The insights gained from our investigations into quinone electrochemistry led us to attempt the construction of a prototype battery system. Our primary goal was to demonstrate the feasibility of utilizing quinones as active materials in an energy storage device, specifically a redox flow battery (RFB).

The underlying hypothesis for this prototype was based on the observation that solutions of reduced quinones can exist at different potentials depending on whether they are under a CO_2 or an argon atmosphere. This suggested the possibility of modulating the cell potential, and hence the energy state of the reduced quinones, by simply purging the solution with CO_2 or argon gas. We hypothesized that this property could be exploited to create a rechargeable battery system where the charging and discharging processes are driven by the interconversion between the reduced quinone species under CO_2 and argon atmospheres.

To illustrate this concept, Scheme 4.2 and Scheme 4.3 show the different charging states of quinone reduction under argon and CO_2 atmospheres, respectively. For reduction under argon, the quinone undergoes two distinct one-electron reduction steps at different potentials. In contrast, strongly coordinating quinones under a CO_2 atmosphere exhibit a merging of the two one-electron reduction processes, occurring at a more positive potential close to -1 V vs. the Ag/AgCl reference electrode, as illustrated in Scheme 4.4.

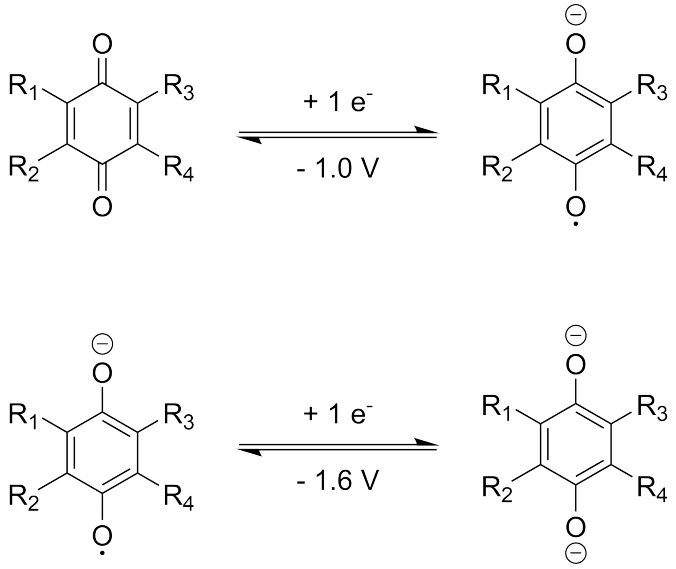

Scheme 4.2: Summary of the different charging state with associated electron counts and voltages (with respect to Ag/AgCl reference electrode, value from naphthoquinone) for quinone reduction under an argon atmosphere.

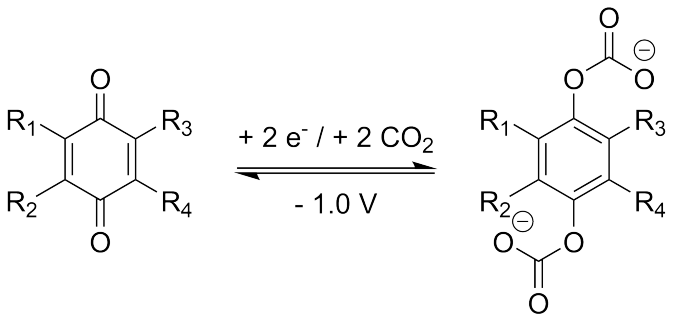

SCHEME 4.3: Summary of the different charging state with associated electron counts and voltages (with respect to Ag/AgCl reference electrode, value from naphthoquinone) for quinone reduction under a CO_2 atmosphere.

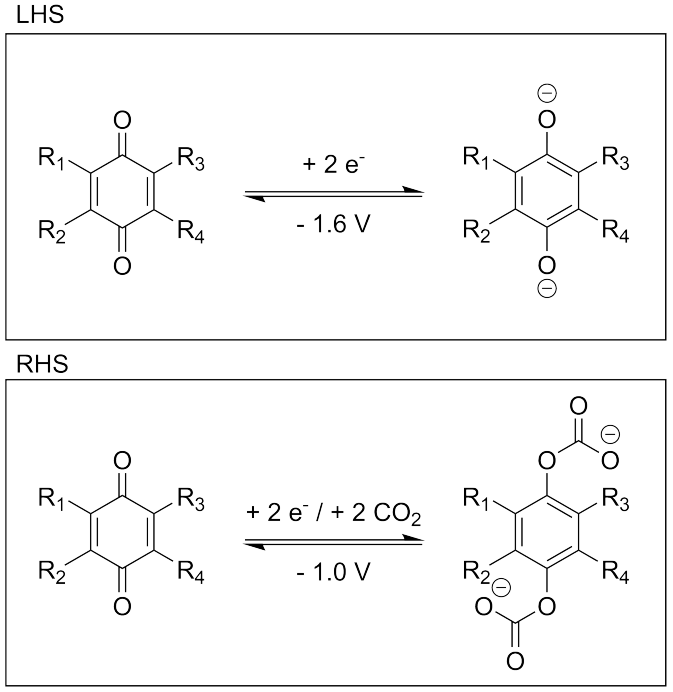

SCHEME 4.4: Overall charging and discharging interaction of quinone with voltage (with respect to Ag/AgCl reference electrode, value from naphthoquinone), in the left-hand side (LHS, charging) and the right-hand side (RHS, discharging).

The shorthand notation of Scheme 4.4 can be written out as follows.

$$Electrode|\mathrm{Q}^{2-}\ (solv, c = 0.001M), Q(solv, C = 0.000M)|| \\ Q(solv, C = 0.001M), \mathrm{Q(CO_2)_2}^{2-}(solv, C = 0.000M), \mathrm{CO_2}(satd.), |Electrode \tag{4.2}$$

Thus, the resulting expected cell potential is:

$$E_{cell} = E_{RHS} - E_{LHS} \tag{4.3}$$

$$E_{cell} = -1V - (-1.6V) = 0.6V \tag{4.4}$$

The proposed battery scheme, depicted in Scheme 4.5, involves a three-stage process to investigate the electrochemical behavior of quinones under these varying atmospheric conditions. Initially, the quinone in the working chamber was reduced under an argon atmosphere, with the counter chamber containing a sacrificial electron donor to facilitate the reduction. In the second stage, the sacrificial donor was replaced with uncharged quinone, which was then purged with CO_2. Finally, the potential difference between the two chambers was measured, allowing for the observation of a spontaneous charge-discharge process.

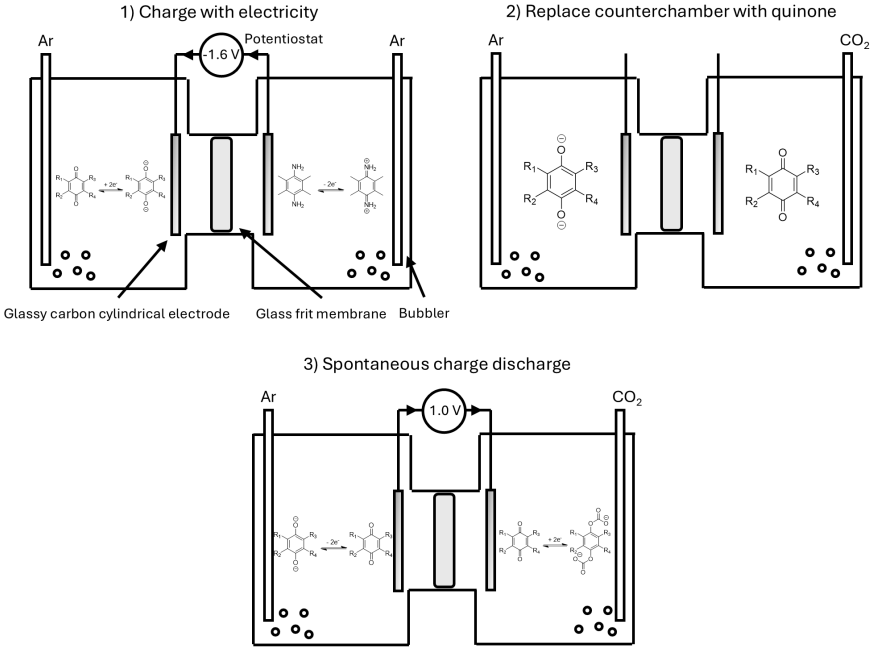

SCHEME 4.5: Proposed redox flow battery system controlled by switching the CO_2 and Ar gas flow between compartments for charging and discharging cycles.

Central to the development of this quinone-based battery system was the selection of appropriate compounds for the counter electrode compartment. Drawing from previous findings on the susceptibility of quinones to decomposition under oxidative

conditions (Section 4.4.2), we chose to employ organic compounds that can undergo chemically reversible oxidation and remain stable in their oxidized state. This approach aimed to mitigate the detrimental effects of oxidative decomposition on the quinone species, thereby enhancing the overall stability and performance of the battery system.

The prototype quinone-based battery demonstrated the capability to store and release electrical energy, albeit with limited charge release efficiency. Under argon purging of the counter chamber, the efficiency averaged 35 ±6%, while CO_2 purging resulted in a slightly improved efficiency of 40 ±4%. This enhanced performance under CO_2 was anticipated due to the positive shift in the reduction potential of the quinone, which theoretically leads to a better potential gradient between the working and counter chambers. Fig. 4.12 compares the CVs in the initial, charged, and discharged states, along with the chronoamperometry of the charge release state indicating the discharge efficiency.

The modest efficiency observed can be attributed to various factors, including the intrinsic redox properties of the quinone species, spontaneous comproportionation (Scheme 4.6), and overall cell design. Despite these limitations, the successful operation of the prototype battery serves as a proof-of-concept, highlighting the potential of quinones as active materials in energy storage applications. Further optimization of battery components, such as the quinone species, electrode materials, electrolyte composition, and cell configuration, may lead to improved charge release efficiency and overall performance. The insights gained from this prototype study provide valuable direction for future research efforts aimed at developing high-performance quinone-based redox flow battery systems, particularly in the context of CO_2 utilization.

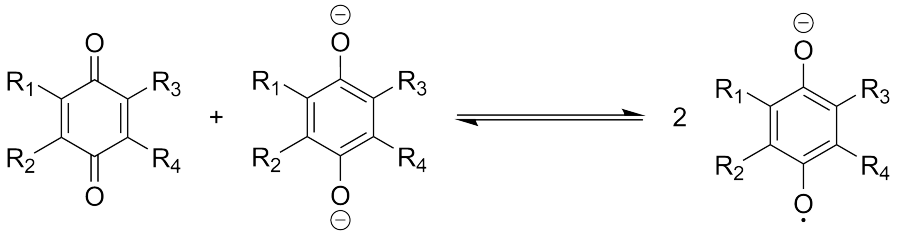

Scheme 4.6: Mechanism for possible comproportionation of present quinone dianion and neutral quinone to quinone radical anion.

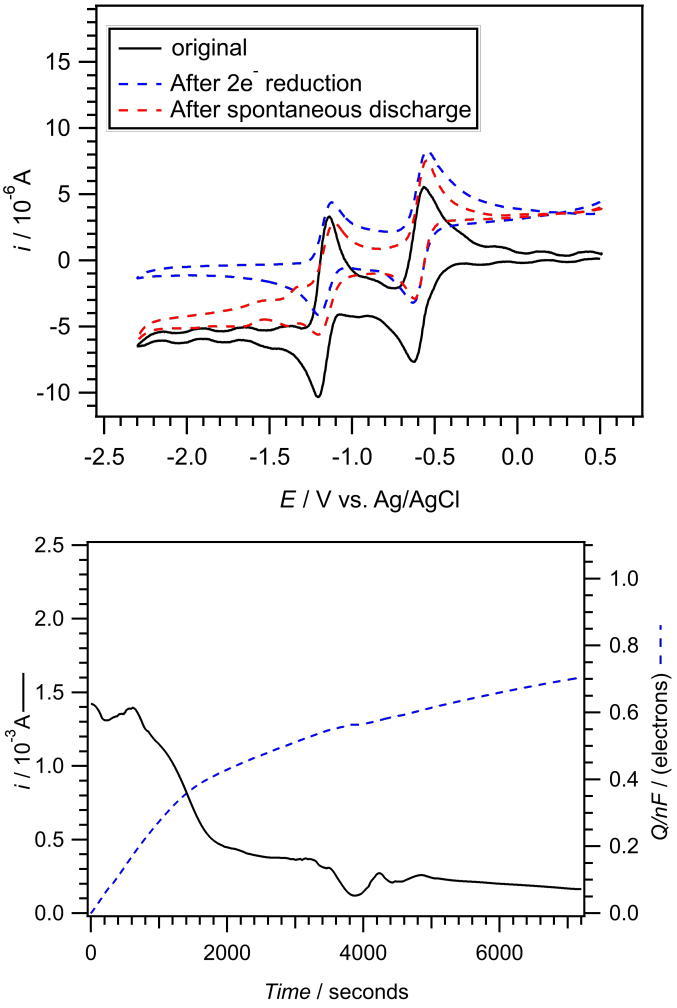

FIGURE 4.12: (Top) cyclic voltammogram and (Bottom) charge discharge chronoamperometry of battery process, based on an experiment with 2 mM menadione in 0.1 M n-Bu_4NPF_6/MeCN.

4.4.5 Limitations and Challenges

Throughout the investigation into the electrochemistry of quinones for CO_2 reduction and energy storage applications, we encountered several key limitations and challenges that warrant further discussion. One of the primary challenges was the susceptibility of quinones to decomposition under oxidative conditions. This issue hindered the reversibility and long-term stability of the redox processes, as the quinone species were prone to irreversible reactions and degradation when subjected to positive potentials. Although attempts were made to mitigate this by employing organic oxidants in the counter electrode, the inherent instability of the oxidized quinone forms remains a significant concern that requires further attention.

In addition to the problems with oxidative stability, the sensitivity of quinone-based systems to molecular oxygen and trace water content in the reaction media also posed substantial limitations. Previous studies have highlighted that the presence of oxygen can lead to parasitic reactions between the reduced quinone species and O_2, resulting in the formation of superoxide radicals and reduced efficiency of the targeted CO_2 reduction processes.[19] Furthermore, the hydrogen-bonding interactions between water molecules and the quinone redox states were found to modulate their reduction potentials and overall stability, potentially impacting the reversibility and performance of the system.[15,16]

Strategies to address the oxygen and water sensitivity, such as molecular engineering of more stable quinone derivatives and the use of concentrated salt solutions, have been explored in recent work.[20,21] However, in the present study, the primary focus was on demonstrating the feasibility of using quinones as active materials in a rechargeable air-battery system, rather than optimizing the long-term stability and reversibility for CO_2 capture and release applications. As such, the decision was made to not delve deeply into the mitigation of oxygen and water effects, as these factors were deemed to have a relatively smaller impact on the proposed battery concept.

Nevertheless, future studies building upon this work should carefully address the limitations posed by oxygen and water, as these parameters can significantly influence the practical deployment and scalability of quinone-based technologies for energy storage and CO_2 utilization. By developing more oxygen-stable quinone derivatives and employing robust electrolyte formulations, researchers can provide a more comprehensive understanding of the challenges and tradeoffs involved in harnessing the potential of these redox-active organic molecules.

Another limitation encountered in this study was the modest charge release efficiency of the prototype quinone-based battery. While the battery demonstrated proof-of-concept operation, the efficiency was limited to 40%, which is not yet competitive with existing energy storage technologies. Improving the efficiency will require a comprehensive optimization of the battery components, including the quinone species, electrode materials, electrolyte composition, and cell design. These aspects have been highlighted in recent work on aqueous quinone flow chemistry for electrochemical CO_2 capture.[22]

It is important to note that the primary focus of the present work was on demonstrating the feasibility of using quinones in a rechargeable battery system, rather than optimizing the system for CO_2 capture and concentration applications. As such, we did not conduct a comprehensive benchmarking of the prototype against existing CO_2 capture technologies. Future studies building upon this work should carefully evaluate the performance and energy efficiency of the quinone-based system in comparison to other CO_2 capture methods, in order to assess its potential for real-world applications in carbon management.

Overall, the limitations identified in this work align with the challenges reported in the literature, particularly regarding the oxidative and oxygen sensitivity of quinone-based systems, as well as the need for further optimization to enhance their performance and practical applicability. Addressing these limitations will be crucial for realizing the full potential of quinone-based energy storage and CO2 utilization systems.

4.5 Conclusion

In this chapter, we have explored the unique electrochemical properties of quinones and their potential applications in CO_2 reduction and energy storage. Our investigations have provided valuable insights into the behavior of quinones under different atmospheric conditions, the impact of proton/hydrogen sources on their redox properties, and their reactivity towards CO_2.

We have demonstrated that the reversibility of quinone redox processes is enhanced under a CO_2 atmosphere compared to an Ar atmosphere, which can be attributed to the positive shift in the second reduction potential observed under CO_2. This finding highlights the potential of quinones as CO_2-binding redox molecules for carbon capture and utilization. However, we also discovered that the application of a positive potential to quinones can lead to their decomposition, emphasizing the need for careful consideration of the oxidative stability of these species.

Our efforts to modify the reduction potential of quinones using hydrogen-bond donors and to acidify the reduced quinone species have shown promise in increasing the stability of the reduced quinones-CO_2 adduct and preventing undesired side reactions. However, further research is necessary to optimize these strategies and

to elucidate the mechanisms governing the formation of desired CO_2 reduction products.

The successful construction and operation of a prototype quinone-based battery serves as a proof-of-concept for the utilization of quinones as active materials in energy storage devices. While the charge release efficiency was modest, this study provides a foundation for future research aimed at optimizing quinone-based energy storage systems.

Overall, our findings contribute to the growing body of knowledge on quinone electrochemistry and its potential applications in CO_2 reduction and energy storage. The insights gained from this study pave the way for the development of innovative and sustainable solutions to address the pressing challenges of carbon capture, utilization, and renewable energy storage. However, further research is necessary to overcome the limitations and challenges identified in this work and to fully realize the potential of quinone-based technologies in these critical areas.

References

(1) Yoro, K. O.; Daramola, M. O. In *Advances in Carbon Capture*, Rahimpour, M. R., Farsi, M., Makarem, M. A., Eds.; Woodhead Publishing: 2020, pp 3–28.

(2) Symons, P. Quinones for redox flow batteries. *Current Opinion in Electrochemistry* **2021**, *29*, 100759.

(3) Huskinson, B.; Marshak, M. P.; Suh, C.; Er, S.; Gerhardt, M. R.; Galvin, C. J.; Chen, X.; Aspuru-Guzik, A.; Gordon, R. G.; Aziz, M. J. A metal-free organic–inorganic aqueous flow battery. *Nature* **2014**, *505*, Publisher: Nature Publishing Group, 195–198.

(4) Mizen, M. B.; Wrighton, M. S. Reductive Addition of CO 2 to 9,10-Phenanthrenequinone. *Journal of The Electrochemical Society* **1989**, *136*, Publisher: IOP Publishing, 941.

(5) Tam, S. M.; Tessensohn, M. E.; Tan, J. Y.; Subrata, A.; Webster, R. D. Competition between Reversible Capture of CO2 and Release of CO2•– Using Electrochemically Reduced Quinones in Acetonitrile Solutions. *The Journal of Physical Chemistry C* **2021**, *125*, Publisher: American Chemical Society, 11916–11927.

(6) Kissinger, P.; Heineman, W. R., *Laboratory Techniques in Electroanalytical Chemistry, Second Edition, Revised and Expanded*, Google-Books-ID: AwuTx14Ro2UC; CRC Press: 1996; 1014 pp.

(7) Hui, Y.; Chng, E. L. K.; Chua, L. P.-L.; Liu, W. Z.; Webster, R. D. Voltammetric Method for Determining the Trace Moisture Content of Organic Solvents Based on Hydrogen-Bonding Interactions with Quinones. *Analytical Chemistry* **2010**, *82*, Publisher: American Chemical Society, 1928–1934.

(8) Elgrishi, N.; Rountree, K. J.; McCarthy, B. D.; Rountree, E. S.; Eisenhart, T. T.; Dempsey, J. L. A Practical Beginner's Guide to Cyclic Voltammetry. *Journal of Chemical Education* **2018**, *95*, Publisher: American Chemical Society, 197–206.

(9) Zito, A. M.; Yang, J. Y. Electrolyte Effects on the Reduction Potential and Carbon Dioxide Binding Affinity of Quinones. *Journal of The Electrochemical Society* **2024**, *171*, Publisher: IOP Publishing, 043502.

(10) Simeon, F.; Stern, M. C.; Diederichsen, K. M.; Liu, Y.; Herzog, H. J.; Hatton, T. A. Electrochemical and Molecular Assessment of Quinones as CO2-Binding Redox Molecules for Carbon Capture. *The Journal of Physical Chemistry C* **2022**, *126*, Publisher: American Chemical Society, 1389–1399.

(11) Schimanofsky, C.; Wielend, D.; Kröll, S.; Lerch, S.; Werner, D.; Gallmetzer, J. M.; Mayr, F.; Neugebauer, H.; Irimia-Vladu, M.; Portenkirchner, E.; Hofer, T. S.; Sariciftci, N. S. Direct Electrochemical CO $_2$ Capture Using Substituted Anthraquinones in Homogeneous Solutions: A Joint Experimental and Theoretical Study. *The Journal of Physical Chemistry C* **2022**, *126*, 14138–14154.

(12) Xu, Y.; Zheng, M.; Musgrave, C. B.; Zhang, L.; Goddard, W. A.; Bukowski, B. C.; Liu, Y. Assessing the Kinetics of Quinone–CO $_2$ Adduct Formation for Electrochemically Mediated Carbon Capture. *ACS Sustainable Chemistry & Engineering* **2023**, *11*, 11333–11341.

(13) Barlow, J. M.; Yang, J. Y. Oxygen-Stable Electrochemical CO $_2$ Capture and Concentration with Quinones Using Alcohol Additives. *Journal of the American Chemical Society* **2022**, *144*, 14161–14169.

(14) Zito, A. M.; Bím, D.; Vargas, S.; Alexandrova, A. N.; Yang, J. Y. Computational and Experimental Design of Quinones for Electrochemical CO $_2$ Capture and Concentration. *ACS Sustainable Chemistry & Engineering* **2022**, *10*, 11387–11395.

(15) Hui, Y.; Chng, E. L. K.; Chng, C. Y. L.; Poh, H. L.; Webster, R. D. Hydrogen-Bonding Interactions between Water and the One- and Two-Electron-Reduced Forms of Vitamin K1: Applying Quinone Electrochemistry To Determine the Moisture Content of Non-Aqueous Solvents. *Journal of the American Chemical Society* **2009**, *131*, Publisher: American Chemical Society, 1523–1534.

(16) Tessensohn, M. E.; Hirao, H.; Webster, R. D. Electrochemical Properties of Phenols and Quinones in Organic Solvents are Strongly Influenced by Hydrogen-Bonding with Water. *The Journal of Physical Chemistry C* **2013**, *117*, Publisher: American Chemical Society, 1081–1090.

(17) Rocha-Ortiz, G.; Tessensohn, M. E.; Salas-Reyes, M.; Flores-Moreno, R.; Webster, R. D.; Astudillo-Sánchez, P. D. Homogeneous electron-transfer reaction between anionic species of anthraquinone derivatives and molecular oxygen in acetonitrile solutions: Electrochemical properties of disperse red 60. *Electrochimica Acta* **2020**, *354*, 136601.

(18) Shi, R. R. S.; Tessensohn, M. E.; Lauw, S. J. L.; Foo, N. A. B. Y.; Webster, R. D. Tuning the reduction potential of quinones by controlling the effects of hydrogen bonding, protonation and proton-coupled electron transfer reactions. *Chemical Communications* **2019**, *55*, 2277–2280.

(19) Jeziorek, D.; Ossowski, T.; Liwo, A.; Dyl, D.; Nowacka, M.; Woźnicki(Deceased), W. Theoretical and electrochemical study of the mechanism of anthraquinone-mediated one-electron reduction of oxygen: the involvement of adducts of dioxygen species to anthraquinones. *Journal of the Chemical Society, Perkin Transactions 2* **1997**, *0*, Publisher: Royal Society of Chemistry, 229–236.

(20) Liu, Y.; Ye, H.-Z.; Diederichsen, K. M.; Van Voorhis, T.; Hatton, T. A. Electrochemically mediated carbon dioxide separation with quinone chemistry in salt-concentrated aqueous media. *Nature Communications* **2020**, *11*, 2278.

(21) Li, C. J.; Ziller, J. W.; Barlow, J. M.; Yang, J. Y. Aqueous Electrochemical and pH Studies of Redox-Active Guanidino Functionalized Aromatics for CO2 Capture. *ACS Organic & Inorganic Au* **2024**, *4*, Publisher: American Chemical Society, 387–394.

(22) Jing, Y.; Amini, K.; Xi, D.; Jin, S.; Alfaraidi, A. M.; Kerr, E. F.; Gordon, R. G.; Aziz, M. J. Electrochemically Induced CO2 Capture Enabled by Aqueous Quinone Flow Chemistry. *ACS Energy Letters* **2024**, *9*, Publisher: American Chemical Society, 3526–3535.

Chapter 5

Probing the Molecular Interactions of Electrochemically Reduced Vitamin B_2 with CO_2

5.1 Abstract

The electrochemical reduction of riboflavin (vitamin B_2) in a dimethyl sulfoxide solvent was examined under a CO_2 atmosphere and compared with results under an argon atmosphere. Variable-scan-rate cyclic voltammetry combined with controlled potential electrolysis (CPE) and analysis by UV–vis and EPR spectroscopies provided insights into the nature of interactions of reduced flavins with dissolved CO_2. Reductive exhaustive CPE experiments under CO_2 indicated an overall two-electron stoichiometry, compared to one-electron reduction under an argon atmosphere, due to the lowering of the formal one-electron reduction potential of the flavin radical anion to form the dianion, which can be rationalized by riboflavin–CO_2 molecular interactions. UV–vis spectroscopic measurements confirmed complete chemical reversibility of the redox transformations over extended time scales. Digital simulation modeling of the voltammetric data enabled extraction of thermodynamic and kinetic parameters for the proposed mechanism, comprising multiple proton-coupled electron transfer steps, diamagnetic anions, radical anions, and neutral radical intermediates enroute to the fully reduced state, as well as evidence of a long-lived solution phase complex of the reduced riboflavin with CO_2.

5.2 Introduction

Riboflavin is the crucial component responsible for redox activity in the cofactors flavin adenine dinucleotide and flavin mononucleotide. These cofactors power numerous biological redox reactions by facilitating electron movement across diverse chemical groups.[1,2] Examples of these reactions include the dehydrogenation of NADPH and d-amino acids. Within membranes, flavoenzymes exhibit greater electron-transfer adaptability than nicotinamide coenzymes (NAD/NADP), handling both single-electron and two-electron transfers.[3–6] This flexibility lets flavins bridge the gap between two-electron donors (like NADH) and single-electron acceptors (such as heme Fe). Importantly, flavins engage in key aerobic processes due to their distinct oxygen interactions.[4]

Similar to quinones, flavins can exist in three oxidation states: flavoquinone (Flox), flavosemiquinone radical ($Fl_{rad}{}^{\bullet-}$), and flavohydroquinone dianion ($Fl_{red}{}^{2-}$). The electrochemical reduction mechanism for vitamin B_2 in an aprotic solution is an ECE

(where E represents an electron transfer and C represents a chemical step) process for cyclic voltammograms recorded between -0.5 and -1.6 V vs Fc/Fc^+ (where Fc = ferrocene).[6] For larger potential windows, additional electron transfer and chemical steps are observed. In buffered aqueous solutions, a chemically reversible electron transfer involving the transfer of two electrons and two protons occurs.[7]

Literature reports have shown that quinones in their reduced forms can undergo molecular bonding with carbon dioxide (CO_2), leading to substantial changes in their formal reduction potentials (E_f^0) compared to those observed under inert Ar or N_2 atmospheres.[8] This binding relationship between quinone and CO_2 has been proposed for utilization for CO_2 capture and concentration.[9–15] Therefore, considering the similar electrochemical behavior of quinones and flavins, experiments were performed in this study to test whether reduced flavins were also able to undergo molecular interactions with dissolved CO_2 and to determine how the overall reduction mechanism changed in a CO_2-rich environment.

Investigations by Tatwawadi et al.[16] and Sawyer and McCreery[17] in inert atmospheres partially characterized the electrochemical reduction of riboflavin (Fl_{ox}) in dimethyl sulfoxide (DMSO) using voltammetry. They observed two reduction processes on the forward scan and several oxidation processes when the scan direction was reversed after first reducing the compound. They concluded that the first reduction wave was a one-electron transfer process to form a radical anion ($Fl_{rad}^{\bullet -}$) while the second electron transfer step also occurred by one electron to form the dianion (Fl_{red}^{2-}), analogous to quinone reductions in aprotic media.[18–21] Complementary electrolysis-EPR experiments by Male et al.[22] corroborated formation of $Fl_{rad}^{\bullet -}$ upon controlled potential electrolysis (CPE) with the potential held just past the first reduction peak. Comproportionation between fully reduced Fl_{red}^{2-} and Fl_{ox} species also appeared to be responsible for $Fl_{rad}^{\bullet -}$ generation in both aqueous and nonaqueous solvents.

Additional cyclic voltammetry (CV) studies by Niemz et al.[6] and Tan and Webster[23] verified that the electrochemical reduction initially follows a one-electron pathway, generating $Fl_{rad}^{\bullet -}$. However, detailed EPR spectroscopic studies and modeling of voltammetric data with digital simulations indicated that the mechanism was much more complicated than simple electron transfer and involved multiple proton-transfer reactions (Scheme 5.1).[6,23] Specifically, a homogeneous reaction of the intermediate $Fl_{red}H^-$ with residual Fl_{ox}^- drives the formation of additional $Fl_{rad}^{\bullet -}$ beyond that

produced via heterogeneous electron transfer at the electrode surface (Scheme 5.1). Spectral monitoring verified the presence of both radical and fully reduced species as reduction products.[23] Definitive voltammetric signatures of starting Fl_{ox} and end Fl_{red}^{2-} facilitated thermodynamic assignments for the multistep mechanism.[23]

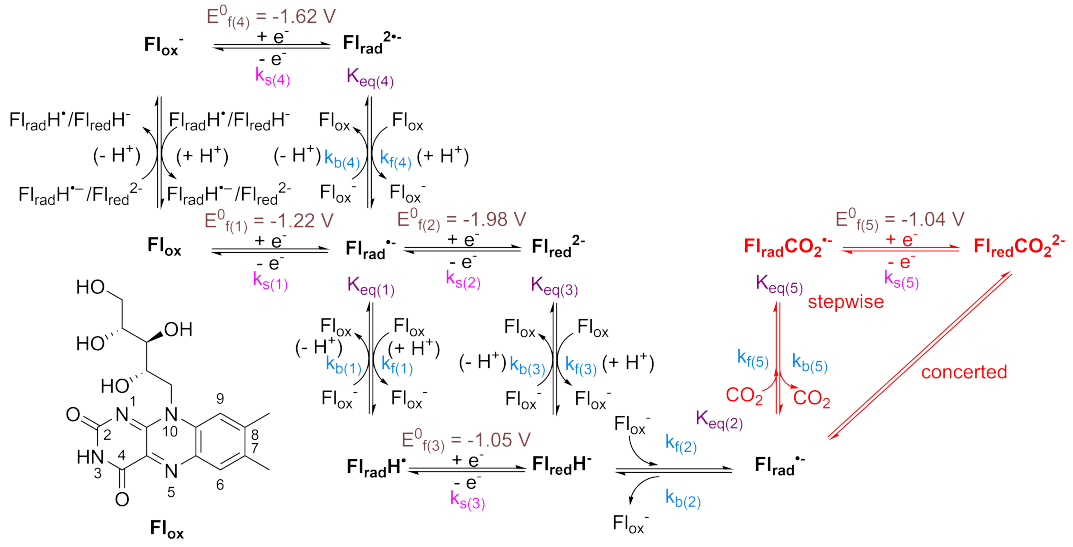

SCHEME 5.1: Mechanism for the Electrochemical Reduction of Riboflavin in DMSO under Ar (Black) or CO_2 (Black and Red). Conditions Determined by Variable Scan-Rate CV Studies.[1]

In this study, CV with varying scan rates and spectroscopic analysis (UV–vis and EPR) were used to identify the species and pathways behind the observed voltammetric processes of riboflavin under a CO_2 atmosphere. Digital simulation procedures were used to model the complex mechanism, characterized by proton-coupled electron transfer (PCET), yielding detailed kinetic and thermodynamic parameters.

[1]Values for equilibrium and kinetic reactions related to the homogeneous chemical processes, as well as electrochemical data linked to the heterogeneous electron transfer steps ($E^0_{f(1)} - E^0_{f(5)}$), can be found in Table 1 and [23]. The counterions for the ionized species are either the cation ($n\text{-}Bu_4N^+$) or the anion (PF_6^-) from the supporting electrolyte.

5.3 Materials and methods

5.3.1 Chemicals

Riboflavin sourced from *Eremothecium ashbyii* and having a purity of at least $\geq$ 98% was procured from Sigma-Aldrich. The supporting electrolyte, n-Bu_4NPF_6, was produced by combining equal molar quantities of a 40% n-Bu_4OH aqueous solution and a 65% HPF_6 aqueous solution. The resulting precipitate was rinsed with water, recrystallized thrice using hot ethanol, and then dried in vacuum for 24 h at 140 °C.

For the preparation of electrochemical solutions, DMSO (from Merck) and the appropriate quantity of n-Bu_4NPF_6 were added to 3 Å molecular sieves (from Fluka) that were dried under vacuum at 250 °C for 6 h in a Buchi Glass Oven B-585. The DMSO/electrolyte mixture was then left in a glass vacuum syringe under a argon atmosphere for a minimum of 36 h.

5.3.2 Electrochemical procedures

CV experiments were conducted with a computer-controlled Eco Chemie Autolab PGSTAT302N with an ADC10M ultrafast sampling module and SCAN250 true linear scan generator module. The working electrode was a 1 mm diameter planar Pt disk, used in conjunction with a Pt wire auxiliary electrode and a silver wire miniature reference electrode (purchased from eDAQ) separated from the test solution through a porous glass frit containing an internal solution of 0.5 M n-Bu_4NPF_6 in MeCN. Accurate potentials were obtained using ferrocene as an internal standard. The electrochemical cells were dried at 110 °C for at least 1 h prior to use. Solutions of riboflavin (1 mM, 0.5 M n-Bu_4NPF_6 in DMSO) for voltammetric analysis were deoxygenated by purging them with high-purity Ar or CO_2 gas, and all voltammetric experiments were conducted at 22(2) °C in a Faraday cage. Potentials were first recorded at an Ag/AgCl reference electrode and then coverted to versus ferrocene/ferrocenium redox couple (Fc/Fc^+) by comparing the voltammetric peak potentials of riboflavin to the Fc added at the end of the experiment.

Digital simulations of the CV data were performed by using the DigiElch 6 software package (Gamry Instruments). The simulation procedure involves matching the experimentally obtained CV curves with CV curves that are theoretically generated based on electrochemical, kinetic, and thermodynamic parameters. The electrochemical input values include the formal potentials, uncompensated solution resistance, capacitance, electrode area, diffusion coefficients, and experimental conditions, including the voltammetric scan rates and scan range. Some information is set based on the experimental conditions, while other parameters are estimated by matching the simulated CV curves with the experimental data. The electrochemical and homogeneous reactions are entered into the software, with each species given a unique identifier, usually based on an alphabet character. The kinetic values for the homogeneous reactions (the forward (k_f) and backward (k_b) rate constants) are estimated from how the voltammetric peaks vary in relative intensity as the voltammetric scan rates are varied, which then allow a calculation of the equilibrium constants ($K_{eq} = k_f/k_b$). The simulations are repeatedly refined until the calculated voltammograms best fit the experimental voltammograms by using identical parameters over a range of voltammetric scan rates.

CPE was performed in a two-compartment electrolysis cell using cylindrical glassy carbon electrodes as the working and auxiliary electrodes and a silver wire as the reference electrode contained in a solution of 0.5 M n-Bu_4NPF_6 in MeCN and separated from the working electrode compartment with a glass membrane.

5.3.3 Spectroscopic experiments

UV–vis spectra were obtained ex situ by electrolyzing solutions of riboflavin in DMSO at 22(2) °C, transferring under Ar or CO_2 atmospheres to a UV flat cell, and recording on a PerkinElmer Model Lambda 750 UV–vis–NIR spectrophotometer. 1 H and 13 C NMR spectra were obtained of electrolyzed solutions of riboflavin in DMSO at 22(2) °C, which were transferred into NMR tubes and recorded using Bruker AVANCE 400 and AVANCE III 400 spectrometers. EPR spectra were obtained from electrolyzed solutions of riboflavin in DMSO at 22(2) celsius, which were transferred to a quartz flat cell and recorded using a continuous-wave X-band Bruker ELEXSYS E500 EPR spectrometer.

5.3.4 Computational methods

The molecular structures were illustrated using Chemcraft and fine-tuned with the BP86 density functional,[24] utilizing def2-SVP (split valence polarization)[25] and def2-TZVP (valence triple-ζ polarization)[26] Ahlrichs basis sets.[27] The effects of solvation were considered within the ORCA suite of programs.[28–31] The final structures of the compounds were confirmed to remain at true energy minima by conducting frequency calculations at the BP86/def2-TZVP level, which resulted in no imaginary frequencies. Atomic charges calculated using Mulliken and the natural bond orbital (NBO) were derived from DFT calculations at the BP86/def2-TZVP level of theory.

5.4 Results and discussion

5.4.1 Cyclic voltammetry

CV of riboflavin (Fl_{ox}) in DMSO under an Ar atmosphere at a scan rate of 100 mV s^{-1} led to a reduction wave observed at approximately -1.25 V vs Fc/Fc^+ as shown as wave 1 in Fig. 5.1 (a) (dashed red trace), due to two overlapping one-electron reduction steps. The initial reduction occurred by one electron to form the radical anion ($Fl_{rad}{}^{\bullet-}$), which abstracted a proton from another flavin to form $Fl_{ox}{}^-$ and $Fl_{rad}H^\bullet$. Because $Fl_{rad}H^\bullet$ is easier to reduce than Fl_{ox}, it immediately underwent a second electron transfer to form $Fl_{red}H^-$ as previously reported.[6,23] When the scan direction was reversed at -1.6 V vs Fc/Fc^+ after first reducing riboflavin, two oxidation waves were observed labeled as wave 2 and wave 3 in Fig. 5.1 (dashed red trace). Wave 2 is associated with the one-electron oxidation of $Fl_{rad}{}^{\bullet-}$, and wave 3 is due to the one-electron oxidation of $Fl_{red}H^-$, with the relative size of the waves varying depending on the voltammetric scan rates.[6,23] When the scan was extended to more negative potentials, two additional waves were detected which have been assigned to the reduction of $Fl_{ox}{}^-$ (wave 4) and reduction of $Fl_{rad}H^\bullet$ (wave 5),[23] as shown in Fig. 5.1 (b).

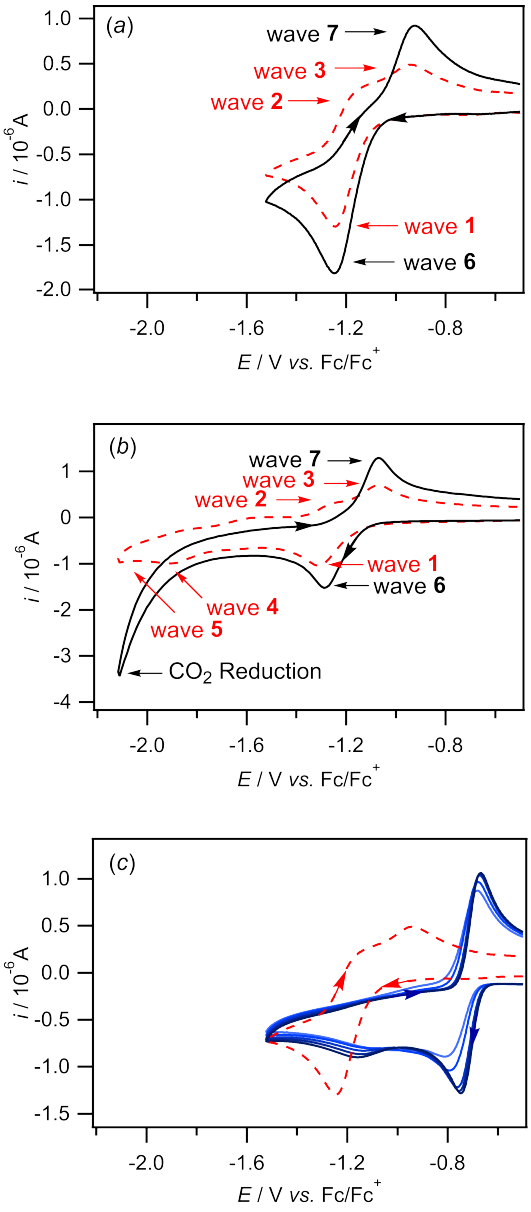

FIGURE 5.1: Cyclic voltammograms obtained for the reduction processes of 1 mM riboflavin in DMSO with 0.5 M n-Bu_4NPF_6 using a 1 mm diameter planar Pt electrode at a scan rate of 0.1 V s^{-1}. (Dashed red line) Ar atmosphere. (Solid black line) CO_2 atmosphere. (a) The scan direction was reversed at -1.5 V vs Fc/Fc+. (b) The scan direction was reversed at -2.1 V vs Fc/Fc+. (c) Trifluoroacetic acid was added in quantities ranging from 1 (pale blue) to 5 (dark blue) equiv under an Ar atmosphere compared to the voltammogram prior to the acid addition (dashed red line).

CV of Fl_{ox} in DMSO under a CO_2 environment at a scan rate of 100 mV s^{-1} led to only one forward reduction peak at -1.3 V (Fig. 5.1 (a) black trace) (wave 6) and one reverse oxidation peak at -1.1 to -0.9 V (Fig. 5.1 (a) and (b), black trace) (wave 7)

when the scan was reversed. The large increase in negative current that is observed in the black trace in Fig. 5.1 (b) at -1.8 V vs Fc/Fc^+ is due to the direct reduction of dissolved CO_2(g). However, when the scan rate was progressively increased above approximately 2 V s^{-1}, the voltammograms began to match what was observed under an argon atmosphere, where waves 1, 2, and 3 were the dominant processes (Fig. 5.2).

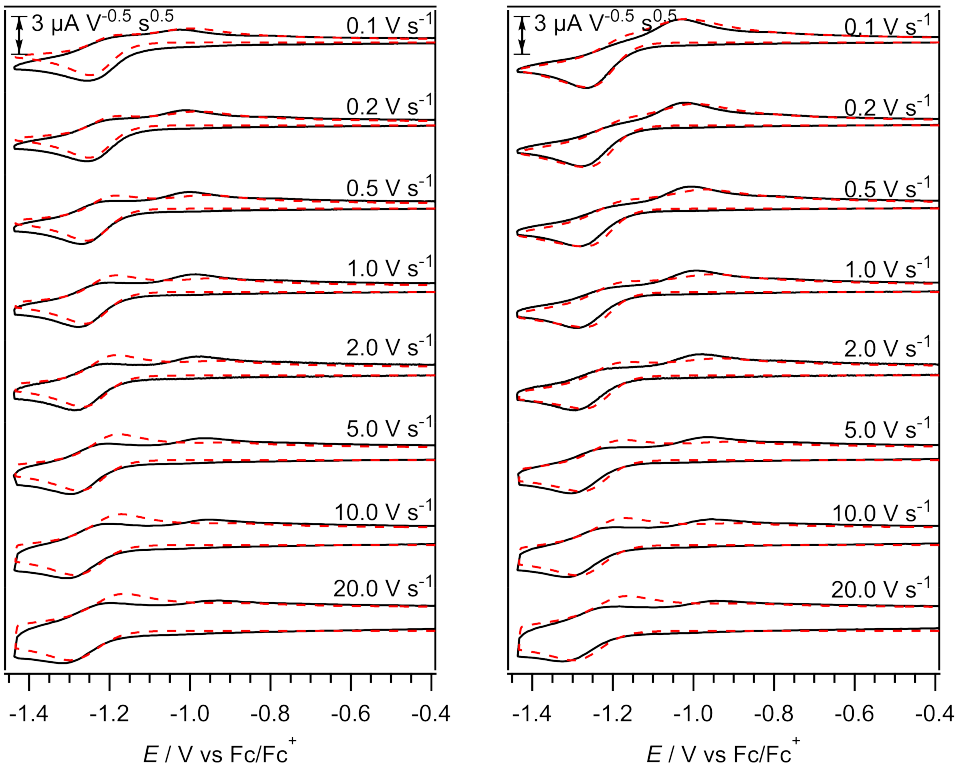

FIGURE 5.2: (Black lines) Cyclic voltammograms with varying scan rates of 1 mM riboflavin in DMSO with 0.5 M n-Bu_4NPF_6 recorded at a temperature of 22(2) °C using a 1 mm Pt electrode. (Red dashed lines) Digital simulations of the CV data based on the mechanism in Scheme 5.1 and parameters given in Table 1 and [23]. (Left) CV curves recorded under an Ar atmosphere. (Right) CV curves recorded under a CO_2 atmosphere. The current data were scaled by multiplying by $\nu^{-0.5}$

Therefore, the results were interpreted based on an initial slow reaction of CO_2 with reduced Fl_{ox} at lower scan rates (<2 V s^{-1}), which was outrun as the scan rate was progressively increased. It is important to note that the change in the appearance of the CV curves under a CO_2 atmosphere is not due to a change in the pH of the solutions due to any conversion of dissolved CO_2 to carbonic acid. Voltammograms recorded in the presence of small amounts of deliberately added

acid do appear as chemically reversible two-electron, two-proton processes as shown in Fig. 5.1 (c) (as expected for flavins in aqueous buffered solution, red dashed line indicated the original voltammogram of Fl_{ox} prior to the acid addition)[32] but are shifted substantially in potential compared to what is observed in Fig. 5.1 (b).

5.4.2 Controlled potential electrolysis

Experiments involving CPE and coulometry were carried out to ascertain the number of electrons involved in the reduction of riboflavin and to estimate the duration of the existence of the reduced entities. Experiments on Fl_{ox} in previous studies in DMSO under argon indicated an overall one-electron-per-molecule reduction stoichiometry for exhaustive electrolysis.[16,23] This aligns with a mechanism whereby approximately half of the starting Fl_{ox} undergoes two-electron reduction, balanced by the remaining half acting as proton donors to form Fl_{ox}^{-} (Scheme 5.1). Thus, despite the two-electron reduction associated with the first voltammetric wave under CV conditions, CPE and coulometry measurements indicate that the reaction proceeds through the transfer of just one electron per riboflavin molecule during exhaustive electrolysis.

CPE experiments on Fl_{ox} were performed under a CO_2 atmosphere with an applied potential of approximately -1.1 V versus an Ag wire (separated via a salt bridge), which is 0.3 V more negative than the reduction peak potential (E_p^{red}). Over the course of electrolysis, the solution changed from yellow to reddish-brown. Fig. 5.3 (a) shows cyclic voltammograms obtained before (black solid line) and after (red dotted line) exhaustive electrolysis. The shift in the potentials of zero current flow seen in the cyclic voltammograms between the start and end of the electrolysis is because the reduced species exists in a charged state.

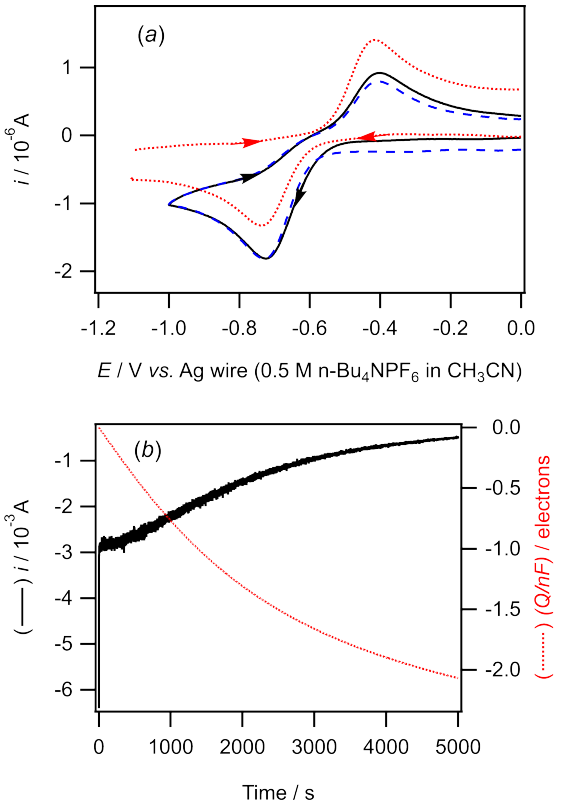

FIGURE 5.3: Voltammetric and coulometric data collected during the CPE of 1 mM riboflavin in DMSO with 0.5 M n-Bu_4NPF_6, conducted under a CO_2 atmosphere at 22(2) °C. (a) CV curves were recorded using a 1 mm diameter planar Pt electrode at a scan rate of 0.1 V s^{-1}. The black line represents the state before reduction of riboflavin. The red dotted line shows the state after riboflavin had been fully reduced. The blue dashed line indicates the state after reduced riboflavin has been fully reoxidized. (b) Graph of the current (left axis) and coulometry (right axis) versus time data collected during the exhaustive reduction of riboflavin -1.1 V versus a silver wire (in the presence of 0.5 M n-Bu_4NPF_6 in MeCN).

The integrated current over time from the electrolysis (Fig. 5.3 (b) molecule (red dotted line) confirming the two electrons stoichiometry of the electrochemical reduction step over extended electrolysis time scales. Applying an oxidizing potential of -0.1 V vs Ag at the completion of the reductive electrolysis led to the regeneration of the starting material, as shown by the blue dotted trace cyclic voltammogram in Fig. 5.3 (a), which closely matched the black trace cyclic voltammogram that was obtained for Fl_{ox} prior to electrolysis. Together with the color change of the electrolysis solution back to yellow, this suggested recovery of riboflavin upon oxidation of the reduced flavin under electrolysis time scales of hours.

5.4.3 *Ex situ* UV-Vis, NMR, and EPR experiments

Electrochemical UV-vis spectroscopic experiments were performed to determine whether the reduced compound(s) under a CO_2 atmosphere could be cleanly oxidized back to the starting material (Fl_{ox}) without reacting to form other products.

In Fig. 5.4, the black line represents the UV-vis spectrum that was captured prior to the start of the electrolysis. The red line depicts the spectrum of the compound that was fully reduced (via 2 e^-). The dotted blue line shows the spectrum that was recorded after the reduced compound had been oxidized back to the initial material. The spectra in Fig. 5.4 corroborate the high-yield regeneration of the starting material following reverse electrolysis. The entire experiment was conducted over an approximate duration of 4 h at a temperature of 22(2) °C.

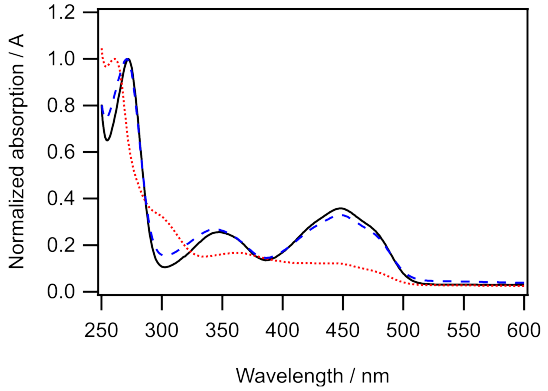

FIGURE 5.4: *Ex situ* electrochemical UV-vis spectra of 1 mM riboflavin in DMSO with 0.5 M n-Bu_4NPF_6, conducted under a CO_2 atmosphere at a temperature of 22(2) °C. The black line represents the state prior to the comprehensive reduction of riboflavin. The red dotted line shows the state riboflavin has undergone, an exhaustive two-electron reduction. The blue dashed line indicates the state after the reduced riboflavin solution had been fully reoxidized through a two-electron reoxidation process.

The reduction mechanism of riboflavin and its interactions with CO_2 were further elucidated through ^1H and ^{13}C NMR spectroscopy and EPR experiments. Solutions of riboflavin that were exhaustively electrolyzed under an Ar atmosphere led to the loss of all of the ^1H or ^{13}C features in the NMR spectra. The disappearance of riboflavin features in the NMR spectra supports the formation of long-lived radical species, which is consistent with the paramagnetic nature of $Fl_{rad}^{\bullet -}$.

In contrast, when a solution containing riboflavin was exhaustively electrolyzed under a CO_2 atmosphere, the reappearance of ^{1}H and ^{13}C NMR features were observed (Figures Fig. A.2 and Fig. 1.3 in Chapter A). This finding indicates that the two-electron reduced state exists as a nonradical dianion, likely due to the formation of a molecular complex with CO_2 ($Fl_{red}(CO_2)_n^{2-}$). This observation supports the hypothesis of CO_2 binding and provides insight into the nature of the reduced flavin–CO_2 interaction.

Complementary EPR experiments provided further evidence of the proposed reduction mechanism. Under an argon atmosphere, the one-electron reduced state exhibited a characteristic radical signal, confirming the formation of $Fl_{rad}^{\bullet-}$. However, the integration of this EPR signal revealed that $Fl_{rad}^{\bullet-}$ was present at only 30–40% of the expected concentration (Fig. A.4 in Chapter A). This finding corroborates the complex reduction state of riboflavin previously described by Tan and Webster, suggesting a dynamic equilibrium between various reduced species.[23]

Furthermore, EPR experiments on the two-electron reduced state under a CO_2 atmosphere led to the disappearance of the radical signal. This observation supports the conclusion that reduction under a CO_2 atmosphere generates a fully reduced dianion species. It is proposed that the presence of CO_2 plays a dual role: it stabilizes the reduced flavins and simultaneously lowers the reduction potential of the $Fl_{red}^{\bullet-}/Fl_{red}^{2-}$ couple. This effect is likely mediated by the formation of a molecular complex, $Fl_{red}(CO_2)_n^{2-}$, as illustrated in Scheme 5.1.

5.4.4 Digital Simulation of CV Data

Scheme 5.1 contains the proposed reduction mechanism of riboflavin in DMSO that was derived from the variable scan rate CV experiments and *ex situ* spectroscopic data. The mechanism involves multiple PCET steps where the flavin molecules and their reduced forms also react homogeneously in comproportionation and disproportionation processes. The simulations were performed using the parameters previously described for riboflavin in DMSO under an argon atmosphere (reaction sequence in black in Scheme 5.1)[23] and with the new steps involving interactions with CO_2 shown in red in Scheme 5.1. The kinetic and thermodynamic parameters used in the simulations for the reactions involving CO_2 are given in Table 5.1. In summary, the simulation method involves iteratively refining the fitting between the

experimental voltammetric curves with the simulated curves over a range of scan rates through continually varying the proposed equilibrium and rate constants and electrochemical parameters. The equilibrium constants and formal potentials are interrelated thermodynamically for the square-scheme components of the mechanism, which aids in the refining of the parameters. For example, if two formal potentials and one equilibrium constant are known, then the second equilibrium constant in the square scheme is automatically calculated.[23] Similarly, in situations where the equilibrium constants are predetermined based on the measured (or estimated) formal potentials of the reactions, then only one rate constant (k_f or k_b) needs to be known as the second can be immediately calculated (from $K_{eq} = k_f/k_b$). This is beneficial in situations where the homogeneous reactions are very fast or relatively slow because the kinetic information that can be extracted from the CV curves is limited by how fast or slow the experimental voltammetric scan can be conducted.

TABLE 5.1: Equilibrium, Rate Constants, and Electrochemical Parameters for the Red Reaction Mechanism Given in Scheme 5.1 That Were Obtained by Digital Simulation of CV Data[2] from Voltammograms Obtained in DMSO Containing 0.5 M n-Bu_4NPF_6 under a CO_2 Atmosphere at 22(2) °C[3]

D_{Fl}/cm^2 s^{-1}	D_{CO_2}/cm^2 s^{-1}	R/Ω	$Fl_{rad}CO_2^{\bullet -} + e^- \rightleftharpoons Fl_{red}CO_2^{2-}$	
			$E^{04}_{(5)}$/v	$k_{s(5)}$/cm s^{-1}
1.6×10^{-6}	1.6×10^{-5}	200	−1.13	0.0004

$Fl_{rad}^{\bullet -} + CO_2 \rightleftharpoons Fl_{rad}CO_2^{\bullet -}$		
$K_{eq(5)}$	$k_{f(5)}$/cm s^{-1}	$k_{b(5)}$/cm s^{-1}
4.62×10^1	6.36×10^2	1.38×10^1

A major mechanistic observation from the cyclic voltammograms is that the rate of reaction between the reduced flavins and CO_2 is slower than the other proton-transfer homogeneous reactions in Scheme 5.1, as evidenced by how at faster scan rates the voltammograms appear similar to that obtained under an argon atmosphere Fig. 5.2. For example, the reaction between $Fl_{rad}^{\bullet -}$ and CO_2 was estimated at 6×10^2 L mol^{-1} s^{-1} (Table 5.1), while the reaction between $Fl_{rad}^{\bullet -}$ and Fl_{ox} to form Fl_{ox}^{-} and $Fl_{rad}H^{\bullet}$ has been estimated to occur approximately 1500 times faster (1×10^6 L mol^{-1} s^{-1}).[23] Nevertheless, the electrolysis and spectroscopic measurements

[2]CV data were recorded with a 1 mm diameter planar Pt working electrode and at scan rates between 0.1 and 20 v s^{-1}.

[3]Formal potentials vs Fc/Fc^+ (add 0.43 V to convert to vs SCE).

[4]Additional values for reactions in Scheme 5.1 are given in [23].

indicate that over longer time scales, the CO_2 adduct is the major stable species produced and it can be oxidized back to the starting material. Therefore, this critically indicates that the interactions of CO_2 with reduced riboflavin must occur after the proton-coupled interactions have occurred (black reactions in Scheme 5.1) and instead must occur with the secondary reduced flavin according to the red reactions in Scheme 5.1 Furthermore, even though PCET reactions occur more quickly than the CO_2 supramolecular binding reactions, the kinetic and equilibrium conditions favor the formation of the $[Fl_{red}(CO_2)_n]^{2-}$ complex as the major long-lived solution phase species. Whether the final electron transfer step occurs concertedly or consecutively (stepwise) remains uncertain, although the reduction of the anion radical to the dianion in the presence of CO_2 (-1 V) occurs at a significantly lower potential than that in an argon atmosphere (-2 V) (Scheme 5.1).

5.4.5 Computational study of interaction between Riboflavin and CO_2

To elucidate the potential molecular interactions between riboflavin and CO_2, a computational study was conducted. In the absence of a stable synthesized product, the investigation was aimed at identifying the most probable binding sites and the stability of the resulting complexes.

Mulliken and NBO calculations were performed to determine the atomic charges of neutral riboflavin (Fl_{ox}) and its reduced forms, ${Fl_{red}}^{\bullet-}$ and ${Fl_{red}}^{2-}$. Fig. 5.5 presents the natural charge for the riboflavin dianion (${Fl_{red}}^{2-}$). The results indicated the presence of three localized negative charge regions, namely, O2, O4, and N5 (numbering from Scheme 5.1), which could potentially serve as binding sites for CO_2. These findings suggest that the electron-rich regions of the reduced riboflavin molecules are more likely to interact with the electron-deficient carbon atom of CO_2.

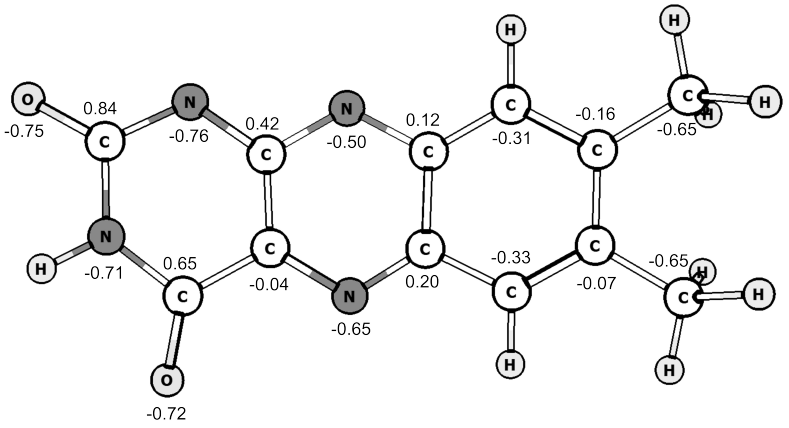

FIGURE 5.5: DFT-optimized structure and associated natural charge for the riboflavin dianion ($Fl_{red}{}^{2-}$).

To further investigate the binding capability of reduced riboflavin with CO_2, a HOMO–LUMO analysis was carried out. The analysis revealed that only the reduced forms of riboflavin: $Fl_{rad}{}^{\bullet-}$ and $Fl_{red}{}^{2-}$, possess the necessary electronic configuration to facilitate binding with CO_2. This observation can be attributed to the increased electron density in the HOMO of the reduced riboflavin species, which allows for a more favorable orbital overlap with that of the LUMO of CO_2.

To gain insights into the stability of the potential riboflavin-CO_2 complexes, structure optimization calculations were performed on $[Fl_{red}(CO_2)_n]^{2-}$. The results showed that while CO_2 binding through O2, O4, and N5 could reach a ground state (N1 and N3 were occupied due to hydrogen bonding with the side chain hydroxyl and hydrogen present, respectively), the complex formed via N5 exhibited the most stable optimized structure. Structures and associated energy levels are presented in the Chapter A (Fig. A.5–Fig. A.12 and Table A.1). This finding aligns with the observations made by Ranjan et al. in their study of the 4,4'-bipyridine system, where they also proposed CO_2 binding at a nitrogen site.[33] The similarity in binding locations between these two systems suggests a common mechanism for the capture of CO_2 by reduced nitrogen-containing heterocycles.

However, a key distinction between the riboflavin system and the 4,4'-bipyridine system lies in the reduction potentials. The riboflavin system exhibits a more positive reduction potential compared to 4,4'-bipyridine. This difference in reduction

potentials has significant implications for CO_2 binding kinetics. The riboflavin system demonstrates a lower CO_2 binding kinetic constant based on digital simulation studies (Table 5.1), which can be attributed to its more positive reduction potential. This slower binding kinetics might initially seem disadvantageous; however, it may offer a benefit in practical applications. The more positive reduction potential of the riboflavin system confers the possible advantage that it may be less susceptible to unwanted side reactions. Nevertheless, a significant issue with riboflavin is its low solubility of a few millimoles in aprotic solvents.

5.4.6 Mechanistic analysis of riboflavin-CO_2 interactions and their impact on redox behavior

The interaction between reduced riboflavin species and CO_2 significantly influences both the electrochemical reversibility and stability of the system. Here we present an integrated analysis of these effects based on our electrochemical, spectroscopic, and computational findings.

Electrochemical evidence for enhanced reversibility

Under a CO_2 atmosphere, cyclic voltammetry reveals the merging of the two one-electron transfer steps into what appears as a single two-electron process at slow scan rates. This behavior contrasts sharply with measurements under an argon atmosphere, where two distinct one-electron transfers are observed. The positive shift of the second reduction wave under CO_2 (from -2.0 V to -1.0 V vs Fc/Fc^+) indicates thermodynamic stabilization of the reduced species through CO_2 binding. Digital simulation of cyclic voltammograms indicates additional processes whereby $Fl_{rad}{}^{\bullet-}$ and $Fl_{red}{}^{2-}$ were stabilized by interaction with CO_2. Controlled potential electrolysis experiments confirm complete chemical reversibility over extended timescales, as evidenced by the clean regeneration of the starting material after oxidation.

Spectroscopic validation of species stability

UV-vis spectroscopy provides direct evidence for the formation and stability of the CO_2-bound reduced species. The characteristic absorption bands observed after reduction (as shown in Fig. 5.4) remain stable over hours, indicating formation of a long-lived complex. Notably, EPR measurements show no radical signal in the reduced solution under CO_2, contrasting with the clear radical signals observed under argon. This absence of EPR signal supports our conclusion that CO_2 binding promotes formation of the diamagnetic dianion species over the radical anion (as shown in Fig. A.4).

Computational insights into binding mechanisms

Density functional theory calculations reveal three potential CO_2 binding sites (O2, O4, and N5), with N5 providing the most stable interaction (-37.136 kcal/mol vs -26.620 and -28.433 kcal/mol for O2 and O4 respectively, as described in the Table A.1). The calculated HOMO-LUMO analysis demonstrates favorable orbital overlap between reduced riboflavin and CO_2, providing a theoretical basis for the experimental observation of enhanced stability.

Comparison with quinone systems

The behavior of riboflavin-CO_2 complexes parallels that observed in quinone systems, where CO_2 binding also stabilizes reduced species. However, riboflavin exhibits unique features, particularly the additional proton transfer interactions that occur prior to CO_2 binding. Despite these mechanistic differences, both systems ultimately form stable CO_2-bound two-electron reduced products, suggesting a common underlying principle in the stabilization of reduced organic species through CO_2 coordination.

This mechanistic understanding - supported by multiple analytical techniques - explains both the enhanced reversibility and stability observed under CO_2 conditions, while providing insights relevant to potential applications in carbon capture and energy storage systems.

5.4.7 Limitation and future directions

While riboflavin shows promise as a redox-active molecule for CO_2 capture, several limitations need to be addressed before practical implementation. Like the quinone systems discussed in Chapter 4, reduced riboflavin species exhibit significant oxygen sensitivity. The presence of O_2 can lead to undesired side reactions and decomposition of the reduced forms, necessitating strict anaerobic conditions for operation. This sensitivity presents a major challenge for real-world carbon capture applications where complete exclusion of oxygen may be impractical.

Another significant limitation is riboflavin's poor solubility in most organic solvents. While DMSO provides a suitable medium for fundamental studies, its high boiling point and hygroscopic nature make it less ideal for practical applications. The development of more soluble riboflavin derivatives or alternative solvent systems would be necessary for achieving the high concentrations needed in practical carbon capture systems.

Additionally, the complex proton-coupled electron transfer mechanisms observed in riboflavin reduction, while interesting from a fundamental perspective, could complicate process control in scaled-up systems. The multiple chemical steps involved may affect the overall kinetics and efficiency of CO_2 capture and release cycles.

Future research should focus on:

- Developing oxygen-stable derivatives of riboflavin
- Improving solubility through structural modifications
- Exploring alternative solvent systems
- Optimizing conditions for reversible CO2 binding and release
- Investigating the long-term stability under repeated capture-release cycles

Despite these limitations, this work provides valuable initial perspectives on leveraging bio-inspired organic molecules for carbon capture applications. The insights gained from studying riboflavin's interactions with CO2 contribute to our understanding of molecular design principles for next-generation carbon capture materials.

5.5 Conclusion

This study elucidated the complex mechanism of riboflavin reduction in DMSO solvent under a CO_2 atmosphere by using a combination of CV, spectroscopy, electrolysis, molecular orbital calculations, and digital simulations. Multiple one-electron transfers coupled to proton transfers occur, forming numerous anionic and neutrally charged intermediates prior to the fully reduced state. CPE combined with coulometry confirmed an overall two-electron stoichiometry, validating the proposed inner-sphere CO_2 interactions. Spectroscopic monitoring verified the reversibility of the redox process after bulk electrolysis. Kinetic modeling enables full extraction of thermodynamic and rate parameters governing this PCET network.

Riboflavin possesses structural commonality with quinones, enabling a similar redox mediation chemistry. Under CO_2 conditions, the second electron transfer step of the anion radical converting to the dianion occurs at a potential lower than that of the first electron transfer process because of complexation interactions of the reduced flavins with CO_2. However, unlike quinones, additional proton-transfer interactions between the reduced flavin molecules occur, but ultimately, all the reduced forms are converted to the CO_2-bound two-electron reduced product, $[Fl_{red}(CO_2)_n]^{2-}$. Therefore, the voltammograms recorded at slow scan rates show the appearance of a concerted two-electron chemically reversible process.

References

(1) Suwannasom, N.; Kao, I.; Pruß, A.; Georgieva, R.; Bäumler, H. Riboflavin: The Health Benefits of a Forgotten Natural Vitamin. *International Journal of Molecular Sciences* **2020**, *21*, Number: 3 Publisher: Multidisciplinary Digital Publishing Institute, 950.

(2) Olfat, N.; Ashoori, M.; Saedisomeolia, A. Riboflavin is an antioxidant: a review update. *British Journal of Nutrition* **2022**, *128*, Publisher: Cambridge University Press, 1887–1895.

(3) Walsh, C. Flavin coenzymes: at the crossroads of biological redox chemistry. *Accounts of Chemical Research* **1980**, *13*, Publisher: American Chemical Society, 148–155.

(4) Bruice, T. C. Oxygen-Flavin Chemistry. *Israel Journal of Chemistry* **1984**, *24*, _eprint: https://onlinelibrary.wiley.com/doi/pdf/10.1002/ijch.198400008, 54–61.

(5) Ghisla, S.; Massey, V. Mechanisms of flavoprotein-catalyzed reactions. *European Journal of Biochemistry* **1989**, *181*, _eprint: https://onlinelibrary.wiley.com/doi/pdf/10.1033.1989.tb14688.x, 1–17.

(6) Niemz, A.; Imbriglio, J.; Rotello, V. M. Model Systems for Flavoenzyme Activity: One- and Two-Electron Reduction of Flavins in Aprotic Hydrophobic Environments. *Journal of the American Chemical Society* **1997**, *119*, Publisher: American Chemical Society, 887–892.

(7) Lovander, M. D.; Lyon, J. D.; Parr, D. L.; Wang, J.; Parke, B.; Leddy, J. Critical Review—Electrochemical Properties of 13 Vitamins: A Critical Review and Assessment. *Journal of The Electrochemical Society* **2018**, *165*, Publisher: IOP Publishing, G18.

(8) Comeau Simpson, T.; Durand, R. R. Reactivity of carbon dioxide with quinones. *Electrochimica Acta* **1990**, *35*, 1399–1403.

(9) Kang, J. S.; Kim, S.; Hatton, T. A. Redox-responsive sorbents and mediators for electrochemically based CO2 capture. *Current Opinion in Green and Sustainable Chemistry* **2021**, *31*, 100504.

(10) Barlow, J. M.; Clarke, L. E.; Zhang, Z.; Bím, D.; Ripley, K. M.; Zito, A.; Brushett, F. R.; Alexandrova, A. N.; Yang, J. Y. Molecular design of redox carriers for electrochemical CO $_2$ capture and concentration. *Chemical Society Reviews* **2022**, *51*, 8415–8433.

(11) Barlow, J. M.; Yang, J. Y. Oxygen-Stable Electrochemical CO $_2$ Capture and Concentration with Quinones Using Alcohol Additives. *Journal of the American Chemical Society* **2022**, *144*, 14161–14169.

(12) Diederichsen, K. M.; Liu, Y.; Ozbek, N.; Seo, H.; Hatton, T. A. Toward solvent-free continuous-flow electrochemically mediated carbon capture with high-concentration liquid quinone chemistry. *Joule* **2022**, *6*, 221–239.

(13) Li, X.; Zhao, X.; Liu, Y.; Hatton, T. A.; Liu, Y. Redox-tunable Lewis bases for electrochemical carbon dioxide capture. *Nature Energy* **2022**, *7*, Number: 11 Publisher: Nature Publishing Group, 1065–1075.

(14) Simeon, F.; Stern, M. C.; Diederichsen, K. M.; Liu, Y.; Herzog, H. J.; Hatton, T. A. Electrochemical and Molecular Assessment of Quinones as CO2-Binding Redox Molecules for Carbon Capture. *The Journal of Physical Chemistry C* **2022**, *126*, Publisher: American Chemical Society, 1389–1399.

(15) Choi, G. H.; Song, H. J.; Lee, S.; Kim, J. Y.; Moon, M.-W.; Yoo, P. J. Electrochemical direct CO2 capture technology using redox-active organic molecules to achieve carbon-neutrality. *Nano Energy* **2023**, *112*, 108512.

(16) Tatwawadi, S. V.; Santhanam, K. S. V.; Bard, A. J. The electrochemical reduction of riboflavin in dimethylsulfoxide. *Journal of Electroanalytical Chemistry and Interfacial Electrochemistry* **1968**, *17*, 411–420.

(17) Sawyer, D. T.; McCreery, R. L. Electrochemical studies of the interactions of riboflavine and of its reduction products with metal ions in dimethyl sulfoxide. *Inorganic Chemistry* **1972**, *11*, Publisher: American Chemical Society, 779–782.

(18) Gupta, V. K.; Jain, R.; Radhapyari, K.; Jadon, N.; Agarwal, S. Voltammetric techniques for the assay of pharmaceuticals—A review. *Analytical Biochemistry* **2011**, *408*, 179–196.

(19) Quan, M.; Sanchez, D.; Wasylkiw, M. F.; Smith, D. K. Voltammetry of Quinones in Unbuffered Aqueous Solution: Reassessing the Roles of Proton Transfer and Hydrogen Bonding in the Aqueous Electrochemistry of Quinones. *Journal of the American Chemical Society* **2007**, *129*, 12847–12856.

(20) Hui, Y.; Chng, E. L. K.; Chng, C. Y. L.; Poh, H. L.; Webster, R. D. Hydrogen-Bonding Interactions between Water and the One- and Two-Electron-Reduced Forms of Vitamin K1: Applying Quinone Electrochemistry To Determine the Moisture Content of Non-Aqueous Solvents. *Journal of the American Chemical Society* **2009**, *131*, Publisher: American Chemical Society, 1523–1534.

(21) Hui, Y.; Chng, E. L. K.; Chua, L. P.-L.; Liu, W. Z.; Webster, R. D. Voltammetric Method for Determining the Trace Moisture Content of Organic Solvents Based on Hydrogen-Bonding Interactions with Quinones. *Analytical Chemistry* **2010**, *82*, Publisher: American Chemical Society, 1928–1934.

(22) Male, R.; Samotowka, M. A.; Allendoerfer, R. D. Simultaneous electrochemical and EPR studies of flavin radical equilibria. *Electroanalysis* **1989**, *1*, _eprint: https://analyticalsciencejournals-onlinelibrary-wiley-com.remotexs.ntu.edu.sg/doi/pdf/10.10 333–339.

(23) Tan, S. L. J.; Webster, R. D. Electrochemically Induced Chemically Reversible Proton-Coupled Electron Transfer Reactions of Riboflavin (Vitamin B2). *Journal of the American Chemical Society* **2012**, *134*, Publisher: American Chemical Society, 5954–5964.

(24) Perdew, J. P. Density-functional approximation for the correlation energy of the inhomogeneous electron gas. *Physical Review B* **1986**, *33*, Publisher: American Physical Society, 8822–8824.

(25) Schäfer, A.; Horn, H.; Ahlrichs, R. Fully optimized contracted Gaussian basis sets for atoms Li to Kr. *The Journal of Chemical Physics* **1992**, *97*, 2571–2577.

(26) Schäfer, A.; Huber, C.; Ahlrichs, R. Fully optimized contracted Gaussian basis sets of triple zeta valence quality for atoms Li to Kr. *The Journal of Chemical Physics* **1994**, *100*, 5829–5835.

(27) Weigend, F.; Ahlrichs, R. Balanced basis sets of split valence, triple zeta valence and quadruple zeta valence quality for H to Rn: Design and assessment of accuracy. *Physical Chemistry Chemical Physics* **2005**, *7*, Publisher: The Royal Society of Chemistry, 3297–3305.

(28) Neese, F. The ORCA program system. *WIREs Computational Molecular Science* **2012**, *2*, _eprint: https://onlinelibrary.wiley.com/doi/pdf/10.1002/wcms.81, 73–78.

(29) Neese, F. Software update: the ORCA program system, version 4.0. *WIREs Computational Molecular Science* **2018**, *8*, _eprint: https://onlinelibrary.wiley.com/doi/pdf/10.1002 e1327.

(30) Garcia-Ratés, M.; Neese, F. Effect of the Solute Cavity on the Solvation Energy and its Derivatives within the Framework of the Gaussian Charge Scheme. *Journal of Computational Chemistry* **2020**, *41*, 922–939.

(31) Neese, F.; Wennmohs, F.; Becker, U.; Riplinger, C. The ORCA quantum chemistry program package. *The Journal of Chemical Physics* **2020**, *152*, 224108.

(32) Tan, S. L. J.; Kan, J. M.; Webster, R. D. Differences in Proton-Coupled Electron-Transfer Reactions of Flavin Mononucleotide (FMN) and Flavin Adenine Dinucleotide (FAD) between Buffered and Unbuffered Aqueous Solutions. *The Journal of Physical Chemistry B* **2013**, *117*, Publisher: American Chemical Society, 13755–13766.

(33) Ranjan, R.; Olson, J.; Singh, P.; Lorance, E. D.; Buttry, D. A.; Gould, I. R. Reversible Electrochemical Trapping of Carbon Dioxide Using 4,4'-Bipyridine That Does Not Require Thermal Activation. *The Journal of Physical Chemistry Letters* **2015**, *6*, Publisher: American Chemical Society, 4943–4946.

Chapter 6

Conclusion

This thesis has explored diverse applications of analytical electrochemistry in addressing critical environmental and pharmaceutical challenges. Through a series of interconnected studies, we have demonstrated the versatility and power of electrochemical techniques in water disinfection, pharmaceutical analysis, and carbon dioxide capture and utilization. The research presented here not only advances our understanding of fundamental electrochemical processes but also paves the way for practical applications in these vital areas.

Electrochemical Water Disinfection

Our investigation into the use of platinized titanium electrodes for the electrochemical inactivation of *Escherichia coli* in water has yielded significant insights into the mechanisms of disinfection and the key factors influencing inactivation efficiency. The study revealed that the inactivation of *E. coli* follows a logarithmic decay pattern, independent of the specific electrolyte used, except for sodium chloride, where the oxidation of chloride to chlorine greatly aids the disinfection process. This finding suggests that in the absence of Cl^-, the primary mechanism of bacterial deactivation is mediated by reactive oxygen species (ROS) rather than specific anions present in the electrolyte.

A crucial discovery was the superiority of the three-electrode configuration over the two-electrode system in achieving higher current throughput, a critical factor for effective water purification. This enhanced performance was attributed to the lower internal resistance of the three-electrode system, facilitated by the inclusion of a reference electrode with a stable potential. The study also successfully identified and quantified hydroxyl radicals generated during water electrolysis using NMR spectroscopy, underscoring their crucial role in the electrochemical inactivation of *E. coli*.

These findings have significant implications for the development of efficient, sustainable, and environmentally friendly water disinfection methods. The demonstrated feasibility of rapid disinfection even at low electrolyte concentrations suggests that electrochemical disinfection could be applied to natural waters without the need for added electrolytes. This opens possibilities for decentralized water treatment solutions, particularly in remote or resource-limited areas.

Electrochemical Detection of Pharmaceutical Compounds

The development and optimization of methods for the detection and quantification of praziquantel in water samples represents a significant contribution to pharmaceutical analysis. By comparing gas chromatography-mass spectrometry (GC-MS) and voltammetric techniques, both utilizing solid phase extraction for sample preparation, we have provided a comprehensive evaluation of their respective strengths and limitations.

While GC-MS demonstrated lower detection limits, the voltammetric method showed comparable accuracy and precision, offering a potentially more cost-effective and portable alternative for on-site testing. This is particularly relevant for monitoring pharmaceutical compounds in aquatic environments, where rapid and field-deployable analytical methods are often required. The successful application of these techniques to praziquantel analysis also provides a framework that can be adapted for the detection of other pharmaceutical compounds in environmental samples.

The study highlights the potential of electrochemical methods as complementary or alternative techniques to traditional chromatographic methods in pharmaceutical analysis. The portability and relatively low cost of electrochemical instrumentation make these methods particularly attractive for field applications and routine monitoring in resource-limited settings.

Carbon Dioxide Capture and Utilization

The exploration of the electrochemistry of organic molecules, specifically quinones and riboflavin (vitamin B_2), for potential applications in carbon dioxide capture and energy storage has yielded valuable insights into the behavior of these systems. The investigation of molecular interactions between reduced organic species and CO_2, as well as their electrochemical behavior under various conditions, contributes to our understanding of potential carbon capture technologies and organic-based energy storage systems.

The study revealed complex mechanisms involving multiple electron transfers coupled with proton transfers, forming various intermediates before reaching the fully reduced state. The observation of enhanced chemical reversibility of quinone redox processes under CO_2 atmosphere compared to inert conditions provides new perspectives on leveraging organic molecule-based electrochemistry for carbon capture technologies.

The prototype quinone-based battery demonstrated in this research, while showing modest efficiency, serves as a proof-of-concept for utilizing quinones as active materials in energy storage applications. The insights gained from this study pave the way for future research aimed at optimizing quinone-based energy storage systems, particularly in the context of CO_2 utilization.

Implications and future directions

In conclusion, this thesis demonstrates significant potentials for electrochemistry in addressing critical environmental challenges. Although research contributes valuable methodologies and insights, several important directions for future research and collaboration emerge.

For water treatment technology, future work should focus on real-world validation through collaboration with treatment facilities to assess long-term stability and cost-effectiveness. Studies examining multi-species bacterial populations and system optimization for portable and remote deployment would enhance practical applicability.

In pharmaceutical analysis, partnerships with environmental monitoring agencies and related industries could validate voltammetric methods across diverse water matrices, while development of multiplexed sensors and integrated systems could expand detection capabilities.

The carbon capture and energy storage research would benefit from synthetic chemistry and material science collaborations to develop more stable quinone derivatives and address oxidative stability challenges. Engineering studies focusing on scaling issues and system integration with renewable energy sources could accelerate practical implementation. Economic feasibility studies comparing these approaches with existing technologies would help guide development priorities.

The diverse applications explored here highlight both the versatility of electrochemical methods and the need for continued innovation. Future work should emphasize interdisciplinary collaboration among electrochemists, environmental scientists, chemical engineers, and industry partners to transition laboratory findings to commercial applications. Particular attention should be paid to standardization, regulatory compliance, and economic viability.

Through such collaborative efforts and focused research directions, electrochemical technologies can play an increasingly important role in environmental protection and sustainable development. The path forward requires balancing fundamental research with practical implementation considerations to develop solutions that are not only technically sound, but also economically viable and environmentally sustainable.

Appendix A

Supporting information for chapter 5

Figures

Tables

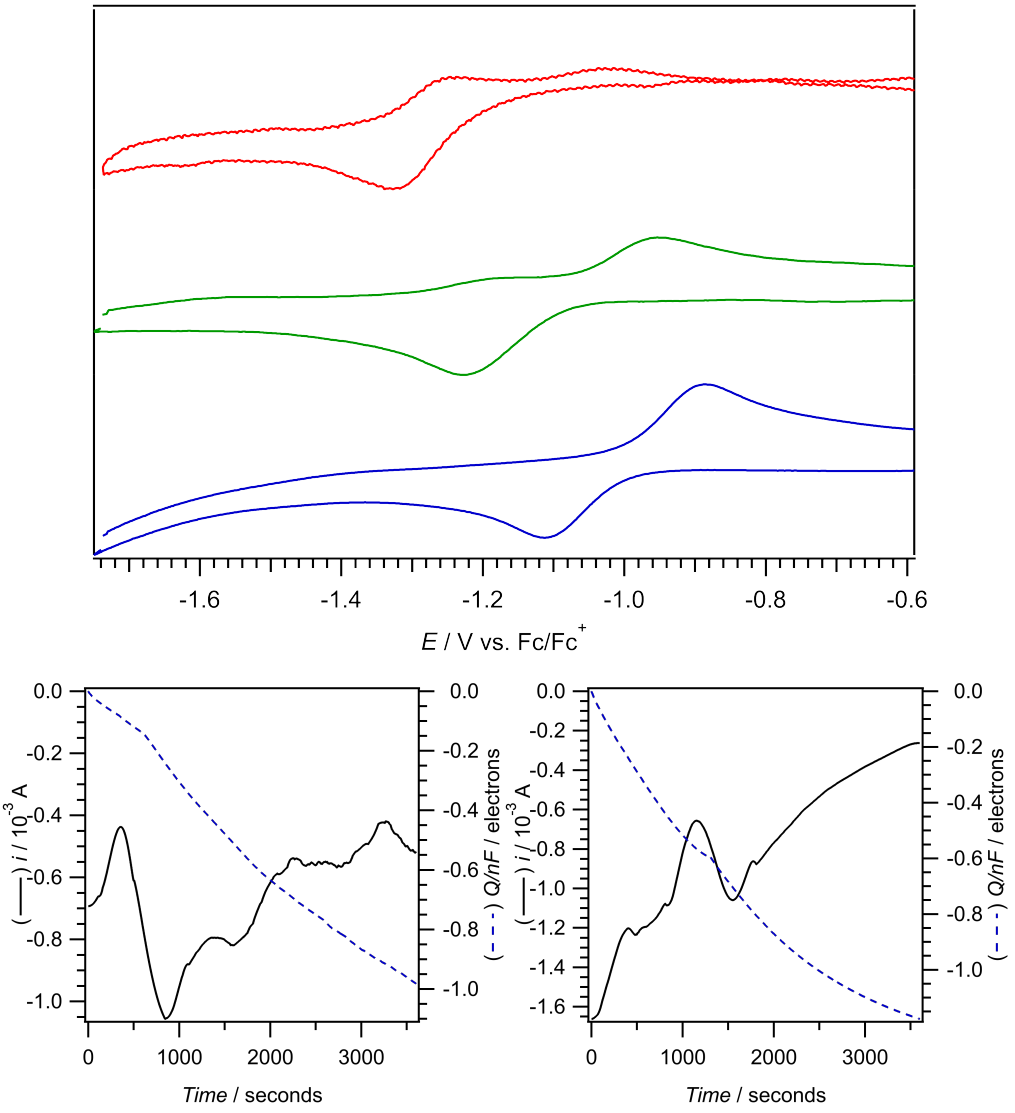

FIGURE A.1: Electrochemical characterization of riboflavin reduction under different atmospheres. (Top) Cyclic voltammograms of 1 mM riboflavin in DMSO with 0.5 M n-Bu_4NPF_6 at 22(2) °C, recorded using a 1 mm diameter planar Pt electrode at a scan rate of 0.1 V s^{-1}. Red trace: initial CV before reduction; Green trace: after one-electron reduction under argon atmosphere; Blue trace: after subsequent one-electron reduction under CO_2 atmosphere. (Bottom) Controlled potential electrolysis data showing current (left axis) and charge passed (right axis) vs. time. Left panel: first reduction step under argon atmosphere; Right panel: second reduction step under CO2 atmosphere at –1.1 V vs. Ag wire (0.5 M n-Bu_4NPF_6 in CH_3CN). All experiments were conducted at 22(2) °C in DMSO with 0.5 M n-Bu_4NPF_6 as supporting electrolyte.

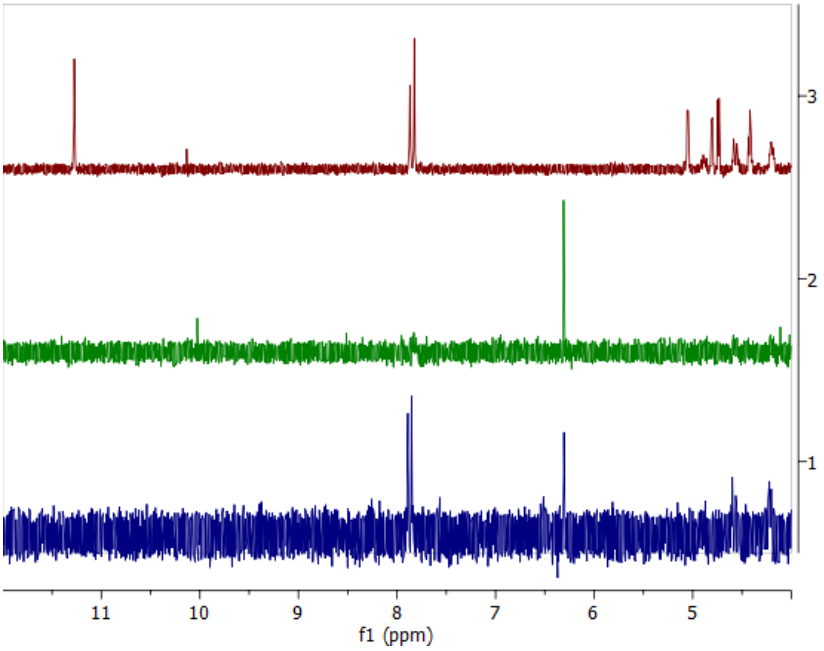

FIGURE A.2: ^{1}H NMR spectra of 1 mM riboflavin solution in DMSO under electrolysis condition (with 0.5 M n-Bu_4NPF_6 in DMSO, 400 MHz). (Red) Before electrolysis. (Green) After one-electron reduction under argon atmosphere. The absence of NMR peaks suggests that riboflavin stays in radical anion form. (Blue) After two-electrons reduction under CO_2 atmosphere. The reappearance of riboflavin features suggests that the reduced riboflavin-CO_2 adducts are in non-radical dianion form. The disappearance of an amine peak at 11.3 ppm is indicative of an interaction from neutral Fl_{ox} to reduced form $Fl_{red}(CO_2)_n{}^{2-}$.

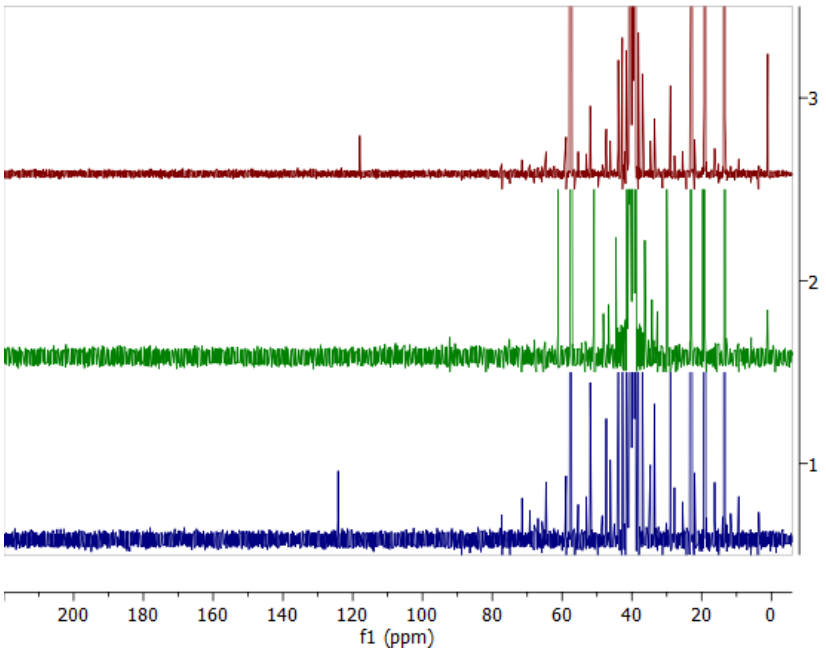

FIGURE A.3: ^{13}C NMR spectra of 1 mM riboflavin solution in DMSO under electrolysis condition (with 0.5 M n-Bu_4NPF_6 in DMSO, 400 MHz). (Red) Before electrolysis. (Green) After one-electron reduction under argon atmosphere. The absence of NMR peaks of riboflavin origin suggests that riboflavin stays in radical anion form. (Blue) After two-electrons reduction under CO_2 atmosphere. The reappearance of riboflavin features suggests that the reduced riboflavin-CO_2 adducts are in non-radical dianion form. The peak at 124 ppm (blue line) is from the dissolution of CO_2 in DMSO.[1]

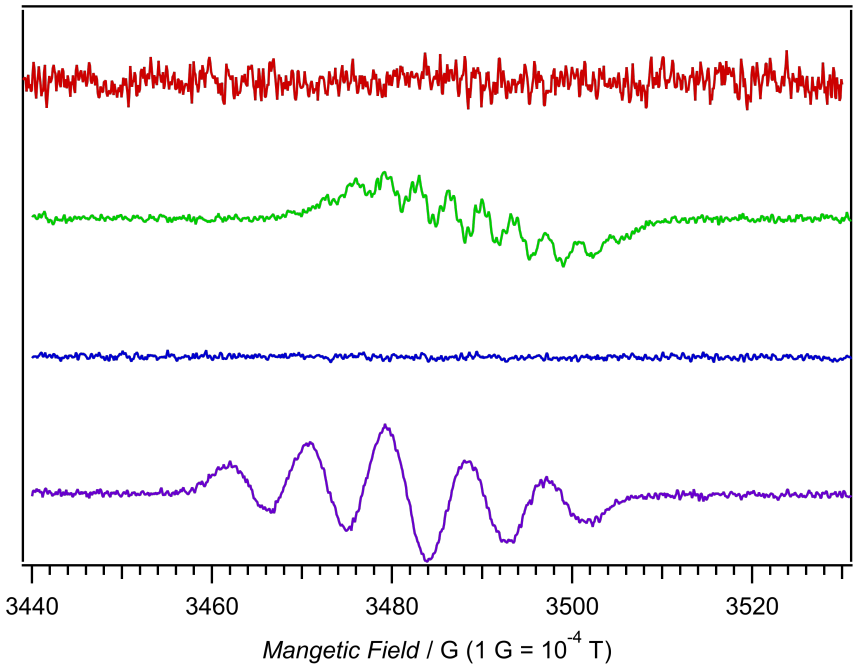

FIGURE A.4: EPR spectra of 1 mM riboflavin solution in DMSO under electrolysis condition (with 0.5 M n-Bu_4NPF_6 in DMSO) (Red) Before electrolysis. (Green) After one-electron reduction under argon atmosphere. (Blue) After two-electrons reduction under CO_2 atmosphere. (Purple) 0.1 mM DPPH in DMSO for scale.

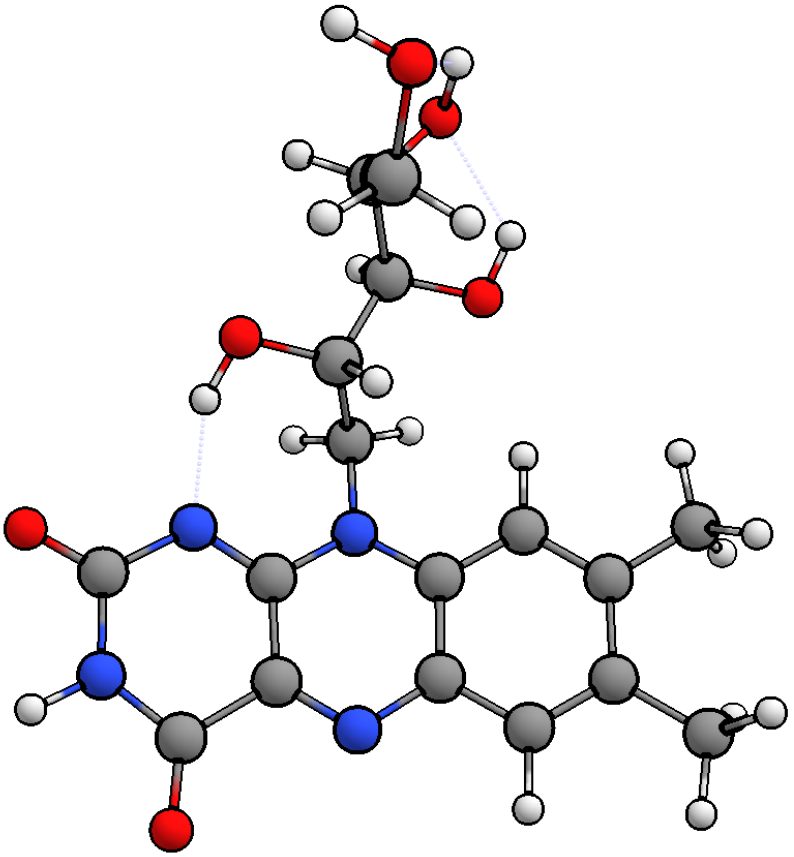

FIGURE A.5: Optimized geometry of riboflavin (Fl_{ox}).

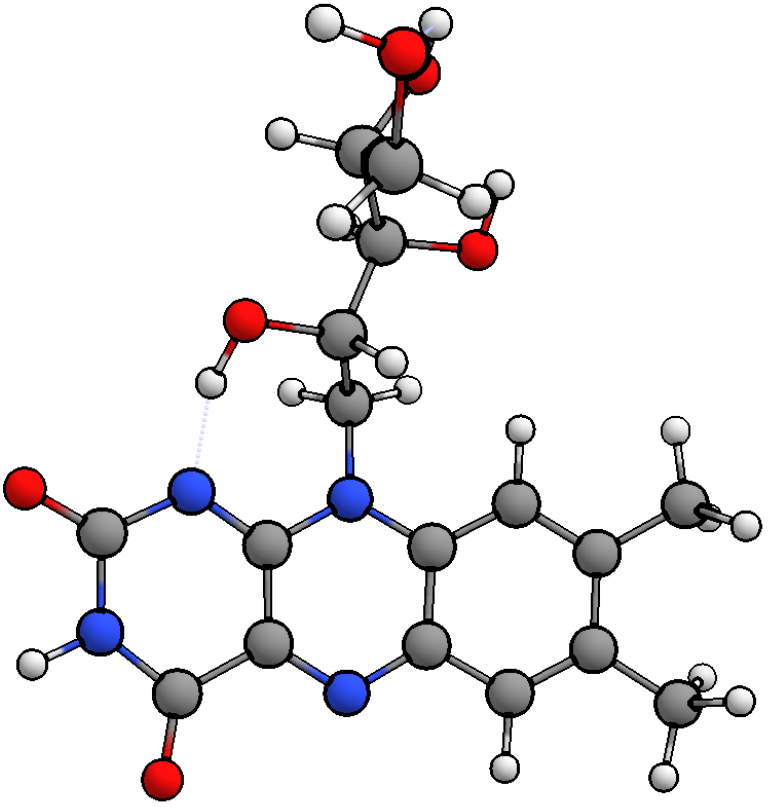

FIGURE A.6: Optimized geometry of riboflavin radical anion ($Fl_{rad}^{\bullet -}$).

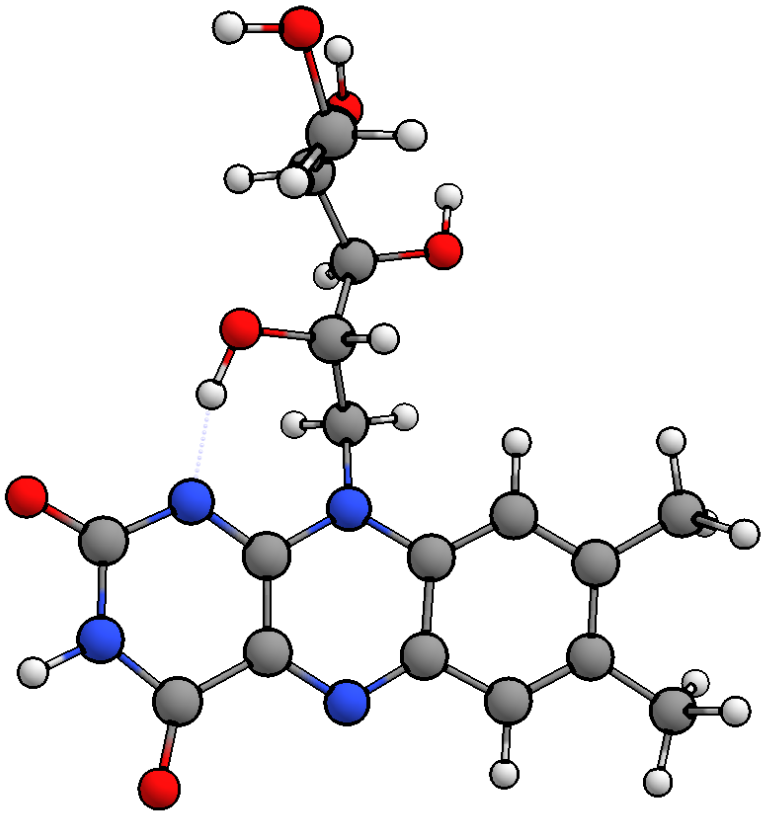

FIGURE A.7: Optimized geometry of riboflavin radical dianion ($Fl_{red}{}^{2-}$).

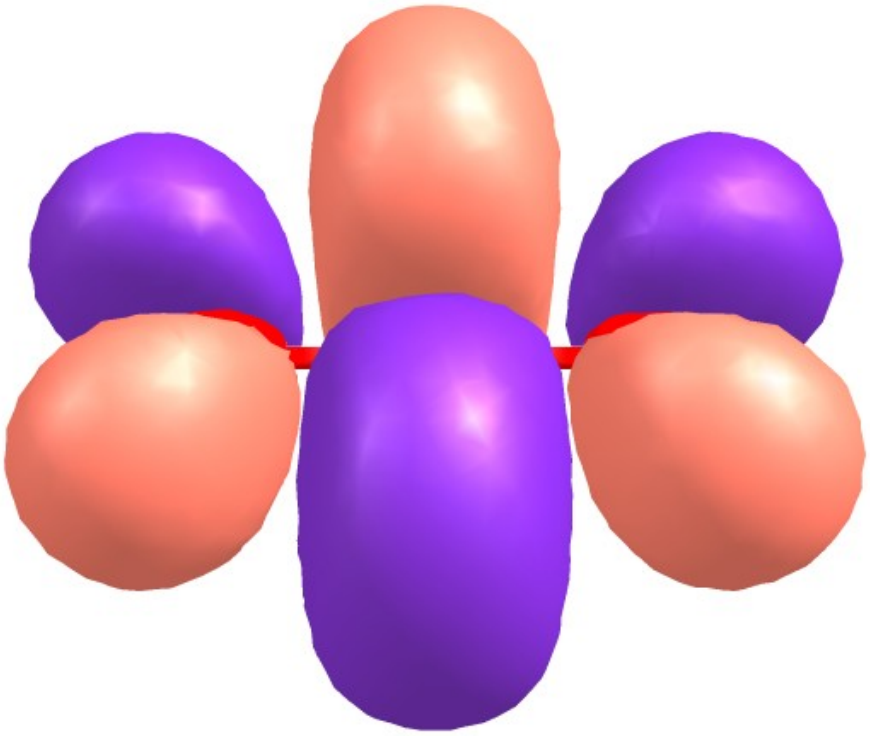

FIGURE A.8: Optimized geometry and the lowest unoccupied molecular orbital (LUMO) of CO_2.

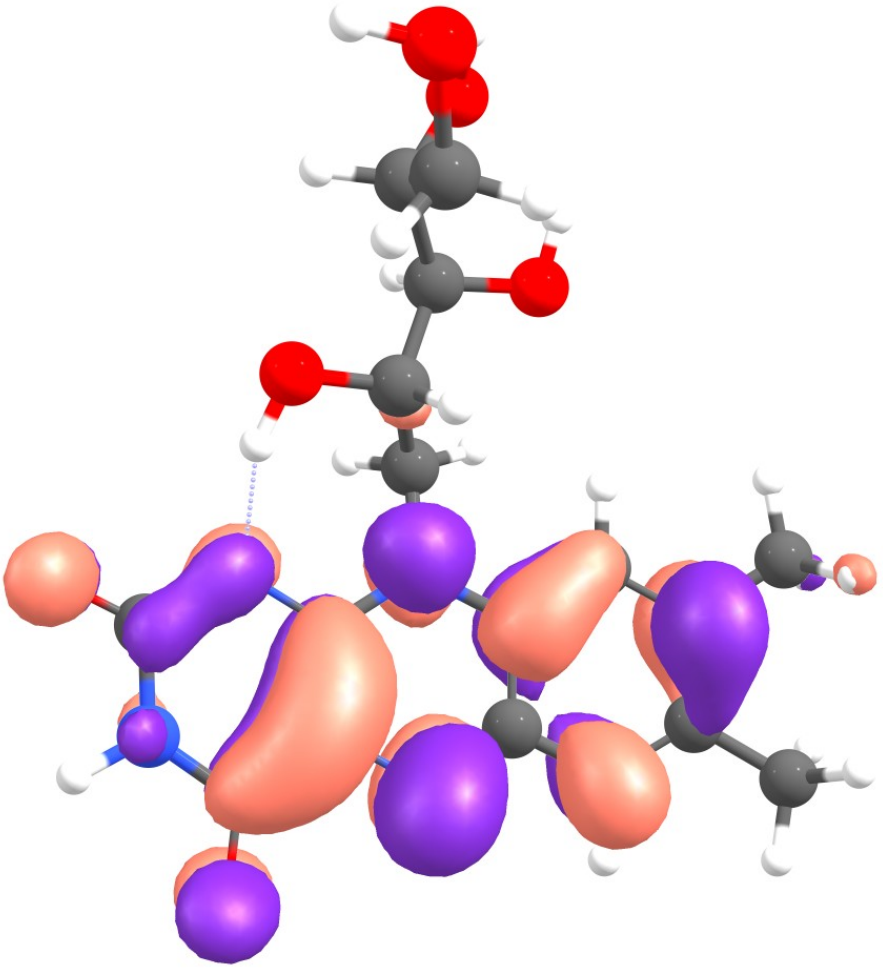

FIGURE A.9: Optimized geometry and the single occupied molecular orbital (SOMO) of riboflavin radical anion ($Fl_{rad}^{\bullet -}$).

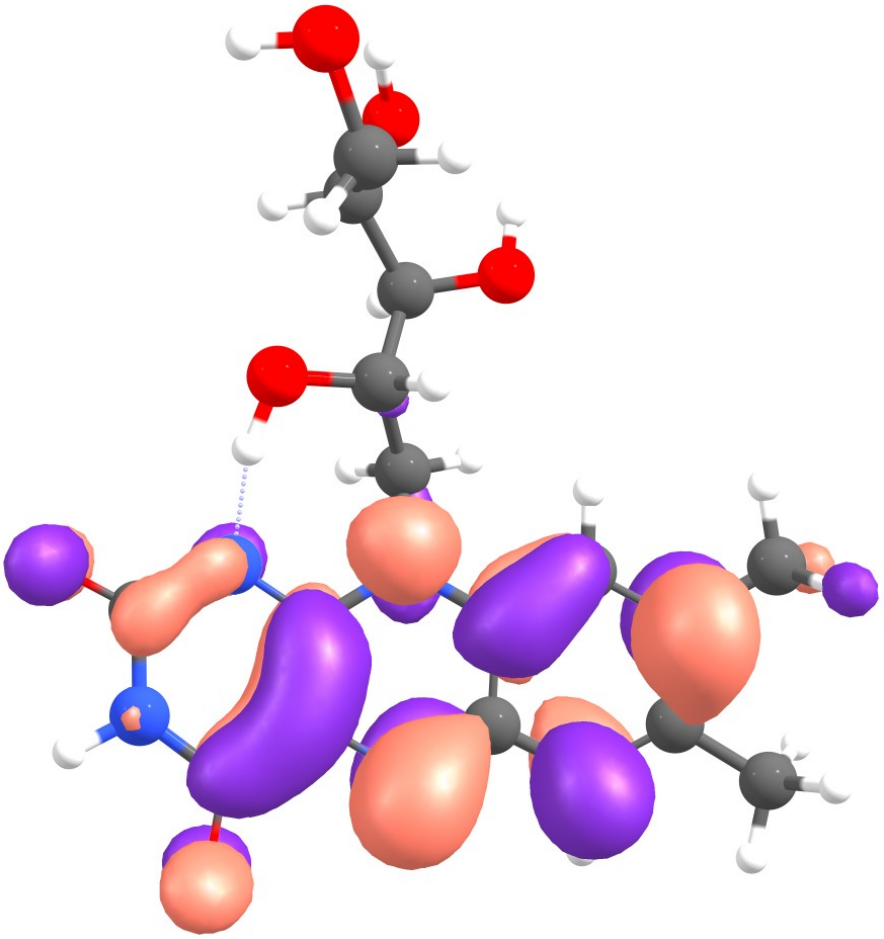

FIGURE A.10: Optimized geometry and the highest occupied molecular orbital (HOMO) of riboflavin radical dianion ($Fl_{red}{}^{2-}$).

TABLE A.1: Relative energies of riboflavin-CO2 adduct ($Fl_{red}(CO_2)^{2-}$) at different binding positions

Name	E(SCF) (Hartree)	ZPE (Hartree)	H (Hartree)
CO_2	-188.45	0.01136	-188.447
$Fl_{red}{}^{2-}$	-1329.40	0.35566	-1329.053
$Fl_{red}(CO_2)^{2-}$ binds at O2	-1517.89	0.37008	-1517.525
$Fl_{red}(CO_2)^{2-}$ binds at O4	-1517.89	0.37031	-1517.527
$Fl_{red}(CO_2)^{2-}$ binds at N5	-1517.91	0.37197	-1517.540

Name	TS (Hartree)	G(gas) (Hartree)	ΔG(gas) (kcal/mol)
CO_2	0.02434	-188.423	
$Fl_{red}{}^{2-}$	0.07797	-1328.975	
$Fl_{red}(CO_2)^{2-}$ binds at O2	0.08474	-1517.440	**-26.620**
$Fl_{red}(CO_2)^{2-}$ binds at O4	0.08405	-1517.443	**-28.433**
$Fl_{red}(CO_2)^{2-}$ binds at N5	0.08316	-1517.457	**-37.136**

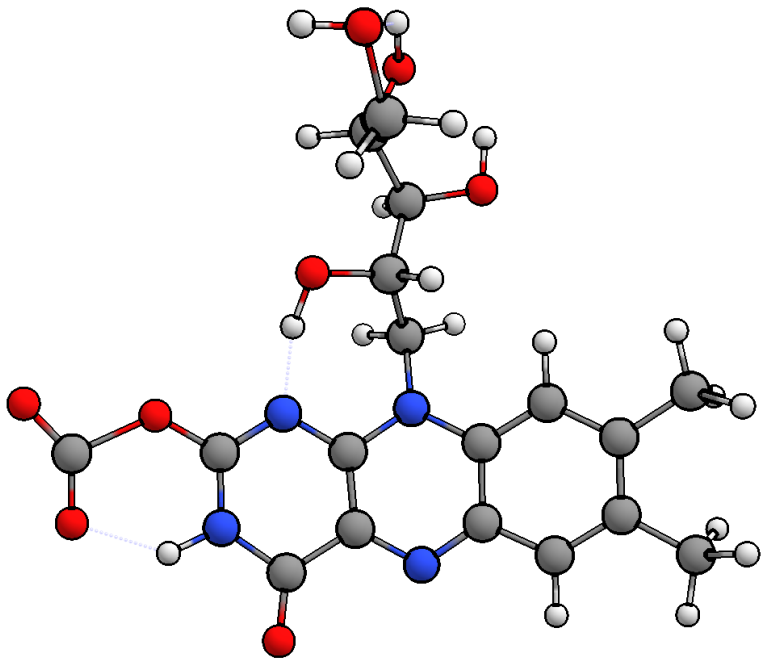

FIGURE A.11: Optimized geometry of $Fl_{red}{}^{2-}$ binding with CO_2 ($Fl_{red}(CO_2)^{2-}$ through O2 position.

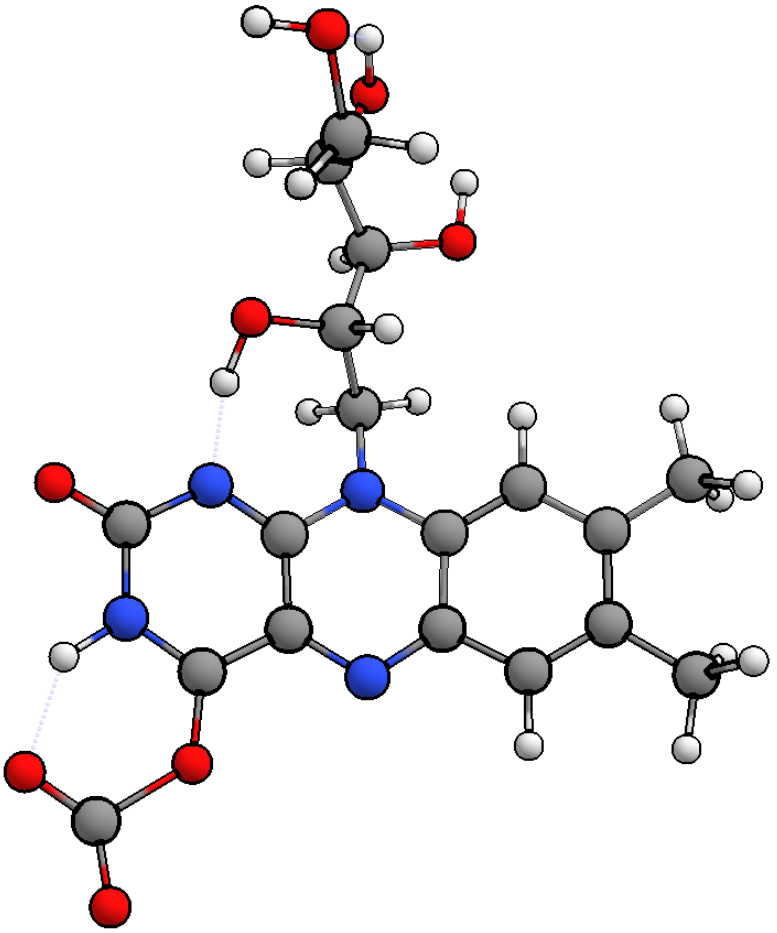

FIGURE A.12: Optimized geometry of $Fl_{red}{}^{2-}$ binding with CO_2 ($Fl_{red}(CO_2)^{2-}$ through O4 position.

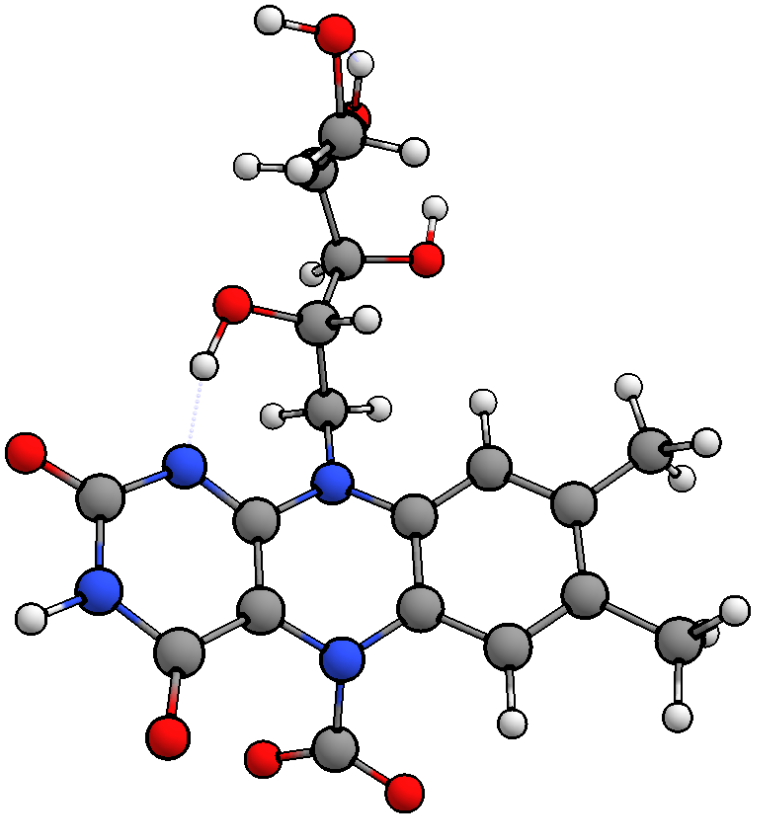

FIGURE A.13: Optimized geometry of $Fl_{red}{}^{2-}$ binding with CO_2 ($Fl_{red}(CO_2)^{2-}$ through N5 position.

Cartesian coordinates of riboflavins and its reduced forms with different binding positions to CO_2

CO_2

C -1.194086 -0.871868 -3.007518
O -0.639595 -0.999309 -1.979692
O -1.748577 -0.744426 -4.035343

Fl_{ox}

O -2.441141 -1.468435 -0.167865
O -2.541074 2.081128 -0.759486
O -5.190614 1.630475 -0.610693
O -5.558454 0.897322 2.011635
O 4.004887 -3.466355 0.616273
O -0.194981 -4.822612 -0.423781
N 0.610279 -0.312359 -0.586572
N 3.206415 -0.783619 0.315647
N 0.157633 -2.571550 -0.488489
N 1.896500 -4.107714 0.058033
C -1.912374 -0.166645 -0.289765
C -0.698592 -0.108677 -1.236961
C -3.021768 0.740898 -0.823749
C -4.349144 0.608067 -0.069065
C 1.433236 0.763607 -0.280656
C 1.016966 -1.596697 -0.329186
C 2.750827 0.489536 0.159963
C 1.021094 2.099101 -0.377402
C 2.394496 -1.766688 0.095798
C -4.248343 0.778189 1.443876
C 1.888679 3.139597 -0.080421
C 3.619294 1.558299 0.445291
C 3.223493 2.871469 0.327417
C 2.879572 -3.169536 0.290074
C 1.398359 4.556693 -0.186857
C 4.180597 3.991597 0.633098
C 0.555566 -3.880200 -0.299164
H -1.598309 0.226427 0.688127
H -0.808810 -0.887216 -1.991436
H -0.663182 0.853019 -1.736240
H -3.224190 0.468996 -1.869223
H -4.769086 -0.378857 -0.291739
H 0.004186 2.340773 -0.651031
H -3.702716 -0.058608 1.885731
H -3.734672 1.708334 1.688440
H 4.620304 1.299537 0.766732
H -1.700675 -2.103094 -0.248480
H -3.315202 2.644748 -0.902489
H -5.893811 1.779169 0.037346
H 0.349258 4.591195 -0.475992
H 1.508091 5.086173 0.763246
H 1.974362 5.119166 -0.927018
H 5.157817 3.600746 0.913608
H 4.316199 4.649102 -0.229691
H 3.820643 4.617344 1.454292
H 2.155842 -5.077780 0.180795
H -5.952552 0.019154 2.067338

$Fl_{rad}^{\bullet-}$

O 2.958644 -0.655612 -1.779883
O 0.835132 2.204460 -2.412331
O 2.172328 3.172286 -0.331430
O 4.683772 3.355136 -1.231341
O 2.432429 -5.700739 -6.097594
O 3.595642 -4.520588 -1.819006
N 1.077804 -1.463445 -4.232786
N 1.169227 -3.135742 -6.518633

N 2.365635 -2.964858 -3.003982
N 2.934764 -5.053180 -3.951575
C 2.030685 0.109114 -2.507492
C 0.831779 -0.724031 -3.498000
C 1.545249 1.260855 -1.617881
C 2.709678 1.974701 -0.912173
C 0.638106 -0.966587 -5.470685
C 1.758399 -2.683650 -4.170041
C 0.673131 -1.873046 -6.593772
C 0.171160 0.348491 -5.636027
C 1.730864 -3.507529 -5.336514
C 3.844611 2.368933 -1.862883
C -0.320664 0.807504 -6.879907
C 0.158755 -1.383065 -7.829986
C -0.335095 -0.082013 -7.990325
C 2.368214 -4.830521 -5.224279
C -0.814096 2.227263 -7.016602
C -0.863155 0.377306 -9.329759
C 2.997207 -4.181741 -2.846077
H 2.487078 0.580423 -3.419239
H 0.579307 -1.454037 -2.203515
H -0.039905 -0.064766 -3.169268
H 0.882627 0.836990 -0.819711
H 3.111786 1.294129 -0.125634
H 0.207893 1.055551 -4.793888
H 4.409955 1.465816 -2.175118
H 3.417243 2.861250 -2.759547
H 0.175172 -2.090860 -8.673632
H 2.848342 -1.616082 -2.114801
H 0.864821 3.019455 -1.861837
H 2.944878 3.783945 -0.341909
H -0.720186 2.776681 -6.059030
H -0.247493 2.797418 -7.787254
H -1.882913 2.273818 -7.326311
H -0.808988 -0.434838 -10.081365
H -1.922976 0.710470 -9.267692
H -0.289971 1.244090 -9.727706
H 3.402505 -5.955524 -3.831930
H 5.199151 2.882460 -0.549410

Fl_{red}^{2-}

O 3.078286 -0.498608 -1.984456
O 0.931528 2.398395 -2.252565
O 2.147192 2.940791 0.074266
O 4.725058 3.173513 -0.636248
O 2.311633 -5.787581 -5.912805
O 3.840512 -4.264807 -1.856459
N 1.233659 -1.324563 -4.375038
N 0.988407 -3.222774 -6.489164
N 2.565082 -2.777228 -3.105988
N 2.996569 -4.932976 -3.893486
C 2.095190 0.281062 -2.612517
C 0.934937 -0.568644 -3.179087
C 1.559186 1.302272 -1.589680
C 2.684564 1.845052 -0.696169
C 0.728237 -0.910901 -5.642316
C 1.860216 -2.586894 -4.261176
C 0.566965 -1.959722 -6.645515
C 0.358733 0.409659 -5.901937
C 1.693536 -3.503392 -5.318714
C 3.881485 2.364340 -1.493105
C -0.273972 0.805163 -7.125932
C -0.105578 -1.530832 -7.847232
C -0.512004 -0.205426 -8.089236
C 2.321187 -4.805894 -5.141367
C -0.683388 2.237228 -7.351276
C -1.209133 0.141727 -9.388523
C 3.170537 -3.984130 -2.875018
H 2.507066 0.882627 -3.469027

H 0.634962 -1.269359 -2.363191
H 0.076044 0.098634 -3.404430
H 0.828482 0.778866 -0.917199
H 3.024121 1.017300 -0.031921
H 0.539655 1.182210 -5.135013
H 4.422927 1.503485 -1.937455
H 3.524198 3.039690 -2.296114
H -0.293275 -2.316638 -8.599791
H 2.952720 -1.489706 -2.356271
H 0.924355 3.092147 -1.556814
H 2.941293 3.508789 0.203951
H -0.423000 2.863101 -6.471663
H -0.194836 2.715384 -8.240173
H -1.784140 2.374848 -7.520623
H -1.333795 -0.757153 -10.028166
H -2.222371 0.580538 -9.224477
H -0.647770 0.900701 -9.984040
H 3.450248 -5.837471 -3.746615
H 5.150028 2.543265 -0.022479

$Fl_{red}(CO_2)^{2-}$, binds at O2

O 3.192199 -0.291605 -2.078489
O 1.012553 2.566508 -2.443047
O 2.215308 3.214299 -0.145607
O 4.787766 3.474376 -0.855381
O 2.435720 -5.613657 -6.034033
O 3.938782 -4.048473 -1.925465
N 1.369516 -1.155025 -4.486494
N 1.184010 -3.041570 -6.617585
N 2.702151 -2.628291 -3.221620
N 3.128975 -4.787221 -4.003590
C 2.206697 0.468420 -2.737192
C 1.058630 -0.401657 -3.293554
C 1.661368 1.508356 -1.743093
C 2.777888 2.102701 -0.870195
C 0.899217 -0.732021 -5.761907
C 1.996863 -2.416259 -4.378961
C 0.770087 -1.764537 -6.777881
C 0.530779 0.590532 -6.018765
C 1.849765 -3.326028 -5.442527
C 3.967067 2.617323 -1.683331
C -0.061527 0.990475 -7.258466
C 0.153528 -1.331615 -7.997788
C -0.255320 -0.004604 -8.242869
C 2.463481 -4.645915 -5.257530
C -0.473222 2.423680 -7.482147
C -0.900987 0.352437 -9.565007
C 3.257914 -3.827793 -3.047067
H 2.628652 1.045803 -3.602891
H 0.769195 -1.105038 -2.477012
H 0.188999 0.251771 -3.518895
H 0.942400 0.994117 -1.051956
H 3.130936 1.308847 -0.172345
H 0.680469 1.356566 -5.239820
H 4.532187 1.756825 -2.097654
H 3.597151 3.254327 -2.511640
H 0.004750 -2.110885 -8.764615
H 3.099602 -1.261048 -2.423582
H 0.996469 3.287027 -1.774810
H 2.996821 3.802285 -0.028736
H -0.242058 3.043904 -6.590479
H 0.041735 2.904190 -8.351688
H -1.567396 2.548161 -7.685101
H -0.990742 -0.539001 -10.219824
H -1.923775 0.779202 -9.437050
H -0.321596 1.122772 -10.126390
H 3.597420 -5.685047 -3.765927
H 5.233309 2.878346 -0.222485
C 4.669580 -5.430581 -1.544829

O 5.199872 -5.293474 -0.455429
O 4.552931 -6.323648 -2.396365

$Fl_{red}(CO_2)^{2-}$, binds at O4

O 2.876388 -0.590780 -1.917067
O 0.873814 2.382524 -2.386139
O 2.055584 3.006012 -0.071551
O 4.655042 3.113752 -0.718524
O 2.230635 -5.656231 -6.165846
O 3.477675 -4.389141 -1.872425
N 1.098380 -1.321333 -4.427477
N 1.040223 -3.100618 -6.655281
N 2.324815 -2.836716 -3.149700
N 2.815064 -4.968788 -3.998946
C 1.972779 0.224252 -2.620259
C 0.798031 -0.575748 -3.220014
C 1.450635 1.303727 -1.656154
C 2.574320 1.853104 -0.762746
C 0.672717 -0.844080 -5.704542
C 1.720390 -2.567668 -4.324271
C 0.617363 -1.829995 -6.772807
C 0.302595 0.485665 -5.916675
C 1.640518 -3.442294 -5.454222
C 3.810837 2.285937 -1.552562
C -0.219568 0.940934 -7.164402
C 0.058546 -1.341791 -8.004457
C -0.348060 -0.011873 -8.206381
C 2.240574 -4.709857 -5.227756
C -0.623540 2.381942 -7.346442
C -0.919502 0.405665 -9.544941
C 2.905428 -4.074193 -2.930922
H 2.461301 0.770387 -3.472317
H 0.460731 -1.286933 -2.431357
H -0.036020 0.116528 -3.451738
H 0.689822 0.834813 -0.977830
H 2.865522 1.053207 -0.043464
H 0.408503 1.218594 -5.099781
H 4.337406 1.386696 -1.934291
H 3.499782 2.925564 -2.402683
H -0.034015 -2.082992 -8.816200
H 2.740872 -1.556759 -2.295121
H 0.881907 3.114803 -1.730697
H 2.864166 3.554712 0.052500
H -0.454293 2.958615 -6.412506
H -0.055657 2.906603 -8.155814
H -1.702754 2.514196 -7.614152
H -0.962614 -0.452530 -10.246863
H -1.951689 0.818610 -9.454796
H -0.315563 1.207011 -10.031610
H 3.223106 -5.931148 -3.946145
H 5.051357 2.507966 -0.062688
C 2.837601 -7.098495 -6.010366
O 3.382082 -7.331062 -4.911857
O 2.649618 -7.728400 -7.039776

$Fl_{red}(CO_2)^{2-}$, binds at N5

O 3.095300 -0.421888 -2.025986
O 0.812771 2.343702 -2.493300
O 2.075650 3.185299 -0.295476
O 4.607945 3.491742 -1.120329
O 3.366234 -5.102152 -6.566359
O 4.391924 -4.003280 -2.234085
N 1.247605 -1.355147 -4.451858
N 1.196954 -3.054933 -6.640407
N 2.819272 -2.671232 -3.295623
N 3.700690 -4.569752 -4.354644
C 2.099084 0.288238 -2.711453
C 0.964219 -0.626994 -3.232752

C 1.534498 1.356173 -1.760595
C 2.654033 2.048997 -0.967883
C 0.900295 -0.819727 -5.713284
C 2.052577 -2.517406 -4.413144
C 0.864851 -1.717792 -6.832243
C 0.542460 0.530329 -5.883704
C 2.038613 -3.344050 -5.534104
C 3.794116 2.548388 -1.856842
C 0.092176 1.030678 -7.129550
C 0.425995 -1.198730 -8.073823
C 0.027293 0.144355 -8.230634
C 3.043850 -4.389328 -5.605842
C -0.310591 2.480581 -7.261696
C -0.458861 0.631269 -9.578134
C 3.665034 -3.750119 -3.214455
H 2.499959 0.842470 -3.604119
H 0.748900 -1.359772 -2.423905
H 0.053223 -0.017154 -3.405458
H 0.864066 0.850914 -1.016363
H 3.061898 1.316165 -0.233813
H 0.589924 1.219208 -5.026417
H 4.376120 1.679589 -2.228672
H 3.374022 3.110585 -2.714557
H 0.340186 -1.929078 -8.890358
H 3.081553 -1.394306 -2.445403
H 0.798692 3.105590 -1.872553
H 2.836671 3.809235 -0.252557
H -0.200499 3.013276 -6.294521
H 0.302816 3.031058 -8.014350
H -1.370422 2.605411 -7.589668
H -0.440469 -0.189365 -10.323137
H -1.502504 1.022470 -9.536625
H 0.162917 1.465984 -9.979039
H 4.399235 -5.316193 -4.343666
H 5.100531 2.958567 -0.466763
C 0.310075 -4.198730 -7.207159
O 0.283216 -5.196428 -6.469213
O -0.247270 -3.930698 -8.294833

References

(1) Li, X.; Zhao, X.; Zhang, L.; Mathur, A.; Xu, Y.; Fang, Z.; Gu, L.; Liu, Y.; Liu, Y. Redox-tunable isoindigos for electrochemically mediated carbon capture. *Nature Communications* **2024**, *15*, Publisher: Nature Publishing Group, 1175.

List of Author's Publications

Journal Articles

- Kongcharoen H.; Coaster B.; Yu F.; Aziz I.; Poh W. C.; Wei M.; Tan M.; **Tonanon P.**; Ciou J.-H.; Chan B.; Webster R. D.; Lew W. S.; Lee P. S. 'Magnetically directed co-nanoinitiators for cross-linking adhesives and enhancing mechanical properties' *ACS Applpied Materials & Interfaces* **2021**, 13, 48, 57851-57863.

- Liangdy A.; Lee W. J.; **Tonanon P.**; Webster R. D.; Snyder S. A.; Lim T.-T. 'Unravelling the synergism of catalytic oxidation and filtration in Co-Mn-oxide impregnated ceramic membrane for intensified degradation of recalcitrant micropollutant with peroxymonosulfate' *Chemical Engineering Journal* **2023**, 454, 140075.

- **Tonanon P.**; Webster R. D., 'Recent Electrode and Electrolyte Choices for Use in Small Scale Water Treatment Applications - A Short Review.' *Current Opinion in Electrochemistry* **2023**, 38, 101211.

- **Tonanon P.**; Jalando-On Agpoon K.; Webster R. D. 'A Comparison of the Detection and Quantification of Praziquantel via Electrochemical and Gas Chromatography Methods in Freshwater and Saltwater Samples.' *Analytical Methods* **2024**, 16 (9), 1323-1329.

- Liangdy A.; **Tonanon P.**; Webster R. D.; Snyder S. A.; Lim T.-T. 'Versatile Fe_3O_4-impregnated catalytic ceramic membrane for effective atrazine removal: Confined catalytic oxidation processes, reactive oxygen species selectivity and performance in real wastewater' *Journal of Environmental Chemical Engineering* **2024**, 12, 3, 112727.

- **Tonanon P.**; Webster, R. D. 'Probing the Molecular Interactions of Electrochemically Reduced Vitamin B_2 with CO_2.' *The Journal of Physical Chemistry B* **2024** 128(44), 10853-10860.

- Liangdy A.; **Tonanon P.**; Snyder S. A.; Webster R. D.; Lim T.-T. 'Surface- and substrate-coated catalytic membrane for mitigating interference of water matrix species in intensified micropollutant confinement oxidation' *Journal of Environmental Chemical Engineering* **2024**, 12, 6, 114750.